# Resonances in Electron Impact on Atoms*†

## George J. Schulz

*Department of Engineering and Applied Science, Mason Laboratory, Yale University, New Haven, Connecticut 06520*

Electrons colliding with atoms can form, at well-defined energies, compound states consisting of the target atom plus the incident electron. The compound states, which are also called "resonances" or "temporary negative ions," often dominate electron collision processes. In this review we discuss the experimental methods which are useful for studying these resonances, and review the results obtained by various investigators. We list the energies and the widths of resonances for H, He, Ne, Ar, Kr, Xe, Li, Na, Hg, and O. The configurations and other properties of resonances in atoms are discussed. Whenever applicable, results are presented in the form of tables and energy level diagrams.

## CONTENTS

## I. INTRODUCTION

This paper and the paper following deal with a special topic in the field of electron impact on atoms and molecules. The object of interest are "resonances," also called "compound states" or "temporary negative ions." These three terms are synonyms and will be used interchangeably. "Resonances" occur at more or less well-defined energies when electrons scatter from atoms or molecules. The object can be considered as a "compound state," in that the incident electron attaches itself to the target atom (or molecule) for times which are longer than the normal transit time through the atom or molecule. Since the projectile is always a negatively charged electron, the "compound state" has a negative charge. Hence the term "temporary negative ion."

The "resonances" can be viewed as nonstationary (short-lived) states of an atom or molecule. In sharp contrast to stationary states of atoms, "resonances" decay by the emission of electrons, not by photons. Our definition of "resonances" in the present context excludes some types of nonstationary states which also can be viewed as resonances. For example, doubly excited states of atoms (e.g., the $2s^2$ and $2s2p$ states in helium) are nonstationary states which decay by electron emission, yielding positive ions. Nevertheless, such states are excited states of the *neutral* atom, and therefore do not meet our definition, namely that the states be temporary negative ions. This limitation of the review is rather arbitrary.

Resonances were discovered almost simultaneously by experiment and theory about 10 years ago, and great progress has been made in our understanding of these phenomena in the past decade. These two review papers represent an effort to discuss the spectroscopy of resonances in a more or less systematic fashion. The review is divided into two parts: In the present paper, we discuss resonances associated with atoms; in the second paper we discuss resonances associated with diatomic molecules. Resonances associated with more complex molecules also exist, but too little is known about them to justify inclusion in the present work.

In both parts of this review we present a concise discussion of the energy levels, the classification of resonances, and their decay. Comparison with theory is presented whenever such comparison is meaningful, but a full exposition of theory is not attempted. Energy level diagrams for resonances are constructed to aid the overview and the tables of values can be found in the appendixes. The discussion is organized by species.

## A. Theory

In atoms, resonances are mostly associated with excited states ("core-excited resonances"). Resonances associated with the ground states of atoms have been established only for the alkalis. One can distinguish between two distinct types of resonances, namely those that lie energetically below the state from which they derive (i.e., below the "parent") and those that lie above. Thus we introduce what may be called the geneology of resonances, a concept actually introduced for a better understanding of resonances in molecules and discussed in more detail in the second paper of this review. A positive ion with a particular configuration of electrons is considered the grandparent. Adding a single electron to this positive ion configuration gives a Rydberg state of the neutral atom or molecule: this is the parent. Adding an extra electron to the parent, we have a particular "resonance."

Resonances which lie below their parent are interchangeably called "closed-channel resonances," "Feshbach resonances," or "Type I resonances" (Taylor *et al.*, 1966, Taylor, 1970). They arise when the interaction potential between the incident particle and the excited state of the target is strong enough to support a bound state. They usually lie approximately 0–0.5 eV below the parent. When the excitation takes place near the center of the resonance, decay into the parent is energetically forbidden, but decay into some other states (nonparents) is allowed. Because decay into nonparents involves a change in configuration of the atoms, Feshbach-type resonances are usually long-lived and their widths are narrow. When such resonances are excited in the high-energy wing, decay into the parent may become energetically possible (Taylor, 1970), and such decay is favored. The end-result of such a decay is often a sharp peak near threshold in the excitation function of the parent state. Such effects are known in both atoms and in molecules.

A special case of a Feshbach-type resonance occurs when the energy level lies near the very top of the potential well. Such a state is called "virtual" and an example is discussed in connection with the $2^1S$ state of helium in Sec. IIIB5.

Resonances which lie above their parents are called "shape resonances" or "open-channel resonances," or "Type II" (Taylor *et al.*, 1966). In this case, the potential forms a penetrable barrier which traps the incident particle near the target. The barrier is formed by the angular momentum of the electron. Thus, we expect $p$-, $d$-, $f$-wave resonances but generally not $s$-wave resonances, since the latter have $l=0$ and thus produce no barrier.

Shape resonances show a preference for decay into their parents and very often dominate the excitation cross section of their parent. Thus shape resonances usually have a shorter lifetime (i.e., larger width) compared to Feshbach resonances. An exception occurs when a shape resonance exists barely above an inelastic threshold (Macek and Burke, 1967). In this case the barrier can be viewed as being very thick (Taylor, 1970) and the resonance becomes long-lived, i.e., the width is narrow; such a case exists in atomic hydrogen.

The presence of resonances is ascertained experimentally by measuring structure in the energy dependence of elastic or inelastic cross sections. Because the structure is often very sharp, monochromatic beams of electrons are needed for such studies and the techniques generally employed are briefly reviewed below. These techniques are also useful for the study of resonances in molecules.

A particular resonance can decay, by the emission of an electron, into many final states. We thus may speak of "channels of decay" for a given resonance. Therefore the existence of a resonance may be detected by measuring the structure in the energy dependence of the cross section of any state which lies energetically below or near the resonance. In fact, sometimes it is possible to detect the existence of a resonance even in a state which lies energetically above the center of resonance. This effect is caused by the "wings" or "tails" of the resonance (Taylor, 1970). Not all decay channels are equally useful for detecting a particular resonance. Often, the branching ratio favors a particular decay and then it is easier to detect structure in the final state which is favored, provided that the nonresonant portion of the cross section is of the same order in the two states. Such phenomena are particularly important in molecules.

The energy dependence of the elastic cross section in the neighborhood of an isolated resonance in the $s$ wave with a single decay channel can be expressed by the Breit–Wigner formula (Blatt and Weisskopf, 1952), $\sigma(E) \sim \pi \lambda^2 \mid A + \{\Gamma/[(E-E_0)+(\frac{1}{2}i)\Gamma]\} \mid^2$. Here, $A$ represents direct "potential" scattering which varies only slowly with energy; $\Gamma$ is the "width" of the state, i.e., the range of energies over which the resonance has a large effect on scattering; $E_0$ determines the location of the resonance; $E$ is the energy; and $\lambda$ is the reduced wavelength of the electron. The cross section off resonance becomes $\pi \lambda^2 \mid A \mid^2$. When direct scattering is small, the cross section near a resonance becomes $\pi \lambda^2 [\Gamma^2/(E-E_0)^2+(\frac{1}{2}\Gamma)^2]$. The maximum cross section then occurs at the resonance energy $E_0$ and the half-width is $\Gamma$. In general, however, interference occurs between direct scattering and resonance scattering so that the shape of the cross section becomes more complicated, leading to destructive and constructive inter-
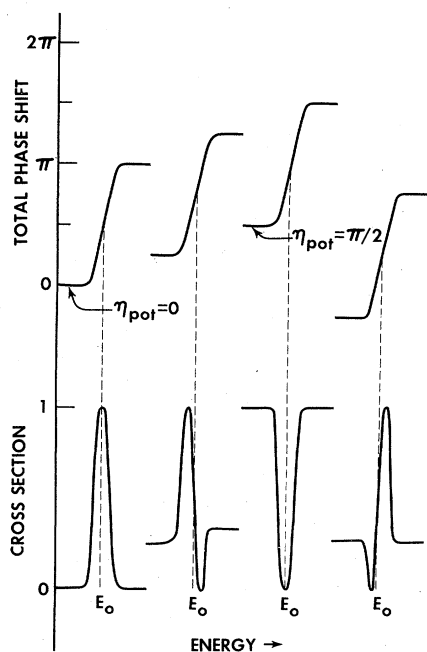
FIG. 1. Partial wave phase shift near a resonance (top portion) and resulting shape of the cross section near a resonance (bottom portion). The figure illustrates the interference between potential and resonance scattering. [After Smith (1966).]

ference. The phase shift $\eta$ which always enters the expression for the elastic cross section [for $s$-wave scattering we can write $\sigma(E) = 4\pi\lambda^2 \sin^2 \eta$], increases by $\pi$ radians as the energy traverses each resonance. This can be seen from the expression for the resonant contribution to the phase shift, $\eta_{res} = -\cot^{-1}[(E-E_0)/\frac{1}{2}\Gamma]$. The smaller the width $\Gamma$, the more rapidly occurs the traversal of the phase shift by $\pi$ radians. In Fig. 1 we plot the phase shift as a function of energy near a resonance for four arbitrary cases. The phase shift for potential scattering is different for each case, but in each case it increases by $\pi$ radians as the energy traverses the resonant energy $E_0$. The shape of the resulting cross section, shown on the bottom of Fig. 1, shows the expected interference structure. The position of $E_0$ is defined to be the energy at which the *resonant portion* of the phase shift has increased by $\frac{1}{2}\pi$; i.e., $\eta_{res} = \frac{1}{2}(2n+1)\pi$. That is the position where the *total phase* shift (consisting of the sum of the phase shifts due to potential and resonant scattering) has increased by $\pi/2$ radians above the phase shift due to potential scattering which prevails just below the resonance.

When we are dealing with inelastic scattering, decay can take place to a state other than the ground state, and the resonant portion of the cross section becomes $\pi\lambda^2[\Gamma_{in}\Gamma_{out}/[(E-E_0)^2+(\frac{1}{2}\Gamma)^2]$. Here $\Gamma_{in}$ is the width for decay into the ground state plus a free electron and $\Gamma_{out}$ is the partial width for decay into the excited state plus a free electron. Then we have $\Gamma = \Gamma_{in} + \Gamma_{out}$.

It is often desirable to evaluate line profiles of resonances using the formula due to Fano (1961) and

to Fano and Cooper (1965a):

$$\sigma(E) = \sigma_a[(q+\epsilon)^2/(1+\epsilon^2)] + \sigma_b.$$

Here, $\sigma_a$ and $\sigma_b$ are the resonant and nonresonant portions of the cross section, $\epsilon = (E-E_0)/\frac{1}{2}\Gamma$, and $q$ is the "line profile index." Simpson *et al.* (1966) describe how one can evaluate the parameter $q$ from experimental measurements. In fact, many authors extract this parameter from their experimentally observed line profiles. Figure 2 shows the line profiles plotted for various values of the parameter $q$.

If one wishes to analyze the line profile in terms of a symmetric and an asymmetric component, one can write (Shore, 1967)

$$\sigma(E) = C(E) + \frac{1}{2}\Gamma B[(E-E_0)^2 + (\Gamma/2)^2]^{-1}$$
$$+ D(E-E_0)[(E-E_0)^2 + (\Gamma/2)^2]^{-1}.$$

The parameters $B$ and $D$, specifying the symmetric and asymmetric components of the line, are constants. They are related to the Fano formula by the equation $B/D = (q^2-1)/(2q)$. Comer and Read (1972) have developed a simple method for obtaining resonance energies from broadened profiles using the formulation of Shore.

Recent reviews of the theory have been assembled by Smith (1966) and by Burke (1968).

## B. Relationship of Theory to Experiment

The search for resonances in atoms by experimental methods consists of a search for structures in various cross sections. In circumstances when this structure is relatively narrow ($\lesssim 300$ meV) and far removed from neighboring resonances, little ambiguity exists. In cases when the structure is broad, further verification is needed. Often, the angular distribution of scattered electrons can elucidate the process involved. In molecules, dissociative attachment and vibrational excitation provide extra evidence. This multiplicity of decay channels often makes the identification of resonances easier in molecules than it is in atoms.

There are many theoretical approaches to the calculation of resonances but a thorough review is beyond the scope of this paper. Nicolaides (1972), in reviewing the field recently, lists many of the pertinent theoretical references. One may rather arbitrarily divide the theories into the following classifications:

(a) Theories using the "scattering viewpoint."

(b) Theories treating resonances as a "decaying state."

(c) Theories treating resonances as special types of bound states using projection operators.

(d) Theories treating resonances as special types of bound states without use of projection operators.

The theories which use the scattering viewpoint, as exemplified by the close-coupling method, essentially simulate a scattering experiment and they calculate cross sections for various processes from the phase

FIG. 2. Natural line shapes for different values of $q$. Reverse the scale of the abscissa for negative $q$. [From Fano (1961).]

$$\frac{(q+\epsilon)^2}{1+\epsilon^2}$$
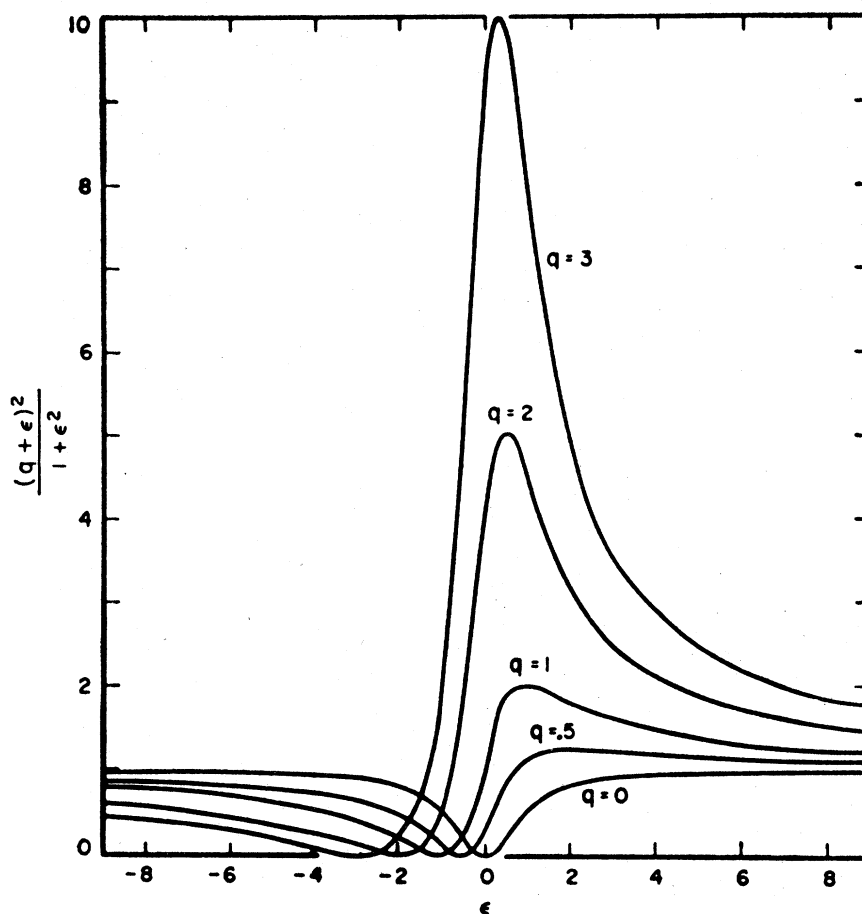
shifts. When the phase shift rises rapidly by $\pi$ radians, the resonance is located. The width is determined from the energy range over which the phase shift rises through $\pi$ radians. This method appears to be very general and gives, in addition to the location and positions of resonances, cross sections for various processes. However, in all but the simplest systems, the computational needs become enormous. Therefore, considerable *a priori* judgement must be exercised as to which states to include to make a particular cross section meaningful. A great deal of relevant insight has been gained by the close-coupling calculations for various atoms and molecules. The frame-transformation theory also belongs in category (a). Here, an expansion is performed in the molecular frame of reference and the region around the molecule is divided into a "core region," and an outer region in which electron correlations are disregarded. This method has had good successes in recent years.

Theories treating resonances as decaying states (which they are) are based on the Kapur–Peierls theory. Here, a stationary value for a complex energy is obtained, which gives both the width and the energy of the resonance. Problems are the need for good wave functions and the need to define a definite radius of

interaction. Both shape and Feshbach resonances can be treated in this manner.

Theories treating resonances by the use of projection operator techniques solve directly for the expectation value of the Hamiltonian, with the decay of the state ignored. The decay can be later introduced to give an estimate of the width of the state, but this is usually a difficult step. Only Feshbach-type resonances can be calculated in this manner.

Similar to the latter category are the techniques which search for locally stationary points of the expectation value of the Hamiltonian. A foremost example is the "stabilization method." Here, one takes a trial function which contains all the knowledge one has about the resonance. Both shape and Feshbach resonances can be calculated in this manner, but the width is again a difficult quantity to extricate.

When scattering amplitudes are calculated, structures in the cross section can be caused by poles, zeros, and branch points in the scattering amplitude. Only the poles should be associated with resonances. The zeros in the scattering amplitude for a single partial wave are associated with Ramsauer minima.

For simplicity of interpretation we assume in this

review that every resonance is characterized by a well-defined energy and width. Also, an attempt is made to associate resonances with one or two molecular orbitals of a negative ion state of the atom or molecule. Actually, a superposition of a few molecular orbitals must always be considered in order to describe a resonance properly. When only a single term is given, it is understood that this is the leading, i.e., dominant, term. Despite the fact that these assumptions oversimplify the problem, they seem to be applicable for most resonances discussed in this review. Exceptions are pointed out in the text. Thus, it is sometimes necessary to invoke the energy dependence of the resonance width and in other cases the resonance center cannot be located precisely from experimental information alone. Sometimes it does not appear to be possible to associate a dominant molecular orbital configuration with a particular resonance.

## C. Isoelectronic and Isostate Comparisons

It is sometimes desirable to deduce the energy levels of resonances, especially those of the Feshbach type, from known energy levels of other atoms which exhibit some similarities with the resonances. This approach is of course only approximate but often the sequence of resonant states and the physical picture can be deduced from such comparisons.

A simple example is discussed by Herzenberg (1971): The lithium atom in its ground state has the approximate electronic structure $1s^2 2s$, and is known to be able to attach an electron with a binding energy of 0.6 eV to form a stable $Li^-$ ion with the approximate structure $1s^2 2s^2$. The nucleus and the two $1s$ electrons in the ion form a small tightly bound core of charge $+|e|$ which provides an attractive potential to hold the two $2s$ electrons, whose wave functions extend far outside the core. A $He^+$ ion with its single $1s$ electron also constitutes a small tight core of charge $+|e|$ to which two electrons can be bound in an approximate configuration $2s^2$, as in $Li^-$. However, the resultant configuration $1s 2s^2$ of $He^-$ lies now nearly 20 eV above the configuration $1s^2$, and can therefore autoionize. It is the state $1s 2s^2$ which shows up as a Feshbach resonance, with a binding energy of about 0.47 eV with respect to the $(1s2s)^3S$ state of He. This binding energy is somewhat smaller than the binding energy of 0.6 eV of the $1s^2 2s$ state of lithium. Using such an approach, one can apply this kind of numerology to other twinned atomic systems.

Kuyatt, Simpson, and Mielczarek (1965) use a somewhat different method of comparison: They consider the known energy levels of doubly excited states in helium $(2s^2, 2s2p, 2p^2, 3s3p, \text{etc.})$. The two excited electrons are moving in a $Z=2$ field, whereas the two electrons in $He^-$ $(1s2s^2, 1s2s2p, \text{etc.})$ are moving in the $Z=1$ field of $He^+$. Kuyatt et al. take the energies of the doubly excited states of helium relative to the energy of $He^{++}$ and divide this energy difference by $Z^2 = 4$ in order to obtain the corresponding energies of

the $He^-$ states relative to $He^+$. There is a fair resemblance between the $He^-$ states thus obtained and the measured values.

Still another comparative method is used by Swanson, Cooper, and Kuyatt (1973). In order to interpret resonances in krypton, they compare the spectrum of resonances, i.e., $Kr^-$, with the isoelectronic atom, RbI. It appears that a fair comparison between these two sets of energy levels can be made if an arbitrary scaling constant is used.

## D. Experimental Techniques

In this section we review briefly the particular experimental techniques which made possible the discovery and the analysis of resonances. The developments described here span a period of about ten years, but they are based on principles which have been known for a much longer period. Actually we are dealing here with a combination of methods which were brought to bear on the problem of resonances in electron collisions with atoms and molecules. Some of the techniques were borrowed from other fields of physics: ultra-high vacuum technology, low-current measurements, particle counting, and signal averaging. Also, progress was partially facilitated by the commercial availability of many of the necessary components. Parallel with these developments was an improved understanding of electron optics (see, e.g., Heddle, 1970; Read, 1970, 1971; Adams and Read, 1972) and the development of new types of electron monochromators (see, e.g., Kuyatt and Simpson, 1967; Klemperer, 1965; Kuyatt, 1968). Good electron monochromators and electron analyzers are a necessary prerequisite for the experimental studies described in this and the following review, since many of the phenomena of interest occur in a very narrow range of energies and thus the use of electron beams with a narrow energy resolution is a *sine qua non*.

Since all of the techniques have been described in the recent literature, in reviews (see, e.g., Bederson, 1968; Kuyatt, 1968) and in books (Hasted, 1964; McDaniel, 1964; Massey and Burhop, 1969) only a very brief outline of the techniques is given here. For details, the reader is referred to the above reviews.

Many combinations of electric and magnetic fields, using appropriate geometrical arrangements and suitable holes or slits, can give chromatic dispersion of electrons and can thus be used for producing monochromatic electron beams. Equally important is the use of metals with desirable surface properties. One wishes to have a surface with a uniform potential and high conductivity. The surface should not be affected by the gas which is being studied. Although many surfaces have been tried by different groups (e.g., gold, Advance, stainless steel, copper) it appears that molybdenum is a most desirable surface.

A variety of geometries are useful for producing monochromatic electrons: The parallel plate and the
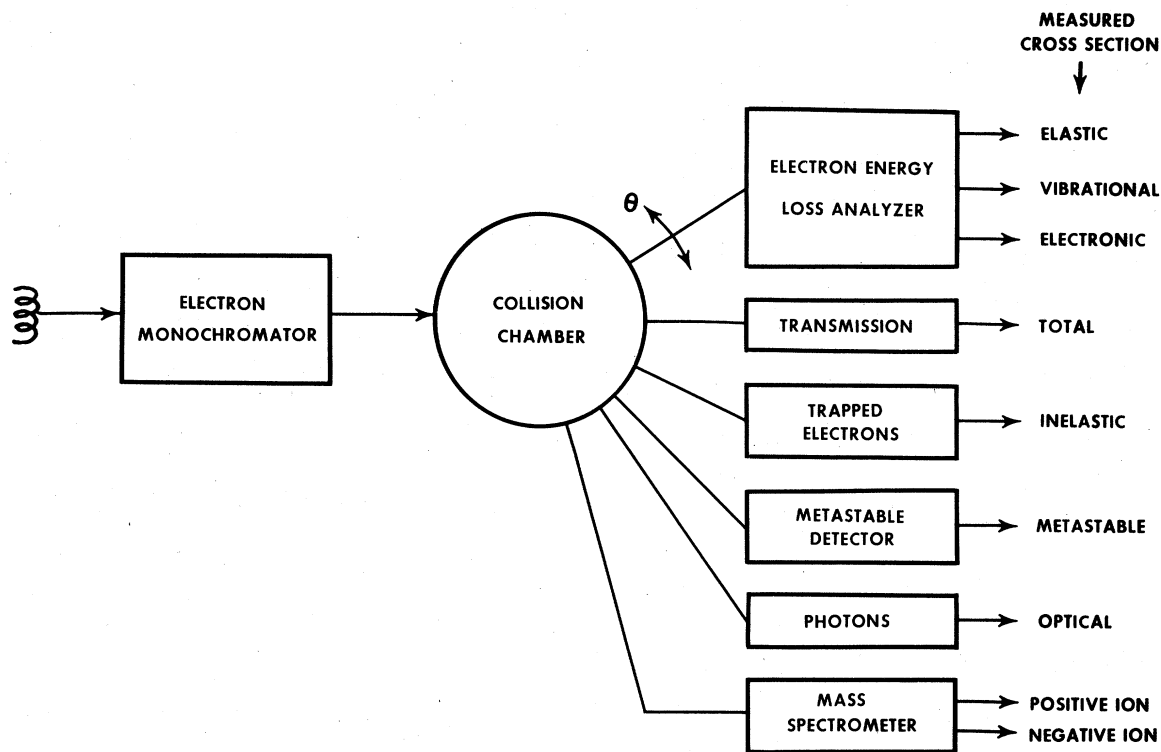
FIG. 3. Schematic overview of experiments which are useful for the study of resonances in atoms and molecules.

coaxial cylindrical "mirror" configurations, the 127° cylindrical electrostatic, and the 180° concentric spherical configurations. For production of very slow (<1 eV) monochromatic electrons, one can use the time-of-flight spectrometer. Monochromatic electrons can also be produced by ionization, using monochromatic photons. Electron monochromators can also be used in series to further improve the energy resolution. It appears that, at the present time, the most widely used monochromators for experiments in which a magnetically field-free region is desired are the 127° cylindrical and 180° concentric electrostatic configurations.

When an axial magnetic field is desired, one can use the retarding-potential difference method. The retarding-potential-difference method relies on the chopping of the electron distribution and thus is not a true monochromator. Although important advances have been made by use of this method, it has been made obsolete by the trochoidal monochromator. Also noteworthy are the 180° magnetic selector and the crossed electric and magnetic selector (Wien filter).

Figure 3 gives an overview of the experiments which are used for the measurement of resonances. The electron monochromator and the collision chamber are common to all experimental arrangements. The detection methods, however, differ widely, and are listed in Fig. 3. Below we discuss the various methods in slightly more detail, without giving credit to the inventors and

users of the methods. Such credit would only duplicate the much more detailed credit given in the subsequent chapters (and in the following paper) when the actual accomplishments are discussed.

### Differential Cross Section Measurements using Electrostatic Monochromators and Analyzers

A typical arrangement used for the measurement of structure in the differential elastic or inelastic cross section is shown in Fig. 4. This type of apparatus is typical of many instruments used in various laboratories to obtain the results discussed in subsequent sections. It is capable of measuring differential elastic or inelastic cross sections and usually it is possible to alter the angle between the monochromator and the analyzer, so that angular distributions of the scattered electrons can be obtained.

Electrons emitted from the filament are focussed, using electrostatic lenses (1–6) on a hole in plate 7, which serves as the input aperture for the monochromator. The monochromator itself may consist either of coaxial cylinders (127°) or concentric hemispheres (180°). Either of these devices should give an energy distribution with a full width at half-maximum of 0.02–0.06 eV. The electrons are focussed onto a molecular beam by the three-element lens system (10, 11, 12). Electrons scattered from the molecular beam pass through the electron optics of the analyzer, through the analyzer proper, and finally impinge on a multiplier and
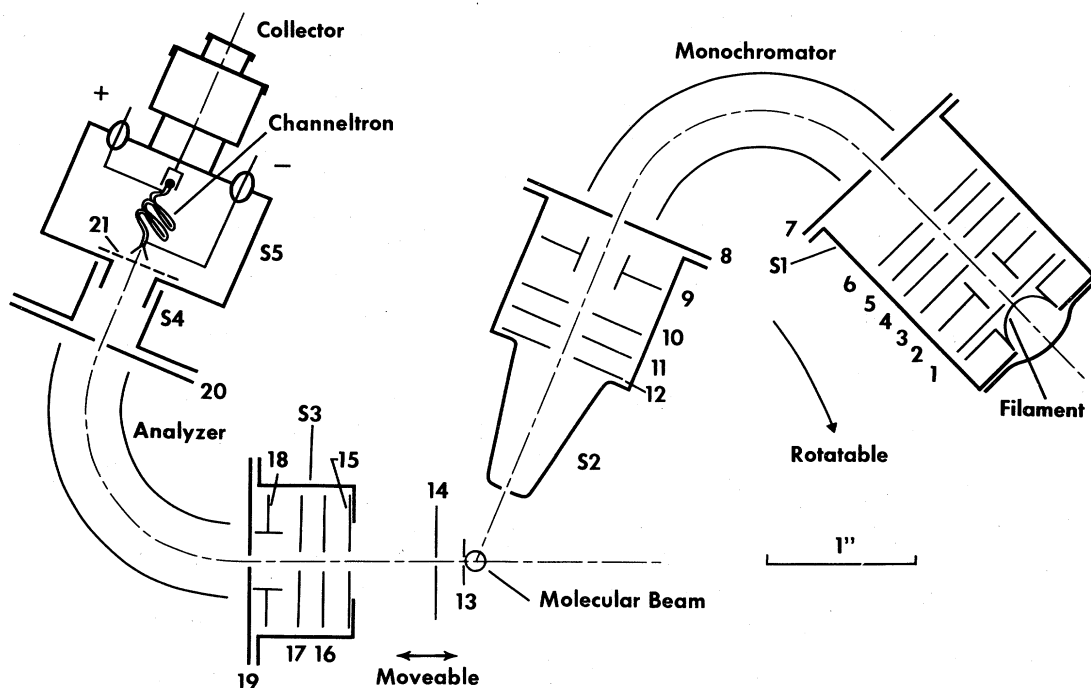
FIG. 4. Schematic diagram of a typical electrostatic monochromator with electrostatic analyzer. Angular distribution can be obtained by rotating the analyzer with respect to the monochromator. Elastic and inelastic differential cross sections can be obtained with such an instrument. [From Pavlovic, Boness, Herzenberg, and Schulz (1972).]

are counted. Use of a well-collimated molecular beam reduces Doppler broadening of the resonances. The electron optics is designed to maintain constant transmission characteristics throughout the spectrometer. Many shields are usually necessary $(S_1-S_5)$ to restrict stray electrons from reaching the multiplier. One usually eliminates magnetic fields from the collision region, either by using a magnetic shield or by using Helmholtz coils.

Double electrostatic analyzers of the type shown in Fig. 4 have given a wealth of information on resonances. Usually, one obtains the energy dependence of the elastic or the specific inelastic cross section at a fixed angle of observation. Structure in such curves is analyzed and the position and the width of resonances can be deduced. Alternatively, one can obtain at a given incident energy the angular distribution of electrons. Such information is valuable for determining the configuration of particular resonances. The inelastic cross sections that have been studied are the vibrational and the electronic cross sections. Rotational cross sections have been studied only in the single case of $H_2$.

### Measurement of Resonances in the Total Cross Section: The Transmission Method

The transmission method can also be used for studying resonances. In the appropriate geometry, the transmitted current $I_t$ through a gas-filled chamber is related to the incident current $I_0$ by the relation $I_t = I_0 \exp(-NQ_tL)$, where $N$ is the gas density, $Q_t$ is

the total cross section, and $L$ is the length of the collision chamber. Small excursions in the cross section $Q_t$ which often indicate the existence of resonances are exhibited by structures in the transmitted current. In fact, when $NQ_tL \gtrsim 1$, then some amplification of the structure takes place; i.e., the percentage change in the transmitted current is larger than the percentage excursion in the cross section. This fact can be utilized for a very sensitive measurement of resonances. A further refinement can be introduced by modulating the energy in the collision chamber and by observing essentially the derivative of the transmitted current.

An example of the arrangement for a transmission experiment is shown in Fig. 5. Here, a trochoidal monochromator is used for creating a monochromatic beam in an axial magnetic field. The electrons then enter the collision chamber region, maintained at a pressure of about $10^{-2}$ Torr, in which a cylindrical electrode M is mounted. A small modulation voltage (0.005–0.06 V) is applied to electrode $M$ so that the electron energy in the collision chamber is modulated. The modulated transmitted signal is detected on the collector C. The retarding electrodes R are used to cut off all those electrons which have made collisions in the collision chamber, so that only the unscattered electrons are transmitted to the collector C. Only under such circumstances is the exponential relationship between the transmitted and the incident current valid.

Copious examples are given in the text showing the sensitivity of this method of measurement, both for
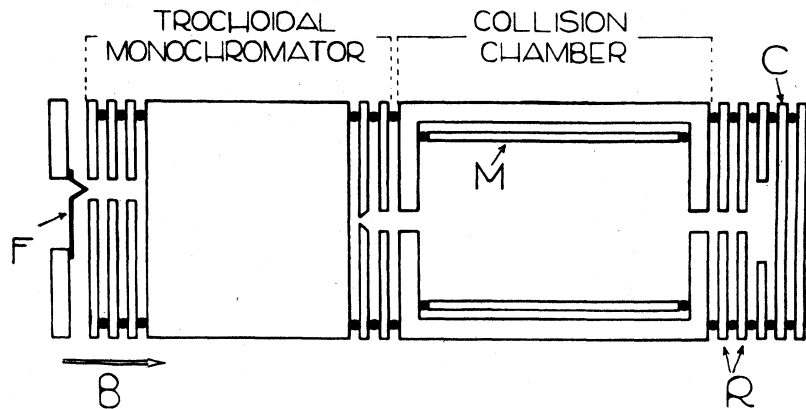
FIG. 5. Schematic diagram of a transmission experiment (top) and the details of the trochoidal mono-chromator (bottom). [From Sanche and Schulz (1972) and Stamatovic and Schulz (1970).]

atoms and for molecules. The high sensitivity for detecting resonances is thus established. However, since one cannot obtain information on the angular distribution of the electrons, one has great difficulty in establishing the configuration of the resonances. Also, it is difficult in this method to establish the final state to which a resonance has decayed. Thus, if one wishes to obtain more detailed information regarding the configuration and the channels of decay, one has to revert to the less sensitive but much more versatile double electrostatic analyzers.

It should be noted that the transmission method for detecting resonances need not use an axial magnetic field. Instead of a retarding electrode (R), one then can use a simple hole or slit for limiting the exit angle. Either method, with or without a magnetic field, should lead to an exponential dependence of the transmitted current with $NQL$. Optical focussing effects, i.e., the energy dependence of the transmitted current in the absence of gas, are inherently different in these two systems of measurement, but the optical focussing effects are probably easier to overcome in the presence of an axial magnetic field. And when one wishes to study resonances in a wide energy range, it is essential that optical focussing effects be small.

*Total Cross Section Measurements using the Ramsauer Method*

The measurement of resonances using the Ramsauer technique is a modern application of possibly the oldest quantitative approach to the measurement of cross sections, originated by Ramsauer and Kollath in the 1920's and 1930's. A review of the early work can be found, e.g., in Massey and Burhop (1969). A modern version of the apparatus is shown in Fig. 6. It is very similar to that used by Ramsauer and Kollath, the major modification being the provision here for differential pumping. Briefly, the electrons from an oxide-coated cathode, or a thoriated iridium filament, are momentum selected by the combination of the three slits, $S_1$, $S_2$, $S_3$, and a uniform magnetic field is applied perpendicular to the plane of the drawing. The electrons are then allowed to interact with the gas to be studied in the scattering cell, and the transmitted electron signal is studied as a function of gas density in the scattering region at a particular value of electron energy. If it is assumed that a current of electrons $I_{c0}+I_{s0}=I_0$ enters the scattering region, the current reaching the collector is given by $I_c(E)=I_{c0}(E) \exp [-\sigma_t(E)Nx]$, where $I_{c0}$ is that part of the current entering the scattering region which would reach the collector in the absence of scattering, $\sigma_t(E)$ is the total cross section, $N$ is the gas density, $x$ is the path length of the electron beam through the scattering chamber, and $E$ is the electron energy. The current reaching the scattering chamber walls is given by $I_s=I_{s0}+I_{c0}[1-\exp(-\sigma_t Nx)]$, where $I_{s0}$ is that part of the current entering the scattering chamber which would reach the scattering chamber walls in the absence of scattering. Then we have $\ln [(I_c+I_s)/I_c] = \ln [(I_{c0}+I_{s0})/I_{c0}]+\sigma_t Nx$. The total cross section is directly determined by measuring the slope of a plot of the left-hand side of this equation vs $N$,
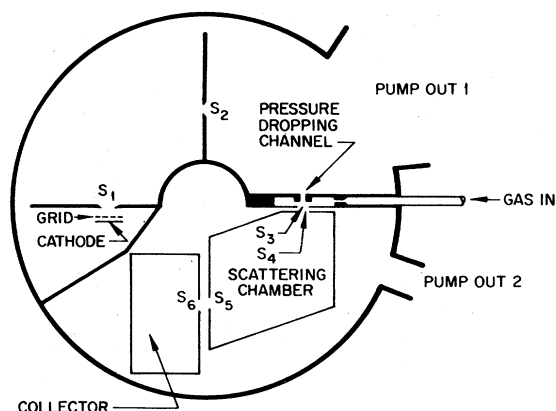
FIG. 6. Schematic arrangement of a modified Ramsauer apparatus for the measurement of total scattering cross section. [From Golden and Bandel (1965).]

at a constant energy. In this kind of selector, two parameters define the electron energy. One is the magnetic field strength and the other is the accelerating voltage. This coupling of the energy to two experimental parameters leads to the fact that the electron energy is usually not continuously variable. Since the energy spread is a function of the electron energy, the study of resonance effects is quite tedious, but resonances have been measured using this method. The advantage of this method lies in the fact that it yields the absolute magnitude of the total cross section at and near the resonance.

## Inelastic Cross Section Measurements using the Trapped-Electron Method

The trapped-electron method has been used for the past 15 years for the measurement of inelastic cross sections, particularly near the threshold of excitation. Basically, the method consists of establishing an electrostatic potential well in which low-energy electrons, resulting from inelastic collisions, are trapped and subsequently collected with a very high efficiency.

Figure 7 shows a schematic diagram of the tube and the variation of potential along the axis. An electron beam collimated by a magnetic field is accelerated into the collision chamber with voltage $V_A$. The collision chamber consists of two end plates and a grid. A cylindrical (or parallel plane) outer collector surrounds the collision chamber. By applying a positive voltage to this collector, with respect to the collision chamber, an electrostatic well, having a depth $W$ (in volts), can be produced along the axis of the tube.

An electron making an inelastic collision just above the threshold for an inelastic process loses most of its energy and is trapped in the well. It spirals back and forth following the magnetic field lines and eventually makes enough elastic collisions to diffuse across the magnetic field to the trapped-electron collector. At an electron energy that exceeds the threshold of an inelastic process by the amount $W$, the electrons have

enough energy remaining to escape over the potential barrier at the end of the collision chamber, and the trapped-electron current vanishes. Therefore, as a function of accelerating voltage, the trapped-electron current is zero below an inelastic threshold, and then grows to a peak which is proportional to the magnitude of the cross section at an electron energy that exceeds the threshold by $W$.

The well depth can be determined by applying a negative voltage to the trapped-electron collector relative to the collision chamber, thus creating a potential barrier in the path of the electron beam. The shift in the electron-beam retarding curve for different values of the applied voltage measures the size of the barrier, which is the well depth with reversed polarity. Other methods for establishing the well depth also exist.

Using the trapped-electron method, sometimes in conjunction with a modulation of the well depth, it is possible to measure an excitation function for several eV above the onset.

A method very similar in concept to the trapped-electron method is the "$SF_6$ scavenger technique." This technique takes advantage of the fact that $SF_6$ has a very large attachment cross section for zero-energy electrons, and a very small cross section for all other energies. Thus one admixes a small amount of $SF_6$ to the gas under study and whenever an inelastic collision takes place, it leads, near threshold, to zero-energy electrons which promptly attach to $SF_6$. By
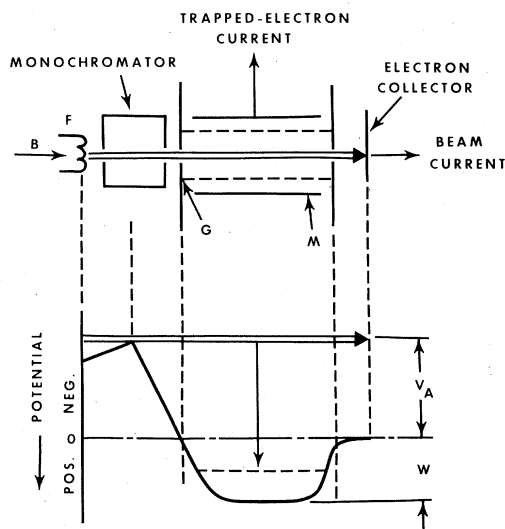


FIG. 7. Schematic diagram of a trapped-electron experiment and potential distribution at the axis of the tube. F is the filament, $P_2$ is the retarding electrode, G is the cylindrical grid forming the collision chamber, M is the cylinder for collection of trapped electrons, E is the electron beam collector, $V_A$ is the accelerating voltage, and W is the depth of the well. The double line in (b) indicates the energy of the electron beam and the arrow indicates the energy lost by an electron in an inelastic collision. The electron energy in the collision chamber is $(V_A+W)$. [From Schulz (1959).]

observing the $SF_6^-$ current using a mass spectrometer, one can obtain information regarding the threshold behavior of inelastic cross sections. Often, the threshold region of inelastic cross sections shows resonance structures.

### Measurement of Cross Sections for Metastable States using Surface Ejection

Measurements of the cross section for production of metastable states can be accomplished with high efficiency if the metastable state to be measured has an internal energy higher than about 10 eV. In this case, one can use for signal detection the ejection of electrons resulting from metastables impinging on a metal surface. Any kind of electron monochromator, magnetic or electrostatic, can be used for producing the monochromatic electron beam. Figure 8 shows a sketch of such an apparatus. If a single metastable state is involved, the current measured on the metastable detector $i_M$ is given by $i_M = i_0 NQL\gamma\alpha$, where $N$ is the gas density, $i_0$ is the current incident on the collision chamber, $L$ is the path length, $\gamma$ is the number of electrons ejected per metastable incident, $\alpha$ is the solid angle subtended by the metastable detector, and $Q$ is the cross section for the particular metastable state. Since atoms may have more than one metastable state (e.g., $2^3S$ and $2^1S$ states for He), and since each metastable state leads to a different $\gamma$, the total curve is not easy to interpret. However, structure in the total metastable cross section is often very pronounced. Examples of such curves are shown in the text.

### Measurement of Optical Excitation Cross Sections

Since resonances can be detected in any decay channel it is obvious that the excitation cross sections to any of the radiating states of atoms should also exhibit structure resulting from resonances. Any kind of monochromator which gives a sufficiently narrow electron energy distribution in conjunction with a sufficiently high electron current is acceptable for such experiments. This type of measurement is particularly suitable for detecting resonances at higher energies, e.g., a few eV below the ionization potential.

Measurements of the optical excitation functions using narrow electron energy distributions are just now receiving attention and a complete analysis of the observed structures is not yet available. Thus this review cannot do justice to this interesting experimental field, but one can anticipate interesting results in the near future.

### Measurement of Positive Ions

Resonances can lie above the ionization potential of the atom. Such resonances can be studied by the methods previously outlined. However, it is now known that such resonances can decay by two-electron emission, yielding a positive ion. It was actually the use of
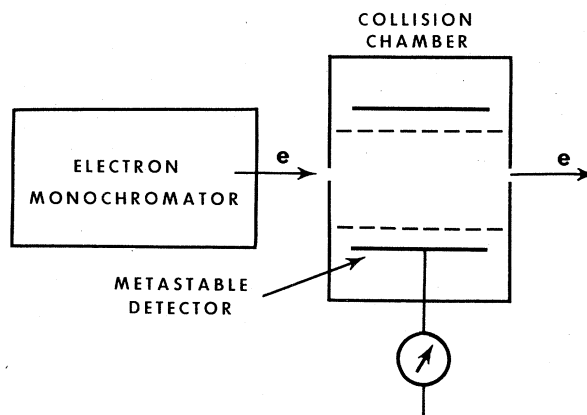


FIG. 8. Schematic diagram of an apparatus for study of metastable excitation by surface ejection of electrons.

the trapped-electron method which established this type of decay (see Sec. IIIC). If one examines the positive ion cross section very carefully, one can observe the resonances lying above the ionization threshold. As described in Sec. IIIC, such measurement must use sophisticated signal accumulation techniques, since the structure in the positive ion cross section is super-imposed on a large monotonically varying background resulting from "direct" ionization. This background signal can be subtracted by use of electronic methods.

When measuring structure in positive ion cross sections, one must be careful to distinguish between "resonances", i.e., temporary negative ions and states of the neutral atom which lie above the ionization potential ("autoionizing states"). Both of these types of states can cause structure in the positive ion cross section.

### Electron-Energy Distributions in Fast Neutral–Neutral Collisions

It has been pointed out by Barker and Berry (1966) that the electron energy distribution of the electrons resulting from collisions of fast neutral atoms could be used for detecting "resonances." The reaction leading to the detection of resonances is of the type

$$He(1s^2) + He(1s^2) \rightarrow He^-(1s2s^2) + He^+(1s)$$
$$\rightarrow He(1s^2) + He^+(1s) + e.$$
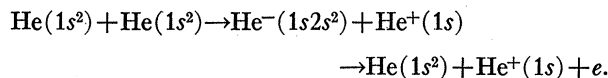
The electrons in the above reaction result from the decay of the $1s2s^2$ resonance and cause interference with electrons produced directly. Thus, structure in the electron energy distribution can be observed.

Actually, pronounced peaks consistent with the above reaction have been observed by Barker and Berry (1966) and by Schowengerdt, Smart, and Rudd (1973), in the energy range up to 150 keV.

However, no new information regarding the location or width of resonances has been generated with this method up to the present time, and thus no further use

can yet be made of this phenomenon. Nevertheless, the reaction itself appears to be of interest to the understanding of electron exchange in neutral–neutral collisions.

### Electron-Energy Distribution in Fast Ion–Neutral Collisions

Fast ion–neutral collisions also lead to electron ejection which can be associated with resonances. When a stable negative ion collides with a neutral atom, the outer electron in the negative ion can be promoted to a resonance state. A peak in the energy distribution of ejected electrons occurs at the energy of the resonance. The results of such an experiment, involving $O^-$ ions, are discussed in Sec. VII.

It is conceivable that the impact of fast positive ions on neutral atoms also could yield electrons associated with resonances. This process would involve electron-exchange, similar to that in neutral–neutral collisions.

### Calibration of Energy Scales

Any discussion of new methods of measurement in the field of electron impact on atoms and molecules must point out the really significant progress which has been made in the past ten years or so in our ability to calibrate the electron energy scale accurately. Usually, the "primary" standard is a known ionization potential or an excitation potential. Important resonances are calibrated against such a standard. The resonances, in turn, can be used as "secondary" standards if they have a natural width which is narrow compared to the electron energy spread. Such a calibration can be performed to an accuracy of ±0.03 or ±0.05 eV, although in some cases even lower values are quoted.

## II. HYDROGEN

From the theoretical viewpoint atomic hydrogen is obviously the simplest system for the calculation of resonances, but measurements in atomic hydrogen are difficult. The combination of establishing a monochromatic electron beam and a source of atomic hydrogen in an experiment proved to be elusive for many years. Thus, it is not surprising that the first indication of resonances in the scattering of electrons by atomic hydrogen came from theoretical work (Burke and Schey, 1962) and the lowest state was identified as $^1S$, lying about 0.6 eV below the $n=2$ state of hydrogen. Since that discovery many determinations using a variety of theoretical methods have been made of the resonant energies.

The position of resonant energies can be evaluated by variational methods as eigenvalues of the Hamiltonian with the open channel projected out. The results thus obtained are approximations to the actual physical resonances in that the shift resulting from the coupling to the neighboring continuum is not included, and the finite width of the state is not considered.

It turns out, however, that the actual shifts are small so that the variational calculations give a close indication of the position of the compound-state energy levels. This can be ascertained from Appendix I, where the results of the variational calculations are indicated by the appropriate symbol.

The position of resonant energies can also be determined by calculating the elastic or inelastic cross section for scattering of electrons with a very fine mesh of incident energies. In such a calculation, the existence of the resonance is exhibited by rapid transit of the phase shift through $\pi$ radians in the vicinity of the compound state. From the variation of the phase shift, one can determine the position and width of the resonance and thus obtain a more complete description of the resonant behavior. The rapid transit of the phase shift through $\pi$ radians is reflected in the behavior of the cross section by the appearance of sharp structure. To calculate the cross section, one must include several states of the target atom. For low-lying levels in hydrogen, it has been shown that it is sufficient to include the three lowest states of the atom in the close-coupling calculation (cc). As a next step, one can do close-coupling calculations with correlations included (ccc). For some calculations it has been found desirable to include six states of the target atom in the calculations (6-state).

Appendix I lists the results of various calculations for the energy and the width of resonances below the $n=2$ threshold. An energy level diagram is shown in Fig. 9. Here, only a single set of energy levels is shown, extending up to the $n=3$ threshold. Of the values listed in Appendix I, it is expected that the most accurate ones are those using an expansion of the wave function in terms of the $1s$, $2s$, $2p$ states of the target, together with up to 20 correlation terms. The results thus obtained are marked (ccc) in Appendix I, following the notation of Burke (1968). The values marked (cc) in Appendix I are obtained by Burke using the $1S$, $2S$, $2P$ states of the target atom in a close coupling expansion. The agreement between the values obtained (cc and ccc) gives confidence that the three-state close-coupling results are reliable. In fact, the good agreement between Burke's values and the values obtained by other investigators is remarkable.

Alternately, one can use the pseudo-state method (ps. st.) developed by Burke, Gallaher, and Geltman (1969) in which the first few states included are atomic eigenstates while higher bound and continuum states are represented by pseudo-states chosen to be orthogonal. The results of these calculations are marked (ps. st.) in Appendix I.

The theoretical values shown in Fig. 9 are those obtained by Burke using the close coupling plus correlation method (ccc). Above the lowest two levels, $^1S$ and $^3P$, and below the $n=2$ threshold of H, there are shown a number of states which converge to the $n=2$ limit. It has been pointed out by Gailitis and Damburg (1963) that the degenerate dipole coupling between the $2S$ and
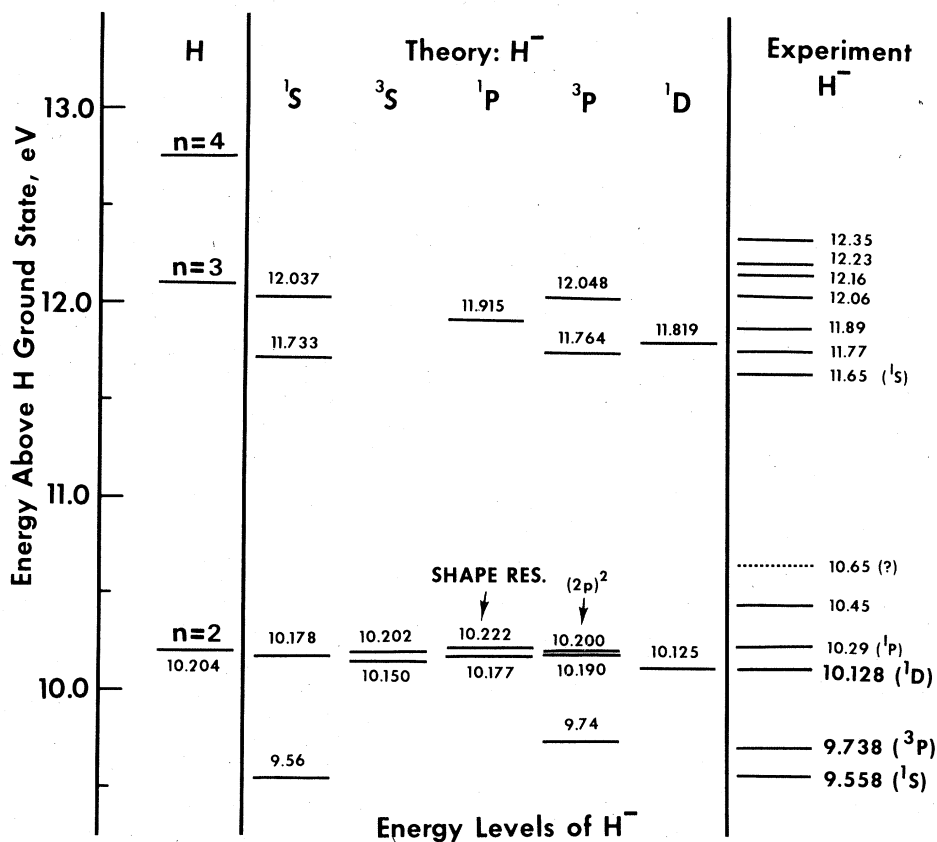
FIG. 9. Energy level diagram for compound states in atomic hydrogen, constructed from the results of theory and experiment. The theoretical values are taken from Burke (1968). Values below the $n=2$ level are also listed in Appendix I (marked ccc) in comparison with other results. The experimental values listed in the figure are those of Sanche and Burrow (1972) for the lowest three resonances and of McGowan et al. (1965, 1969) for the remainder.

**H**     **Theory: H⁻**     **Experiment H⁻**

Energy Above H Ground State, eV

Energy Levels of H⁻

---

$2P$ states of hydrogen produces, at large distances, an $r^{-2}$ potential. This potential is sufficiently attractive to support an infinite number of bound states $(S, P, D)$ in the absence of coupling to the ground state of hydrogen.

The state marked $(2p)^2$ in Fig. 9 is a $^3P$ state, but with even parity whereas all the other states in the $^3P$ column are of odd parity. If LS coupling is a good approximation, the $(2p)^2$ state does not participate in elastic scattering, nor does it decay to the ground state. The value quoted for the $(2p)^2$ state has been calculated by Drake (1970) by Holøien (1960).

Just above the $n=2$ state of hydrogen, Taylor and Burke (1967) find a core-excited shape resonance $^1P$. Using a three-state plus twenty correlation term approximation, the energy is found to be 10.22204 eV and the width $\Gamma = 0.0151$ eV. This width is unusually narrow for a shape resonance. As is common for shape resonances, the mechanism for the $^1P$ resonance is provided by the angular momentum barrier, together with the short-range nuclear attraction. Because the resonance lies so close to the $n=2$ state, the barrier is very thick, and the penetrability very low. As pointed out in Sec. I, such circumstances lead to a narrow width. The existence of such a resonance close to the threshold of an inelastic process dominates the behavior of the inelastic cross section near threshold.

The tabulated data of Taylor and Burke (1967)

show that the $^1P$ resonance exhibits itself by a peak in the elastic cross section near 10.222 eV. This peak, being only 1.3% of the elastic cross section would be difficult to observe experimentally. Nevertheless, this peak in the elastic cross section provides an example of the decay of a core-excited shape resonance into the elastic decay channel.

The six higher states of H⁻ (near $n=3$) shown in Fig. 9 are the result of a close-coupling calculation involving the $1s$, $2s$, $2p$, $3s$, $3p$, and $3d$ states (Burke et al., 1966, 1967). The energies and the widths for these states have been obtained by Macek and Burke (1967) and are also discussed by Burke (1968).

## A. Resonances in the Elastic Cross Section

As previously mentioned, experiments with monochromatic electrons in atomic hydrogen are among the most difficult. The first confirmation of the theoretical considerations was the experiment of Schulz (1964a) who found a peak in the unscattered electron current transmitted through atomic hydrogen at an electron energy of $9.70 \pm 0.15$ eV. For various technical reasons, the electron energy distribution in this early experiment was insufficient to resolve the $^1S$ and the $^3P$ resonances. Very recently, Sanche and Burrow (1972) succeeded in resolving these states in a transmission experiment which uses many improvements developed
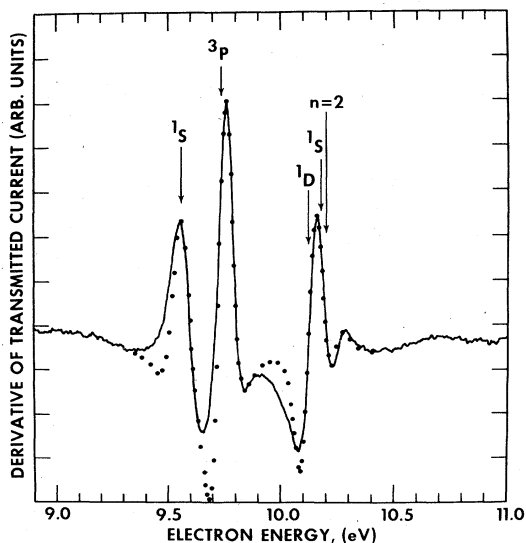
FIG. 10. Derivative of the transmitted current vs electron energy in atomic hydrogen. The experimental results are shown by the solid line. The points are the best fit that can be obtained from the theoretical shape of the cross section, but leaving the energies and the widths of the resonances as parameters. The computer program which is used for obtaining these points includes Doppler broadening and approximates the electron energy distribution by a Gaussian function with a half-width of 70 meV. The energies and widths which give the best fit to the experiment are listed in Appendix I. The arrows point to the energies of the major resonances obtained using close coupling plus correlation. [From Sanche and Burrow (1972).]

over the past few years: A trochoidal monochromator is used and the electron energy in the collision chamber modulated in a manner similar to that introduced by Sanche and Schulz (1972). A plot of the derivative of the transmitted current (which is the primary measurement in this type of experiment) vs electron energy is shown by the solid line in Fig. 10. The energies of several compound states (taken from the theoretical calculations cited in Fig. 9) are also shown in Fig. 10. The points in Fig. 10 are calculated from theory in the following manner: Sanche and Burrow (1972) take the theoretical values of the nonresonant phase shifts which are believed to be "exact" and use the energies and widths of the resonances in single-level Breit–Wigner formulas as parameters. They fold these results with a Gaussian electron energy distribution of appropriate width (70 meV), and include Doppler broadening. Then they calculate the derivative of the transmitted current. The values for energies and widths of the resonances which give the best agreement with experiment are listed in Appendix I and the derivative of the transmitted current vs electron energy which is obtained when these optimum values are used is shown by the points in Fig. 10. This experiment therefore shows that the theory using close-coupling plus correlation (ccc) is in agreement with experiment.

Kleinpoppen and Raible (1965) performed a crossed-beam experiment and found a decrease in the cross section (which corresponds to an increase in transmitted

current) at an electron energy of 9.73±0.12 eV, as shown in Fig. 11. In addition, less pronounced structure around 10.1 eV was observed by Kleinpoppen and Raible, but was not discussed in their paper, probably because the authors did not consider it a sufficiently reliable observation. However, it is clear from Fig. 10 that such structure around 10.1 eV is expected to be visible.

The third experiment bearing on the subject of experimental observation of resonances below the $n=2$ threshold of hydrogen was performed by McGowan, Clarke, and Curley (1965) and their results are shown in Fig. 12. At first sight, this experiment shows little resemblance to the results of Kleinpoppen and Raible. However, McGowan (1966, 1967) points out that there is a strong variation of the differential cross section with angle: The interference between the potential and the resonant scattering causes the structure of the differential elastic cross section to depend strongly on the angle of observation. In order to demonstrate this effect, McGowan (1966) calculated the differential elastic scattering cross section in the region of the resonances, at selected angles of observation. Figure 13 shows the results of these calculations in comparison with some experiments. The experimental results of Kleinpoppen and Raible (taken at 94°) resemble the shape of the theoretical curve for $\theta = 100°$. The experimental data of McGowan, Clarke, and Curley resemble the theoretical curve at 90°, as shown on the bottom left-hand portion of Fig. 13. A more detailed comparison is shown in Fig. 14. Here, the width of the $^1S$ resonance is left as a parameter. The best fit to experiment is obtained when the width of the $^1S$ resonance is taken to be 0.043±0.006 eV, in good agreement with the value of 0.0475 eV given by Burke.

The sharp hump observed just below the $n=2$ level of hydrogen in Fig. 12 can be ascribed to the effect of the $^1D$ state (Ormonde, McEwen, and McGowan, 1969). Figure 15 shows a detailed comparison between theory and experiment in the region 9.9–10.2 eV,
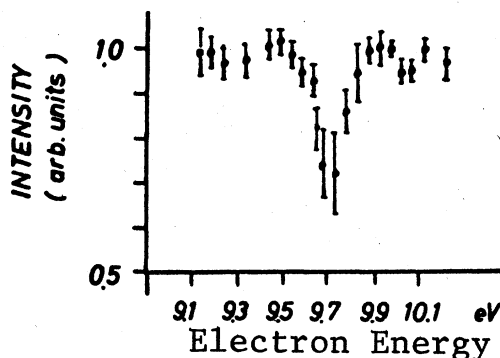


FIG. 11. Elastic cross section for electrons on atomic hydrogen. The angle of observation was 94°, and the width of the energy distribution about 0.1 eV. [From Kleinpoppen and Raible (1965).]

FIG. 12. Differential scattering cross section in hydrogen. The angle of observation is 90° with respect to the bombarding electrons. The position of the three lowest resonances, $^1S$, $^3P$, and $^1D$, are shown. [From McGowan, Clarke, and Curley (1965) and McGowan (1970).]
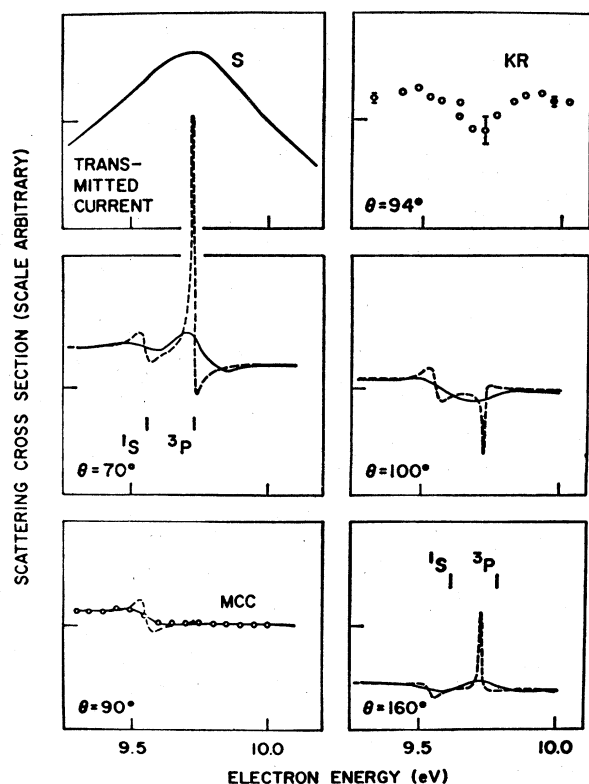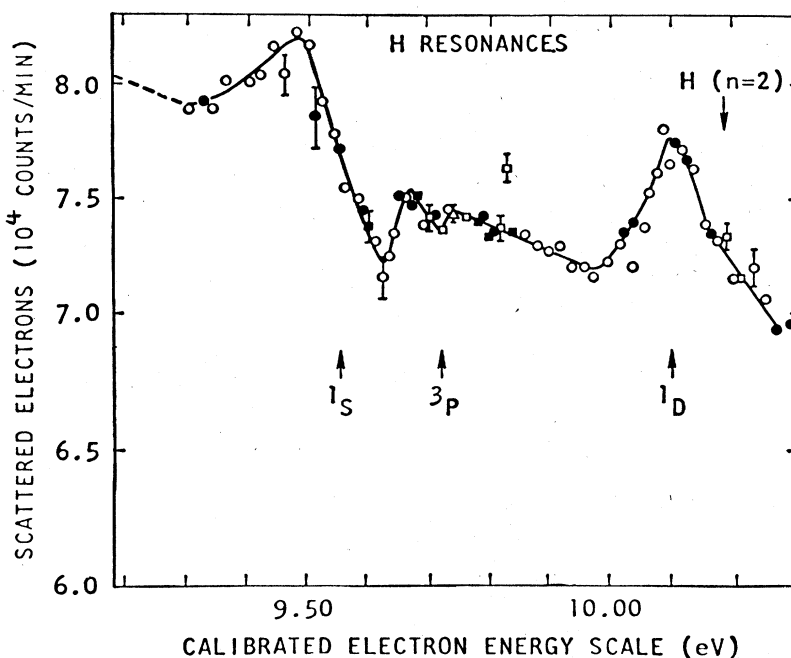


FIG. 13. The experimental results of Schulz (S), Kleinpoppen and Raible (KR), and McGowan, Clarke, and Curley (MCC) compared with the differential scattering calculations of McGowan (1966, 1967) for different scattering angles $\theta$. The dashed line corresponds to the calculated cross section for an angular window of 15°. The position of the $^1S$ resonance is taken to be 9.56 eV and its width 0.04 eV. The $^3P$ resonance is taken to be at 9.73 eV with a width of 0.01 eV. The solid line represents the same calculation with the experimental value of the electron energy distribution (0.06 eV) folded in. [From McGowan (1966).]

when the $^1D$ state alone is considered. The agreement in Fig. 15 must be, presumably, considered fortuitous because a valid comparison between theory and experiment must also include the $S$, $P$, and $^3D$ contributions. For a comparison at 90°, such as is the case for McGowan's experiment, the $P$-wave contribution to the cross section should be zero. Figure 16 shows the valid comparison between theory and experiment. The $^1D$ compound state of $H^-$ seems to be the dominant contribution near 10.1 eV.

It is clear from the work of McGowan that experiments on the angular distribution of electrons in the neighborhood of the $^1S$ and $^3P$ resonances in hydrogen are strongly dependent on the angle of observation and on the acceptance angle of the apparatus. Further work with much better angular resolution will be necessary before a really satisfactory check of the very elaborate theory can be made.

## B. Resonances in the Inelastic Cross Sections

Resonances lying above the $n=2$ state of hydrogen seem to be most pronounced in the inelastic cross section. Figure 17 shows the cross section in the $2p$ excitation from threshold to about 3 eV above threshold. Structure in the cross section is evident and the location of this structure is transposed onto the energy level diagram, Fig. 9. Also shown in Fig. 17 are the theoretical curves. The sharp onset of the $2p$ excitation cross section results from the proximity of the $^1P$ shape resonance, which is almost coincident with the $n=2$ level. This sharp peak near threshold seems to be consistent with the earlier experimental results of Chamberlain, Smith, and Heddle (1964) which were obtained
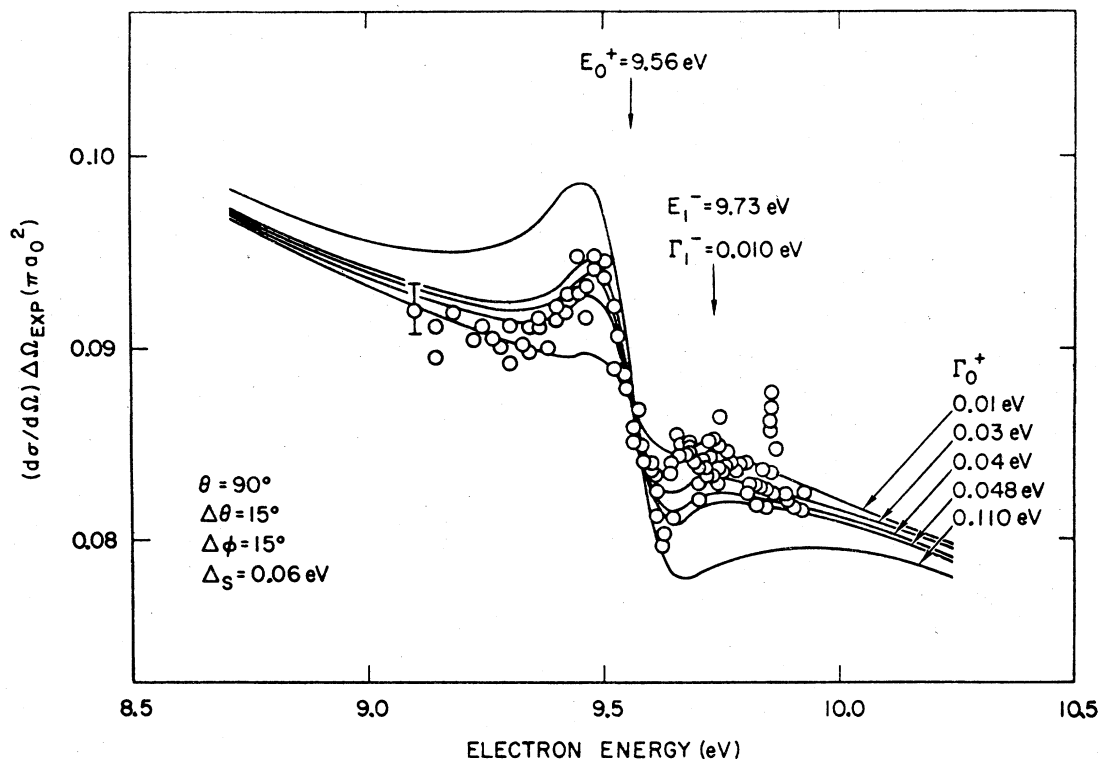
FIG. 14. Comparison between experimental and calculated cross sections in the region of the $^1S$ and $^3P$ resonances in hydrogen. The positions of the two resonances are fixed at 9.56 and 9.73 eV, respectively, and the width, $\Gamma_0^+$ of the $^1S$ resonance is varied from 0.01 to 0.110 eV. The best fit to the experimental data, indicated by the circles, is obtained when $\Gamma_0^+ = 0.043 \pm 0.006$ eV. [From McGowan (1967).]

with a broader electron energy spread. Also, the sharp peak near threshold is consistent with theory.

Two subsidiary peaks in the experimental curve shown in Fig. 17 occur at $10.45 \pm 0.03$ eV and at $10.65 \pm 0.03$ eV, i.e., just above the $n=2$ state of hydrogen. According to McGowan et al. (1969), the first of these is statistically real and the second is not. McGowan et al. argue that the 10.45-eV peak may be an interference effect of the first resonance, as calculated by Marriott and Rotenberg (1968), or another shape resonance. Geltman and Burke (1970) used the pseudo-state expansion theory in an attempt to confirm the experimental structure near 10.45 and 10.65 eV. Their theory, however, shows no signs of the experimental structures and shows a smooth behavior in this energy range. It should be remarked that the pseudo-state expansion theory has achieved measures of success, notably in calculating the ratio of excitation cross sections $\sigma(1s-2s)/\sigma(1s-2p)$ in remarkably good agreement with the experiment of Ott, Kauppila, and Fite (1970).

Below the $n=3$ state of hydrogen, a number of resonances appear in both the experimental and theoretical curves of Fig. 17. For the lowest $^1S$ resonance, agreement exists between theory and experiment as to position and width. The dominant feature of the theory

below the $n=3$ threshold is the $^1D$ resonance near 11.8 eV, but the dominant feature of the experimental curve appears about 0.1 eV higher. McGowan et al. (1969) argue that the theory is insufficient to predict the position of the $^1D$ resonance accurately and that more states need to be included in the theory to give the proper position for the $^1D$ resonance. Thus it may be more desirable to correlate the "dominant" features of experiment and theory.

The broad maximum in Fig. 17 just above the $n=3$ threshold appears to be a core-excited shape resonance (McGowan et al., 1969).

### C. A Resonance Involving $H^{--}$

Electron impact experiments on neutral atoms cannot give information on the possibility of the existence of resonances which involve doubly charged negative ions, e.g., $H^{--}$. In order to gain such evidence, one has to perform experiments in which electrons collide with negative ions. Such an experiment has recently been reported by Walton, Peart, and Dolder (1970). They studied the reaction $e + H^- \rightarrow H + 2e$ in a beam experiment; their results are shown in Fig. 18. Noteworthy is the sharp structure appearing near 14.5 eV, which Walton et al. (1970) attribute to a state of $H^{--}$, with a lifetime of about $10^{-15}$ sec.

Taylor and Thomas (1972) calculated the position and designation of the state responsible for the experimental structure, using the stabilization method which is described in detail by Taylor (1970) and by Hazi and Taylor (1970). Taylor and Thomas (1972) find that a short-lived resonant state, $H^{- -}$, with a configuration principally $(2s)^2 2p\ ^2P^0$ and an admixture of $(2p)^3$, exists at an energy of 14.8 eV and that its width can be estimated to be about 1 eV. The calculated energy and the lifetime are in good agreement with the experiment of Walton *et al.* (1970). Taylor and Thomas further point out that they find another resonance with a largely $(2p)^3$ wave function at some higher, unspecified energy.

The geometric structure of the $H^{- -}$ ion has been studied by Herzenberg and Ton-That (1973). They suggest that the only geometry which can lead to a quasistationary state must have all three electrons located at about the *same distance from the proton*, near the corners of an equilateral triangle. Then all three electrons comprising the $H^{- -}$ ion are attracted to the proton. By minimizing the expectation value of the Hamiltonian with respect to parameter controlling the



FIG. 16. Comparison of experimental and theoretical cross sections in the energy range 10.0–10.2 eV, for 90° scattering in atomic hydrogen. The theory (close-coupling) includes the $^1D$ and $^1S$ resonances as well as the $^{1,3}S$ and $^{1,3}D$ background phase shifts. The theoretical results are averaged over a 15° cone and folded with the experimental beam width. The absolute scale for the experimental points is obtained by normalizing the measured differential cross section in the region below the lowest $^1S$ resonance to the calculated cross section in that region. [From Ormonde, McEwen, and McGowan (1969).]
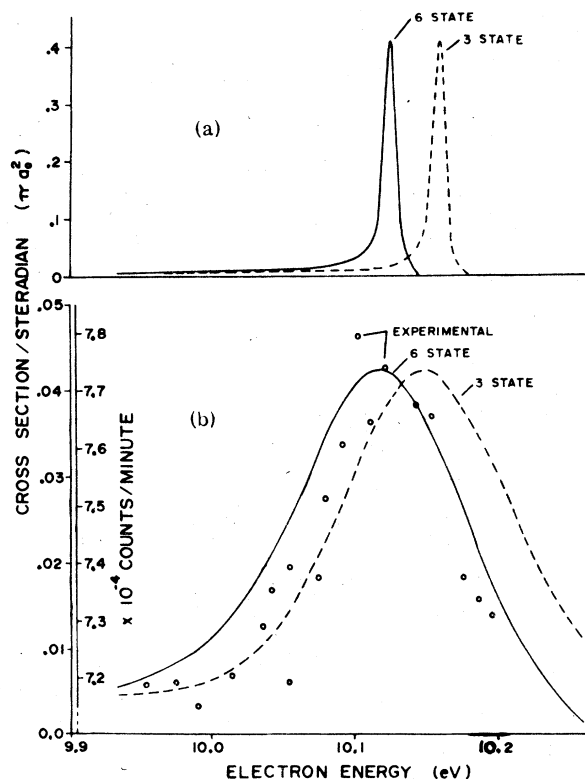


FIG. 15. (a) Close-coupling $^1D$ cross sections over the resonance region. (b) $^1D$ cross sections folded with the resolution of the experimental electron beam. The theoretical calculations correspond to the left-most scale, and the experimental points to the scale on the right. Because the measurements are relative, the results are displayed as shown in order to emphasize the agreement in shape between theory and experiment. [From Ormonde, McEwen, and McGowan (1969).]
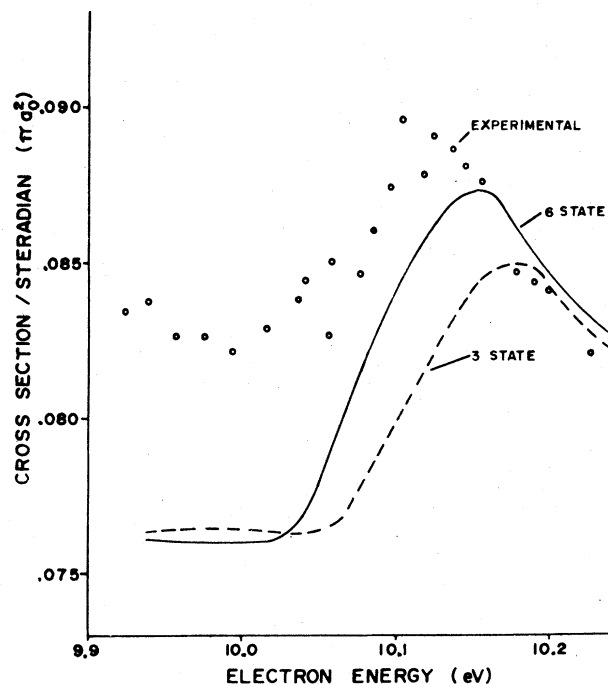
radial distance of the electrons from the proton and the angles between the electrons, they find a quasistationary state. Their value for the energy of this state is 11.9 eV (compared to 14.5 eV for the experimental value quoted above) and a lower limit for the width is $\Gamma > 0.3$ eV. The contribution of the $s^2p$ configuration is 87%, that of the $p^3$ configuration is 10%.

Herzenberg and Ton-That also find an analogous state in $He^-$, at an energy of 45.9 eV, with all three electrons equidistant from the nucleus. This state could provide an interpretation for the broad resonance around 50 eV (see Sec. IIIC) observed in helium by Crooks *et al.* (1972).

Other doubly charged negatives have recently been observed using mass spectrometry (Baumann *et al.*, 1971). In this experiment, negative ions are formed in a Penning source. Electric and magnetic deflection experiments confirm that doubly charged negative ions are present in the beam. The ions which have been identified are $O^{- -}$, $Te^{- -}$, $Bi^{- -}$, $F^{- -}$, $Cl^{- -}$, $Br^{- -}$, and $I^{- -}$. The lifetime of the above ions must be relatively long in order for them to survive their trip through the mass spectrometer ($\sim 10^{-6}$–$10^{-7}$ sec). This is in contrast to $H^{- -}$, for which the lifetime is about $10^{-15}$ sec. Fano (private communication) suggests that a plausible
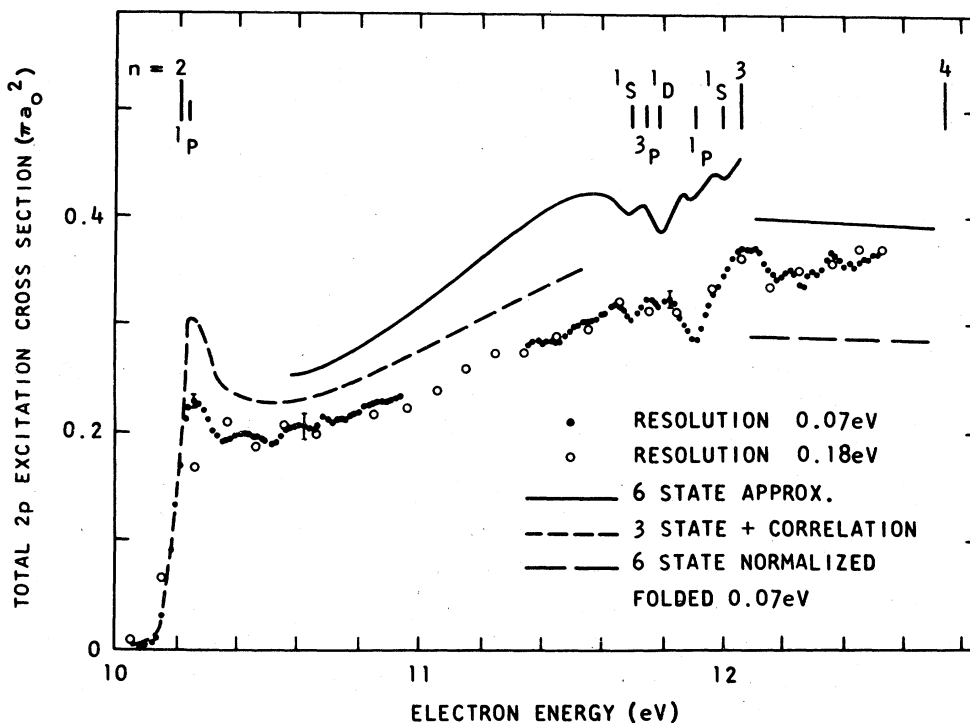
FIG. 17. Total $2p$ excitation cross section in hydrogen. The high-resolution experimental data indicated by the closed points were obtained with an energy spread of 70 meV and the low-resolution data, indicated by the open circles, were obtained with an energy spread of 180 meV. The experimental data are from McGowan, Williams, and Curley (1969). The cross section is plotted on an absolute scale, referenced to the values of Long, Cox, and Smith (1968). Also shown is the "six-state close-coupling" theory of Burke et al. (1967) and the "three-state close-coupling plus electron correlation" theory of Taylor and Burke (1967), into which the experimental resolution (70 meV) has been folded. [From McGowan, Williams, and Curley (1969).]

explanation for these long-lived negative ions could be a sextet of the type $3p^4(^3P)4s4p^2$ for $Cl^{--}$ and a configuration $2p^3(^4S)3s3p^2$ for $O^{--}$. The energy of these levels is not known.

## III. HELIUM

As we review the field of resonances and go from atomic hydrogen to helium, the most striking effect is the decrease in theoretical effort and the increase in experimental effort. Thus the guidance for classifying the structures found by experimentalists is not too extensive, and experiments usually precede theory. In fact, much of the classification has been obtained from experimentally measured angular distribution. The experiments performed to date have analyzed structures in the $2^3S$, $2^1S$, $2^3P$, and $2^1P$ cross sections as well as in the total elastic and total metastable cross section.

The discovery of resonances in atoms came from measurements of the structure in the elastic cross section, as shown in Fig. 19. This type of experiment, especially when it is coupled with a measurement of angular distributions (Fig. 20), gives a great deal of information regarding the width, symmetry, and shape of the resonance, especially for resonances lying below the first electronically excited state of the atom.

For resonances lying above the first electronically excited state, as in the case of core-excited shape

resonances associated with $n=2$ and higher-lying states, it is advantageous to study structures in the electronically excited states, such as $2^3S$, $2^1S$, $2^3P$, $2^1P$, etc. The decay into these final states is usually preferred.

For an overview of all the sharp resonances occurring by electron impact, it is advantageous to use a transmission experiment. These types of experiments, pioneered by Kuyatt, Simpson, and Mielczarek (1965), can be made very sensitive to sharp structures in the cross section by modulating the electron energy and thus performing a differentiation of the transmitted electron current with respect to energy. Such experiments have been performed for all rare gases by Sanche and Schulz (1972). A sample of their data for helium is shown in Fig. 21. The advantage of this type of experiment is the overview of the location of resonances on the energy scale. The disadvantage lies in the limited information: One generally cannot deduce the symmetry, the width, or the exact shape. Nor is it possible to observe broad resonances (e.g., shape resonances) very clearly. Various elastic and inelastic cross sections must be measured at different angles of observation to fill out the picture.

As an aid to the subsequent discussion, Fig. 22 shows an energy level diagram of the lowest states of neutral He and the position of resonances, as observed by

various investigators, both experimentally and theo-
retically. The solid horizontal lines indicate those
resonances which seem well established at the present
time.

## A. Classification of Energy Levels in He

It has already been pointed out that the levels of the
compound states in helium and other gases arise from
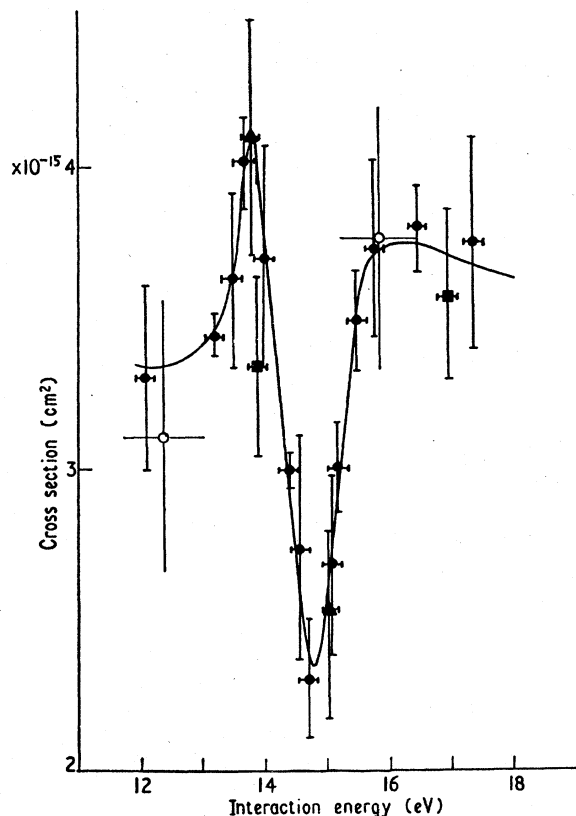the addition of an electron to a particular excited state



FIG. 18. Cross sections for detachment from H⁻ by electron
impact. The symbols ■, ●, and ▲, respectively, refer to measure-
ments with inclined beams in which the ion beam laboratory
energies were 7, 8, and 10 keV. The open circles denote earlier
measurements by Peart *et al.* (1970). Estimates of energy resolu-
tion and 90% confidence limits of random error are shown for
each point. [From Walton, Peart, and Dolder (1970).]

of the atom. The resulting state lies, for the case of
Feshbach resonances (also called "closed channel"
and core-excited resonances), below the energy level
of the parent. Thus one can think of these states as
negative ions with a definite electron affinity, in the
range of about 1/2 eV. It is also possible for the com-
pound state to lie *at* the energy of the parent state
("virtual states") or *above* the parent state, by up to
3 eV. Thus one can list all the relevant configurations
which can be derived from an excited state of helium,
plus an additional electron. From the lowest states of
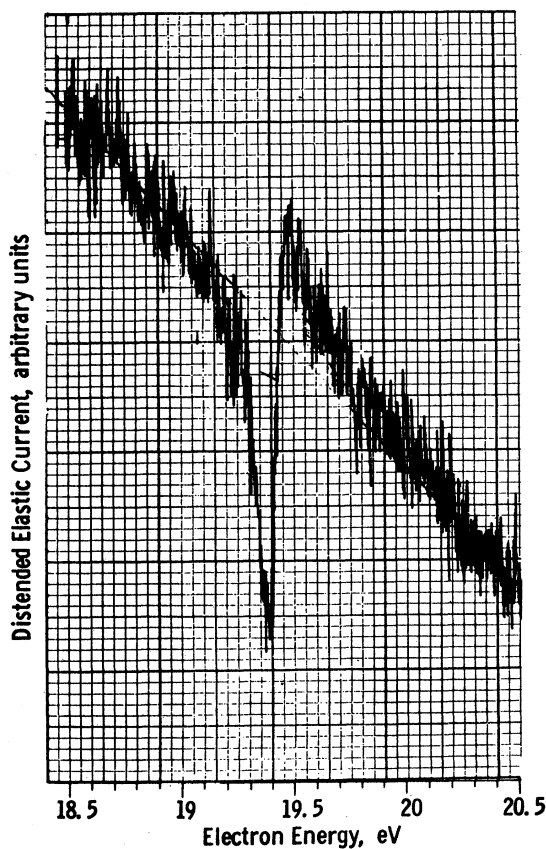helium, $1s2s$ and $1s2p$, we can write the states listed in



FIG. 19. The original observation of the $(1s2s^2)$ $^2S$ resonance
in helium. The angle of observation is 72° and the elastic cross
section is measured. The decrease in the cross section near 19.3 eV
is approximately 14%. [From Schulz (1963).]

Table I. The superscripts designate states of odd and
even parity. The $2s2p$ configuration can lead to $^3P$ and
$^1P$ states. The addition of a $1s$ electron to this term
results in two distinct $^2P$ states of different energy for
the $1s2s2p$ configuration. One of these states has spins
of the outer electrons parallel ($^2P_{\uparrow\uparrow}$), the other anti-
parallel ($^2P_{\uparrow\downarrow}$). The "parents" of these two states are
the $(2s2p)^3P$ and $(2s2p)^1P$ states, respectively.

The $(2p)^2$ configuration, being composed of two
equivalent electrons, results in $^1S$, $^3P$, and $^1D$ states.

TABLE I. Possible states of He⁻.

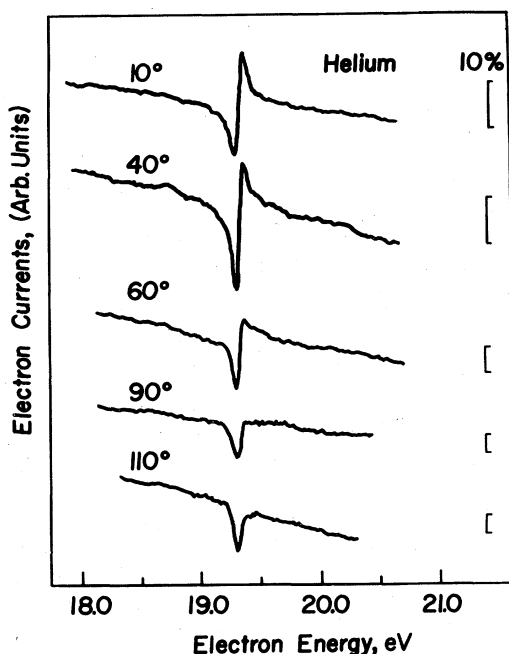| | Outer electrons equivalent | Additional states for nonequivalent electrons (unlikely) |
|---|---|---|
| $1s2s^2$ | $^2S^e_{\uparrow\downarrow}$ | $^2S^e_{\uparrow\uparrow}$ |
| $1s2s2p$ | $^2P^o_{\uparrow\uparrow}$, $^2P^o_{\uparrow\downarrow}$, $^4P^o$ | ... |
| $1s2p^2$ | $^2S^e_{\uparrow\downarrow}$, $^2D_{\uparrow\downarrow}$, $^2P^e$, $^4P$ | $^2S^e_{\uparrow\uparrow}$, $^2P^e$, $^2D^e_{\uparrow\uparrow}$ |

FIG. 20. The appearance of the $(1s2s^2)$ $^2S$ resonance in helium at different angles of observation. The vertical lines indicate a 10% change in the differential elastic cross section. [From Andrick and Ehrhardt (1966).]

Adding a $1s$ electron, we obtain $^2S$, $^2P$, $^4P$, and $^2D$ states. These are the only allowed states within the LS coupling scheme, which is expected to be applicable for the case of He⁻.

It was first pointed out by Fano and Cooper (1965) that there are restrictions on the quantum numbers of the compound states that can be reached by the collision of an electron with a ground-state helium atom $(^1S)$. The *parity* and the *total angular momentum quantum* number $J$ of the input channel must be invariant in the collision. They must be conserved for the system $e + \text{He}(^1S)$ and for the system He⁻. The spin quantum number $S$ and the orbital angular momentum quantum number are each individually conserved only insofar as LS coupling is applicable. This should be the case for helium.

We can eliminate all the quartet states in Table I because these would require a spin–flip. Also, we can eliminate, as pointed out by Kuyatt *et al.* (1965) the state $^2P^e$ resulting from the $1s(2p)^2$ configuration. The parity of this state is necessarily *even*. In order to produce this state from $^1S$ state of helium (parity even), the electron must have a parity $(-1)^l$, where $l$ is the orbital angular momentum. In order to produce a $P$ state from an $S$ state, we must have $l=1$, e.g., odd parity. Thus we cannot conserve parity and must
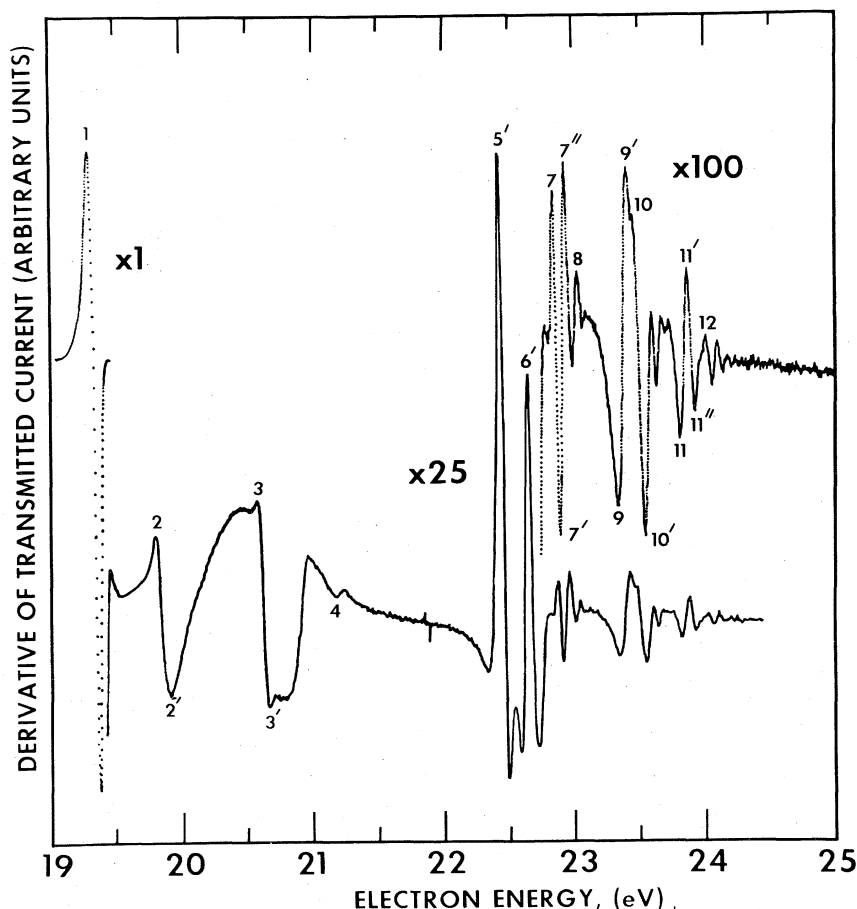


FIG. 21. Derivative of transmitted current vs electron energy in helium, below ionization. The gain of the amplifier is increased by a factor of 25 for the lower portion of the curve and by a factor of 100 for the inset in the upper right, compared to the region around 19.3 eV. The excursion around 19.3 eV corresponds to a change in transmitted current of about 10%. The smaller excursions (e.g., #12) thus correspond to a change in transmitted current of about 0.01%, which is the limit of this transmission experiment. [From Sanche and Schulz (1972).]

FIG. 22. Survey of energy values for resonances in helium. On the left-hand side of the diagram we show the lowest energy levels in He. The names of the authors are indicated above; just below the names we indicate the decay channels in which the resonances are observed. The dots indicate the position at which structures have been observed. Two theoretical columns are also included. Burke *et al.* (1969) calculate the widths of the $^2P$, $^2D$, and $^2F$ resonances and these are indicated by the vertical lines. The full horizontal lines indicate those resonances which seem firmly established. The many extra resonances found by Golden *et al.* (1970), as well as the resonance at 19.45 eV (dashed horizontal line), have been put in doubt by the results of Sanche and Schulz (1972) and must be seriously questioned at the present time. [From Sanche and Schulz (1972).]
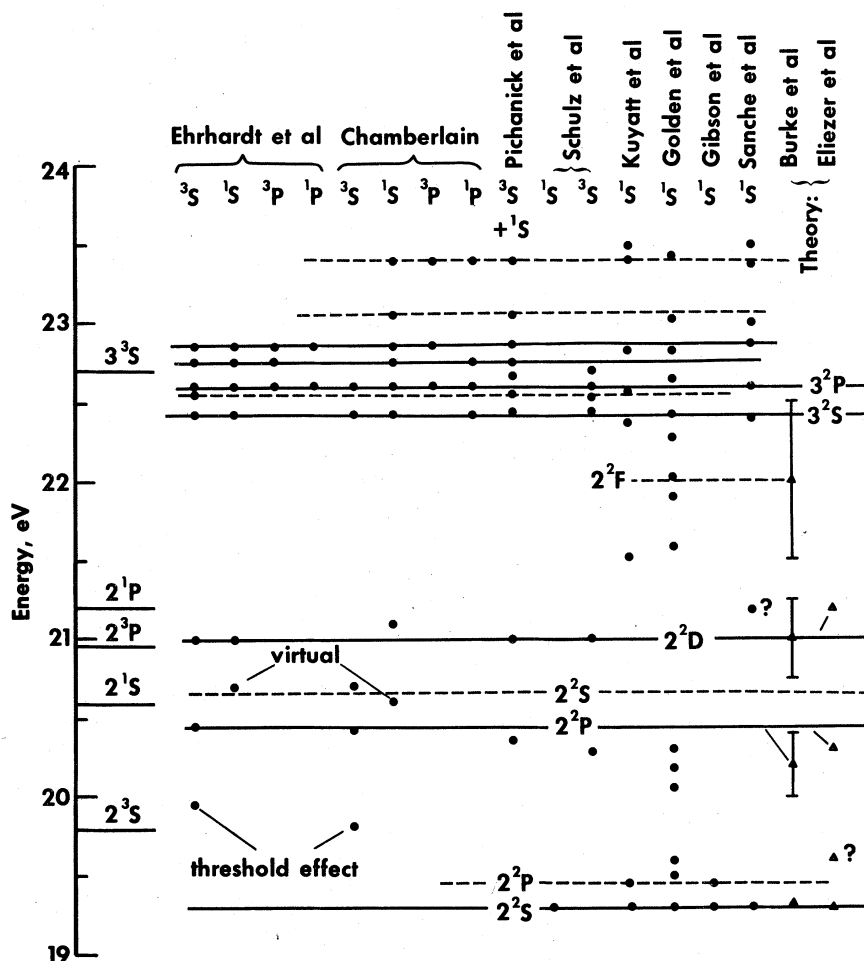
cross out the $^2P^e$ state in Table I. This leaves us with one state from the $1s2s^2$ configuration, $^2S^e$, two states from the $1s2s2p(^2P^0)$ configuration (one with spins in the outer shell parallel, one antiparallel), and two states from the $1s2p^2$ configuration $^2S$ and $^2D$. The total number is 5.

If the electrons in the outer shell are not equivalent, then we have to write $1s2p2p'$, where $2p'$ stands for electrons in an $np$ orbital $(n=2\rightarrow\infty)$ and additional states are possible, as postulated by Golden and Zecca (1970). These additional states are also listed in Table I, although they may not be real possibilities.

## B. Resonances from 19.3 eV to the Ionization Potential

In this section we discuss resonances above the lowest $2^2S$ at 19.34 eV, and list them in a sequence of increasing energy. An attempt is made to establish the reliability of each determination. At the outset it must be stressed that differences in energy which are *less than* the observed width of these resonances (i.e., about 0.05 eV) must be ignored. Resonances can exhibit a different shape, depending on the angle of observation, or the acceptance angle at a fixed angle, or depending on the decay channel in which they are observed. Only a complete analysis involving phase shifts could establish a reliable guide to such differences.

### 1. 19.34 eV $(1s2s^2, {}^2S)$

The resonance occurring near 19.3 eV was the first to be measured experimentally for an atomic system. Although some discrepancies as to the exact energy and width emerged initially, all the experimental values have converged to the region 19.30–19.35 eV. Appendix II lists some of the recent values obtained by experiment and by theory. Figure 19 reproduces the original measurement of this resonance obtained by observation of elastic scattering at an angle of 72 degrees, in a double electrostatic analyzer. Simpson and Fano (1963) confirmed the existence of this resonance and classified it as the $1s(2s)^2 \, {}^2S$ state. Further experimental confirmation came from a Maier–Leibnitz type experiment of Fleming and Higginson (1963). Andrick and Ehrhardt (1966) obtained the angular dependence in the region of 19.3 eV and confirmed that the resonance appears in the $s$-wave. Figure 20 shows that the
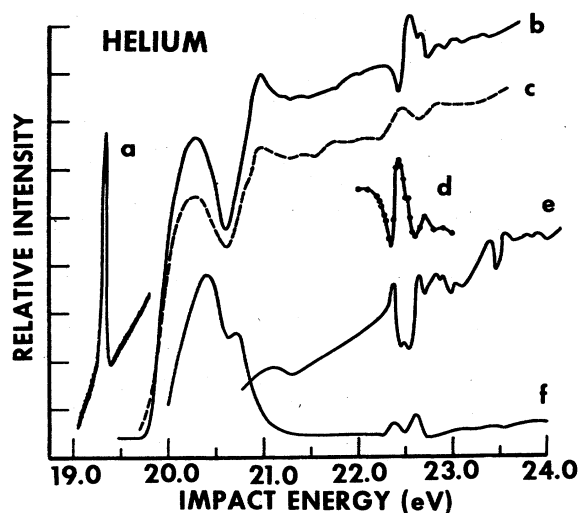
FIG. 23. Comparison of cross sections for production of metastables in helium. (experiments) a—resonance at 19.3 eV observed in a transmission experiment; b—total metastable cross section (Pichanick and Simpson, 1968); c—total metastable cross section (Schulz and Fox, 1957); d—$2^3S$ differential cross section at 72° (Schulz and Philbrick, 1964); e—$2^1S$ differential cross section at 0° (Chamberlain, 1967); f—$2^3S$ differential cross section at 0° (Chamberlain, 1967). [From Pichanick and Simpson (1968).]

resonance can be clearly observed at 90°, at which angle the $p$ wave disappears. An analysis of the phase shift shows that the phase shift of the $s$ wave for potential scattering is 100 degrees, for the $p$ wave 25 degrees, and for the $d$ wave 4 degrees. These phase shifts can be compared with a subsequent study of Gibson and Dolder (1969) who obtained $\eta_0=110°$, $\eta_1=17°$, and $\eta_2=3°$. The agreement with the theory of LaBahn and Callaway (1964) is satisfactory. The variation of the resonance shape with angle is attributed to the interference of the $s$-wave with the other partial curves. Whereas the width of the resonance was estimated by Andrick and Ehrhardt (1966) to be 15–20 meV, more detailed analysis by Gibson and Dolder gives a value of 8 meV for the natural width at half-height, in good agreement with previous estimates. The value of 8 meV for the width of the resonance at 19.3 eV is probably the best experimental value available at this time. Appendix II compares the widths deduced from experiment and from theory. The latest calculations of this width, due to Temkin et al. (1972) and Sinfailam et al. (1972) give values of 14 and 15 meV, respectively.

### 2. 19.45 eV (?)

A small structure was observed by Gibson and Dolder (1969) in the differential elastic cross section just above the $2^2S$ resonance. This structure is most pronounced at an angle of observation of 54.5° and disappears at 90°. The angular distribution is indicative of a resonance in the $p$ wave and we would deduce that the designation of

the state is $(1s2s2p)$ $^2P^0$. The signal-to-noise ratio with which the 19.45 resonance was observed at 54.5° was only unity, and thus this observation alone cannot be considered to be conclusive. However, this resonance was observed at the identical energy in the transmission experiment of Kuyatt, Simpson, and Mielczarek ("peak" at 19.43±0.01 eV, "dip" at 19.47±0.01 eV), but was visible only on the runs with the highest energy resolution. Also, Golden and Zecca (1970) observed structure in their transmission experiment ("peak" at 19.47 eV, "dip" at 19.52 eV). Andrick and Ehrhardt (1966), whose experiment is similar to the experiment of Gibson and Dolder, did not observe the structure at 19.45 eV. Neither did Pavlovic (private communication) observe this resonance in an experiment which was specifically performed to study this resonance. Sanche and Schulz (1972) consider the 19.45 eV resonance a spurious effect resulting from the replication of the $(1s2s^2)$ $^2S$ resonance by electrons which have lost energy on collision with slits.

In their theoretical study, Eliezer and Pan (1970) found a $^2P$ root at 19.6 eV, but it "stabilized rather poorly." The latter authors consider the evidence unconvincing. Burke did not obtain such a state. Neither did Temkin, Bhatia, and Bardsley (1972), who made a purposeful attempt, using their quasi-projection theory, to find states below 19.8 eV. Similarly, Sinfailam and Nesbet (1972) searched for resonances below the $2^3S$ state with a fine mesh using a variational technique which takes polarization and correlation effects into account. They, too, find no evidence for resonances apart from the $^2S$ resonance. Thus we must conclude that the existence of a resonance at 19.45 eV is uncertain and in serious doubt.

### 3. 19.5–20.3 eV

Between 19.5 and 20.3 eV only Golden and Zecca (1970) have observed resonances. These authors observe 4 structures, each exhibiting a peak and a dip. The assignment given to these structures and the energies (in eV) of the peak and the dip are: $(1s2p^2)^2D_{\uparrow\uparrow}$: 19.58/19.62; $(1s2p^2)^2D_{\uparrow\downarrow}$: 20.04/20.10; $(1s2s2p)^2P_{\uparrow}{}^0$: 20.17/20.21; $(1s2p^2)^2S_{\uparrow\uparrow}$: 20.3/20.35. No one else has observed structure attributable to resonances in this energy range (19.5–20.35 eV), although other transmission experiments in fact had a higher sensitivity for observing resonant structures. One would have to invoke some special features of Golden and Zecca's apparatus which would make this particular apparatus more sensitive to the particular resonances in the energy range under discussion. The angular acceptance angle for forward-scattered electrons could possibly be such a feature, but up to now very little attention has been given to such considerations.

Until the structure in this energy range is reproduced by other experiments, one must retain a skeptical attitude regarding the reality of the 4 structures in the

FIG. 24. Energy dependence of $2^3S$ cross section at 0° and 72°. The solid lines are from the close-coupling theory of Burke, Cooper, and Ormonde (1966). The dashed curves are experimental: The 72° data are from Schulz and Philbrick (1964) and the 0° data from Chamberlain and Heideman (1965). The first peak in the cross section curves is attributed to the $^2P$ resonance and the second to the $^2D$ resonance. [From Burke, Cooper, and Ormonde (1966).]
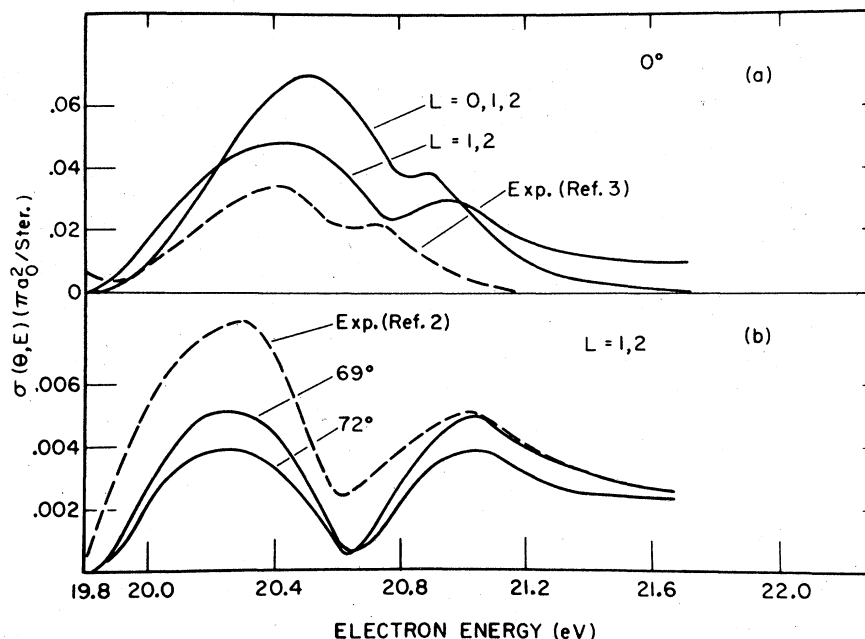
energy range 19.5–20.3 eV. We should note that the last of these structures coincides in energy with the broad $2^2P$ shape resonance discussed in the following section.

### 4. 20.3–20.45 eV ($2^2P$)

The total cross section for excitation of the $2^3S$ state exhibits a maximum at about 0.5 eV above threshold as shown in Fig. 23. It has been pointed out by Baranger and Gerjuoy (1957) that such behavior can best be explained by considering that the inelastic process proceeds via a compound state. By fitting the total $2^3S$ cross section with a Breit–Wigner one-level formula, they obtained a very good fit to the experimental cross section for metastable production ($2^3S+2^1S$) of Schulz and Fox (1957). The parameters that resulted in the best fit located the position of the resonance at 20.2 eV with a width of about 1.0 eV. More detailed theoretical considerations by Burke, Cooper, and Ormonde (1966), using the close-coupling approach, confirmed these ideas. Burke *et al.* found that the major peak of the $2^3S$ cross section occurs within the range of the $p$-wave resonance, which they calculate to occur at 20.2 eV with a width of 0.52 eV. Another smaller peak at the $^2D$ resonance (21.0 eV) is also found in this calculation. These considerations then lead us to associate experimentally determined maxima of the $2^3S$ cross section with the existence of compound states.

If the width of the $p$-wave resonance is anywhere near the value quoted by Burke *et al.* (0.52 eV), it is not surprising that the observed location of this maximum varies depending on angle and the mode of observation. Whereas the total $2^3S$ cross section peaks at 20.3–20.35 eV, (see, for example, Schulz and Fox, 1957; Pichanick

and Simpson, 1968) the differential cross section peaks near 20.45 eV (Chamberlain, 1967; Ehrhardt and Willmann, 1967; Ehrhardt, Langhans, and Linder, 1968). It is doubtful that this discrepancy, of the order of 100 meV, is instrumental. In fact, the "shifting" of the peak is dramatically demonstrated in Fig. 24, due to Burke *et al.*, which shows a shift in the location of the peak in the $2^3S$ cross section by almost 200 meV between an angle of observation of 0° and 72°. Thus it is impossible to define, without a detailed analysis, the exact center of this resonance.

Ehrhardt and Willmann (1967) find that the angular distribution of the scattered electrons which have excited the $2^3S$ state around 20.45 eV (see Fig. 25) exhibits a $p$-wave character, so that the designation of this resonance as $2^2P$ seems established.

### 5. Effects near the Thresholds of the $2^3S$ and $2^1S$ Excitation Cross Section

The differential cross sections for both the $2^3S$ and the $2^1S$ states exhibit a small peak within 150 meV of threshold. This behavior has been observed in two independent experiments, one performed by Chamberlain and Heideman (1965), who analyzed the inelastically scattered electrons in the forward direction, and the other by Ehrhardt and Willmann (1967) and by Ehrhardt, Langhans, and Linder (1968), who observed inelastically scattered electrons at 10–90°. The latter experiments show that the angular dependences of the structures near both the $2^3S$ and the $2^1S$ thresholds are isotropic, indicating an $s$ wave. The peaks occur at 19.95 eV (140 meV above the $2^3S$ threshold) and just above 20.6 eV, respectively.

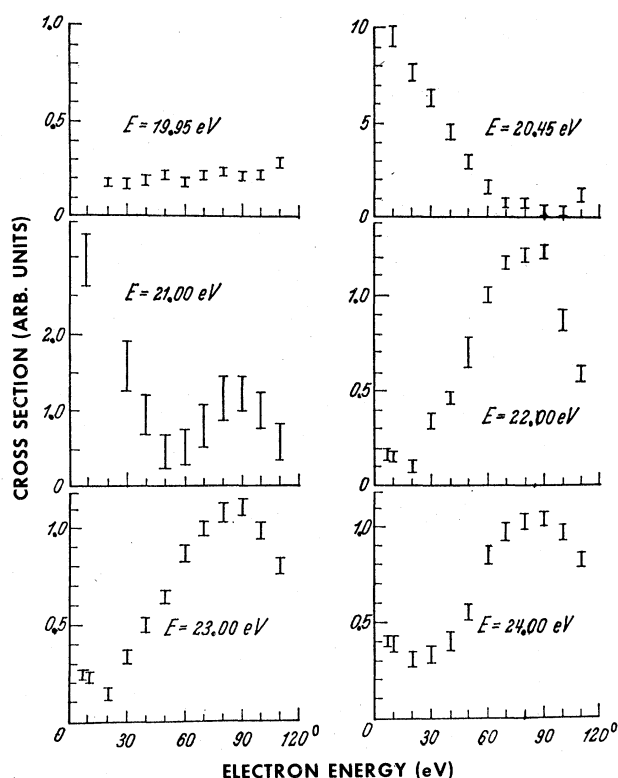The results of Ehrhardt *et al.* (1968) are shown in

FIG. 25. Angular distribution of electrons having excited the $2^3S$ state in helium. The incident electron energy $E$, is indicated. The angular dependence at 19.95 eV corresponds to an $s$ wave, at 20.45 eV to a $p$ wave and at 21.00 eV to a $d$ wave. All curves are experimental. [From Ehrhardt and Willmann (1967).]

Fig. 26. However, it seems that a note of caution is appropriate in analyzing the behavior of these excitation curves within the first 0.5 eV of threshold. This regime involves electrons which possess only 0–0.5 eV of energy after the collisions and which must be accepted by the electron analyzer. For the curves of Fig. 26 to be meaningful, it is desirable that no energy discrimination be present in this energy range. This requirement imposes a very severe demand on the electron optics which must exhibit a complete absence of chromatic aberration in the range 0–0.5 eV. This problem has not yet been solved. Also, there should be a complete absence of stray electric and magnetic fields, which could cause severe discrimination problems. It is probable that the curves of Fig. 26 are afflicted, within 0.5 eV of their thresholds, by an error of unknown magnitude, i.e., a correction factor of unknown shape should be applied to these curves.

One can obtain an indication of the seriousness of the problem outlined in the previous paragraph by taking the ratio of cross sections for the $2^3S$ excitation at two different energies, e.g., the ratio $\sigma(20.45 \text{ eV})/\sigma(19.95 \text{ eV})$. This is the ratio of cross sections near the center of the $^2P$ resonance to the peak near threshold. For the curve of Fig. 26, this ratio is about unity (at 70°), whereas it is about three (at 60°) in the older work of Ehrhardt and Willmann (1967). One should prefer, at

the present time, the data shown in Fig. 26, due to Ehrhardt, Langhans, and Linder (1968) in preference to the older data of Ehrhardt and Willmann since the former authors have made a study of the energy discrimination in their apparatus and have come to the conclusion that the error is less than 50% in the energy range within 300 meV of the $2^3S$ threshold.

The experimentally measured width of the threshold structure near the onset of the $2^3S$ state is about 150 meV and thus should have been noticed in measurements of the total cross section for the $2^3S$ state. Although the resolution of many of the experiments on the total excitation of the $2^3S$ state had sufficient resolution, such a structure was not observed (see, e.g., Schulz and Fox, 1957) and the total $2^3S$ cross section rises to a broad maximum near 20.3 eV. Pichanick and Simpson (1968) made a careful examination of the threshold region with the purpose of examining the threshold structure (see Fig. 23), but failed to find any indication of its existence. If one integrates the theoretical differential cross section over all angles to obtain the total cross section, the threshold structure becomes almost invisible [Burke et al. (1967) and Linder, private communication] and thus the threshold structure near 19.95 eV cannot be observed in the total cross section for exciting the $2^3S$ state.
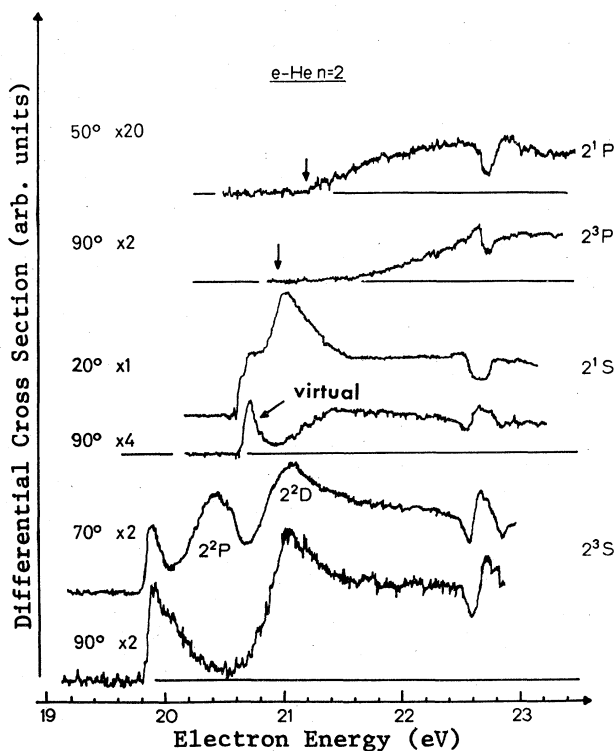


FIG. 26. Energy dependence of the differential cross sections for the excitation of $2^3S$, $2^1S$, $2^3P$, and $2^1P$ levels of helium near threshold, at selected angles of scattering. The angle of observation is indicated, for each curve, on the left-hand side. The number following the designation of angle indicates the enlargement of the particular curve with respect to the $2^1S$ curve at 20°. Experimental. [From Ehrhardt, Langhans, and Linder (1968).]

Although the structures near the thresholds of the $2^3S$ and $2^1S$ states have a similar appearance, the interpretation advanced by Ehrhardt (1969) for the two effects is very different.

Ehrhardt and Willmann (1967) find that the threshold peak at 19.95 eV in the $2^3S$ differential excitation cross section is independent of angle. Thus they deduce that the threshold peak appears in the $s$-wave. In a number of publications, Ehrhardt et al. (1967, 1968, 1969) point out that the threshold effect is caused by the *tail* (i.e., the wings) of the $2^2S$ resonance, whose center is located at 19.34 eV. This conclusion relies heavily on the fact that the theoretical work of Burke and of Taylor could not account for other $^2S$ resonances in this energy range. In his review, Taylor (1970) further discusses the qualitative aspects of threshold peaks in inelastic cross sections caused by core-excited resonances lying below the inelastic threshold.

It is pointed out by Herzenberg (private communication), that very *sharp* peaks in inelastic cross sections near threshold can not be explained *quantitatively* in such a simple fashion. Rather, one has to realize that the decay width for a Feshbach resonance (e.g., $2^2S$ in helium) shows an abrupt increase in a narrow energy range starting at the inelastic threshold. Thus, in the case of helium, one can understand how a narrow width ($\sim 8$ meV) below the threshold of the $2^3S$ state can be reconciled with a width considerably broader ($\sim 1$ eV) above the $2^3S$ state. This argument should



FIG. 28. Differential inelastic cross sections in the energy range 22.4–23.5 eV for helium. The structures are due to the $n=3$ compound states. The final state and the angle of observation are indicated for each curve. [From Andrick, Ehrhardt, and Eyb (1968).]

be applicable generally to the threshold excitation of those states which are parents of Feshbach resonances.

It would be satisfying if the threshold structure in the $2^1S$ state could be explained along similar lines. However, there seem to be good reasons to invoke a different explanation. This explanation is based on the work of Burke et al. (1967) and of Burke, Cooper, and Ormonde (1969) who calculated, using close-coupling methods, the cross section for the transition $e+\mathrm{He}(2^3S)\rightarrow \mathrm{He}(2^1S)+e$. They found a sharp peak at the threshold of the $2^1S$ state, which they attributed to a $^2S$ resonance close to the threshold of the $2^1S$ state. The existence of such a resonance would, of course, also affect the cross section $e+\mathrm{He}(1^1S)\rightarrow\mathrm{He}(2^1S)+e$.

The elastic cross section for scattering of electrons from the $2^1S$ state has a very large value ($1430\pi a_0^2$) near the $2^1S$ threshold, in the $l=0$ partial wave, again indicating the existence of a $^2S$ resonance near the $2^1S$ state. The threshold behavior of the elastic cross section for scattering from the $2^3S$ state is markedly different. Thus Ehrhardt et al. (1968) attribute the threshold structure near the $2^1S$ onset to a $^2S$ state existing near the $2^1S$ state and designate the $^2S$ resonance as a "virtual" state. On this model, the electron is captured just at the upper plateau of the potential well and experiences a phase shift. Taylor (1970) describes this
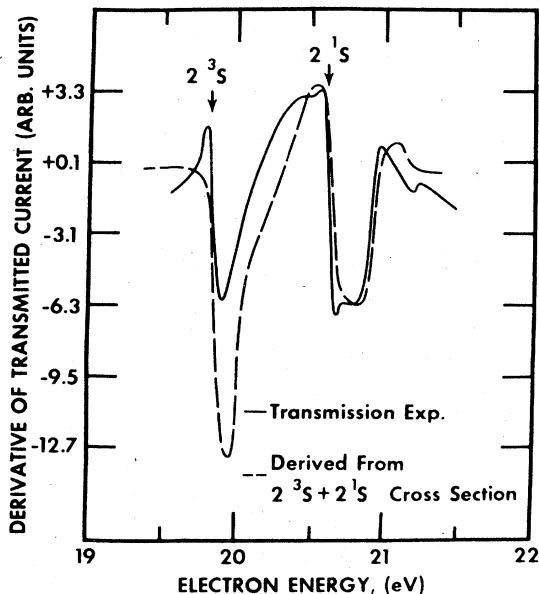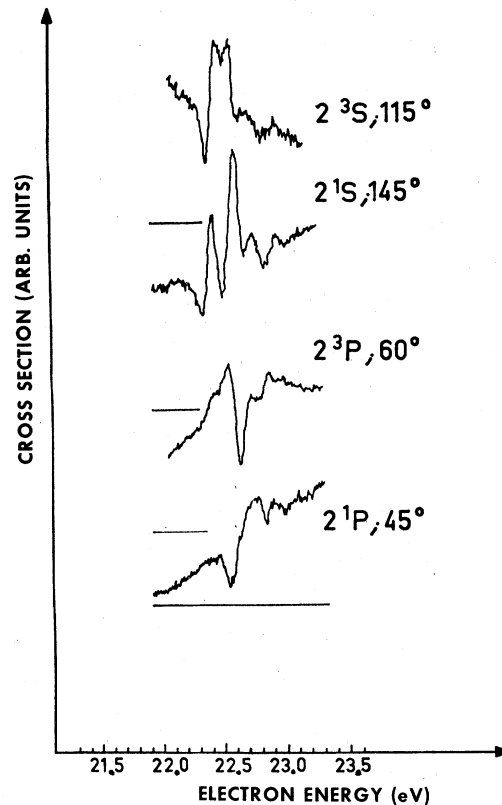


FIG. 27. An expanded view of the derivative of the transmitted current in the neighborhood of the lowest inelastic thresholds in helium. The solid line shows the experiment of Sanche and Schulz (1972) and the dashed line is obtained from the total metastable cross section. The two curves are normalized to each other in the region of the $2^1S$ excitation. The rise in the transmission curve just below the threshold for the $2^3S$ and $2^1S$ states is interpreted as a Wigner cusp in the elastic cross section. [From Sanche and Schulz (1972).]
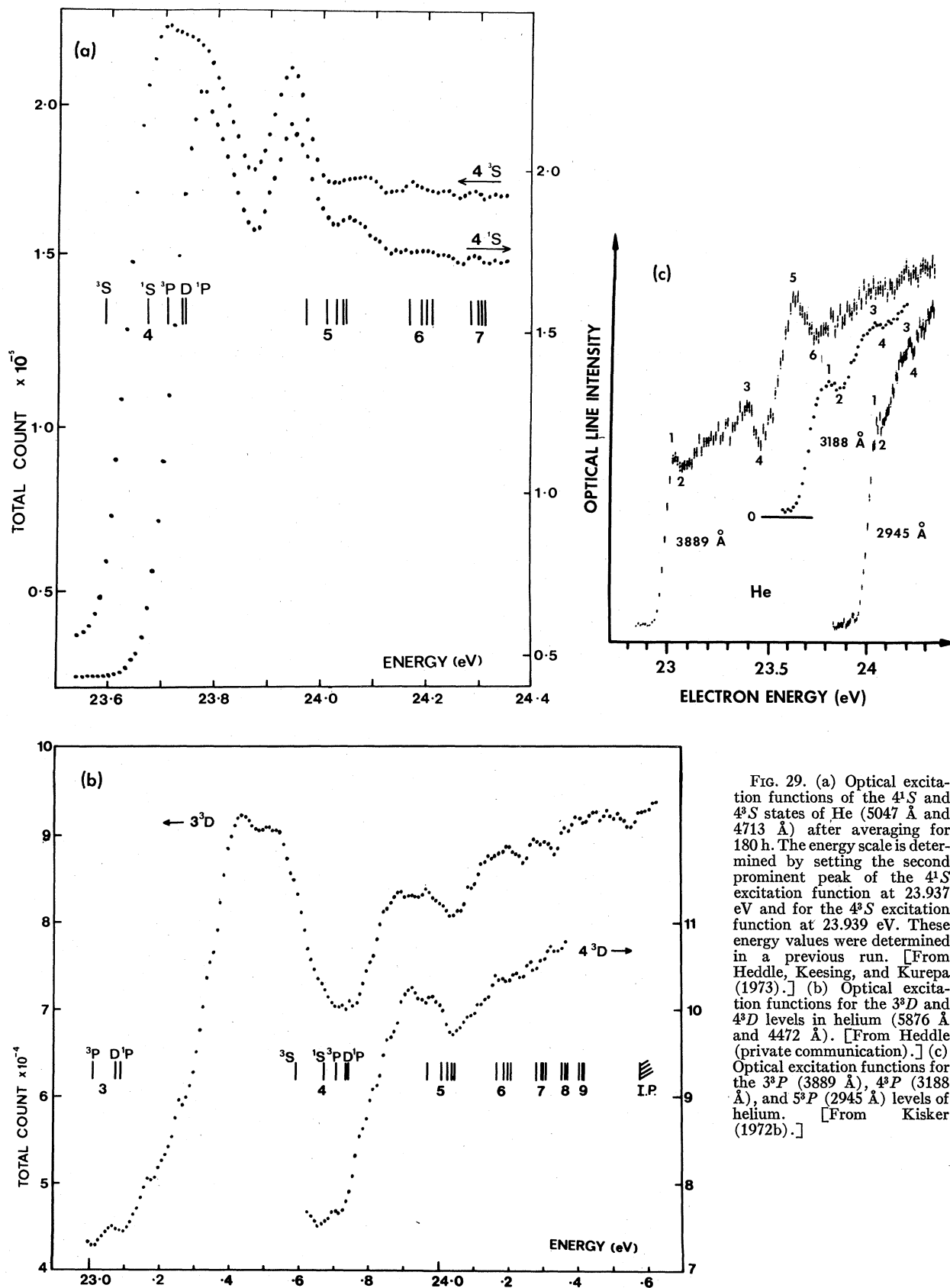
FIG. 29. (a) Optical excitation functions of the $4^1S$ and $4^3S$ states of He (5047 Å and 4713 Å) after averaging for 180 h. The energy scale is determined by setting the second prominent peak of the $4^1S$ excitation function at 23.937 eV and for the $4^3S$ excitation function at 23.939 eV. These energy values were determined in a previous run. [From Heddle, Keesing, and Kurepa (1973).] (b) Optical excitation functions for the $3^3D$ and $4^3D$ levels in helium (5876 Å and 4472 Å). [From Heddle (private communication).] (c) Optical excitation functions for the $3^3P$ (3889 Å), $4^3P$ (3188 Å), and $5^3P$ (2945 Å) levels of helium. [From Kisker (1972b).]

virtual state as a "bound" state that just slipped out of the potential well.

Taylor (private communication) describes the formation of the two $2^2S$ states as follows: The $2^3S$ state mixes with the $2^3P$ state, thus forming a polarization potential which combines with the low screening in excited states to form a well. The electron binds in this well and we get a resonance below the $2^3S$ state. Similarly, the $2^1S$ and $2^1P$ states mix to give a resonance below the $2^1S$ state. Both resonances have a $^2S$ character. As the two $^2S$ channels mix, the two states split apart. The lower $^2S$ state moves down to 19.3 eV and the upper $^2S$ moves up and slips out of the well, to become virtual. This approach, if substantiated by calculations, provides a very picturesque way to visualize the two low-lying s-wave resonances in He. In fact, experiments in other rare gases seem to indicate that such a picture is applicable there too.

The designation of the virtual state in terms of orbitals is by no means clear. Table I indicates that the only $^2S$ state which is not accounted for has the $1s2p^2$ configuration. However it is not suggested that this is the proper answer, since the $1s2p^2$ may have a very large width, and may lie at higher energies.

The resonance near the $2^1S$ threshold also strongly influences the superelastic cross section $e + He(2^1S) \rightarrow He(2^3S) + e$. This cross section exhibits a strong peak near zero energy. A very large average cross section for this process ($\sim 3 \times 10^{-14}$ cm$^2$) for 300°K electrons had been previously measured by Phelps (1955) and the theory of Burke et al. (1969) shows agreement with this large value, which was not completely understood until the resonance process was invoked.

### 6. Structure in the Elastic Cross Section near the $2^3S$ and $2^1S$ Thresholds (Wigner Cusps)

The opening of an inelastic channel should be accompanied by the appearance of a cusp in the elastic cross

FIG. 30. Derivative of the transmitted current in helium in the region of doubly excited states. The vertical lines show the positions of the $2s^2$ and $2s2p$ excited states of helium. [From Sanche and Schulz (1972).]
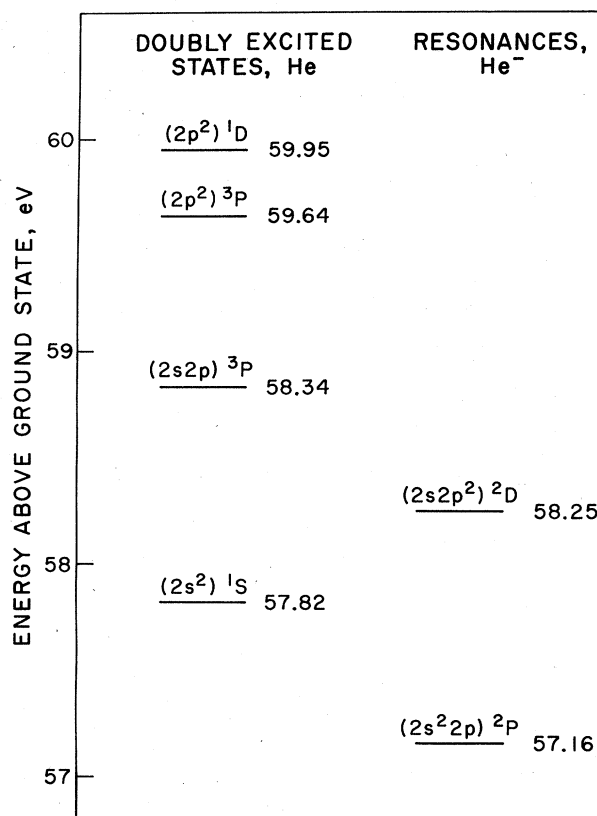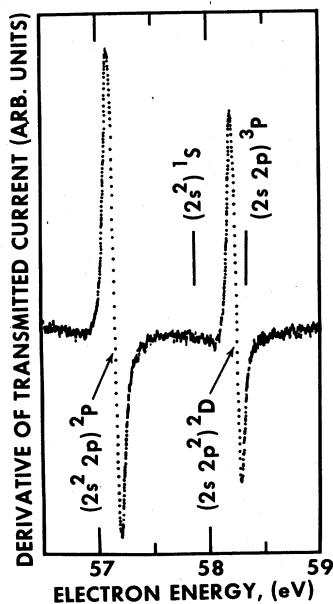
FIG. 31. Energy level diagram for the lowest doubly excited states of helium and the two associated compound states, He$^-$.

section (Wigner, 1948; Baz 1958). Such a cusp has been observed recently in a transmission experiment in helium (Sanche and Schulz, 1972) as a sharp increase in the transmitted current and its derivative just below the threshold for the $2^3S$ and $2^1S$ states. The results are shown in Fig. 27. In the differential elastic cross section at 90°, the Wigner threshold cusp appears as a downward step which causes the cross section to decrease by about 1% (Cvejanovic, Comer, and Read, 1973).

### 7. 21.0 eV ($2^2D$)

The experimental determination of the location of the $2^2D$ resonance comes from the observation of a well-pronounced peak in the $2^3S$ and $2^1S$ cross sections at various angles of observation as shown in Fig. 26. The decay into the elastic channel has not yet been observed. The designation as $^2D$ comes from the angular distribution and from theoretical considerations. The experimental observations are as follows:

$2^3S$ excitation: Schulz and Philbrick (1964) observed a peak, at 21.0 eV with a width of about 0.4 eV, at an angle of 72°. Ehrhardt and Willmann (1967) extended the angle of observation to include the range 7–110°. The angular distribution at 21.0 eV is found to be characteristic of a $d$ wave, as can be seen in Fig. 25. Chamberlain (1967) studied forward-scattered electrons having excited the $2^3S$ state and finds structure at
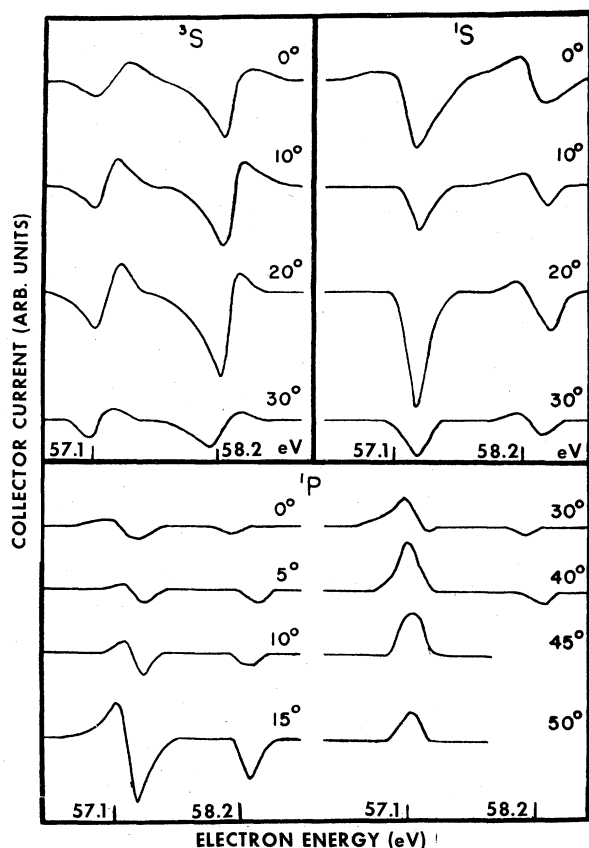
FIG. 32. Typical line shapes of the 57.1- and 58.2-eV resonances $(2s^22p$ and $2s2p^2)$, as observed in $^3S$, $^1S$, and $^1P$ inelastic channels. The angles of observation are indicated on the figure. The ordinate is in arbitrary units and the zeros are displaced. The energy scale is accurate to about 0.2 eV. [From Simpson, Menendez, and Mielczarek (1966).]

20.7 eV, which probably results from the $^2D$ resonance. The position of the peak resulting from the $^2D$ resonance shifts to lower energies (i.e., from 21.0 eV to 20.7 eV) as the angle of observation is decreased (Linder, private communication). In view of the large width of this resonance and the possibility for interference, such a shift is not unusual.

$2^1S$ excitation: The $^2D$ resonance at 21.0 eV is also prominent in the $2^1S$ excitation, as reported by Ehrhardt, Langhans, and Linder (1968) particularly at small angles of observation (10°~50°) and in forward scattering (Chamberlain, 1967).

In the total metastable excitation, which measures the sum of the $2^3S$ and $2^1S$ excitation, a peak occurs at 21.0 eV. This peak can be attributed, in retrospect, to the $^2D$ state.

The theoretical work on the $^2D$ state appears fairly consistent. Burke et al. place the $^2D$ state at 21.0 eV, and ascribe to it a width of 0.4 eV. The stabilization technique of Taylor gives a value of 20.3 eV (Eliezer and Pan, 1970). Also, the $^2D$ state is prominent in the calculated cross section for electron excitation of the $2^1S$ state from the $2^3S$ state (Burke et al., 1967). The theory of Burke et al. (1969) shows that both the elastic

and inelastic cross sections for electron impact on the low-lying metastable states in helium are dominated by the presence of the $^2P$ and $^2D$ resonances.

### 8. 22.42–24 eV $(3^2S, 3^2P, etc.)$ Optical Excitation Functions

The data of Fig. 21 show many partially overlapping structures starting near 22.42 eV and extending to the ionization potential of helium. The lowest of these structures have been studied in the differential inelastic cross sections and are shown in Fig. 28. The values of the energies are listed, together with the suggested designations, in Appendix IIIa.

Very recently optical excitation functions have been studied using monochromatic electrons. Kurepa and Heddle (1972) have studied the following excitation functions: $4^3S{\to}2^3P$ (4713 Å); $4^1S{-}2^1P$ (5047 Å); $3^3S{-}2^3P$ (7065 Å); $4^1D{-}2^1P$ (4922 Å); $4^3D{-}2^3P$ (4472 Å); $3^3D{-}2^3P$ (5876 Å). Heddle, Keesing, and Kurepa (1973) have further analyzed the $4^1S$ and $4^3S$ excitations. Kisker (1972) has reported data on the $3^3P{\to}2^3S$ (3889 Å) and the $4^3P{\to}2^3S$ (3188 Å) lines.

Kurepa and Heddle (1972) detected seventeen structures, many of which appeared rather small, in the energy range 22.80–24.08 eV. Appendix IIIa lists the more prominent structures observed in this work. Also, Appendix IIIa lists large structures observed by Kisker (1972) in the $3^3P$ excitation and $4^3P$ excitation functions.

Most of the observations on structures in the optical excitation functions have not yet been analyzed in sufficient detail, so that any assignment is preliminary.
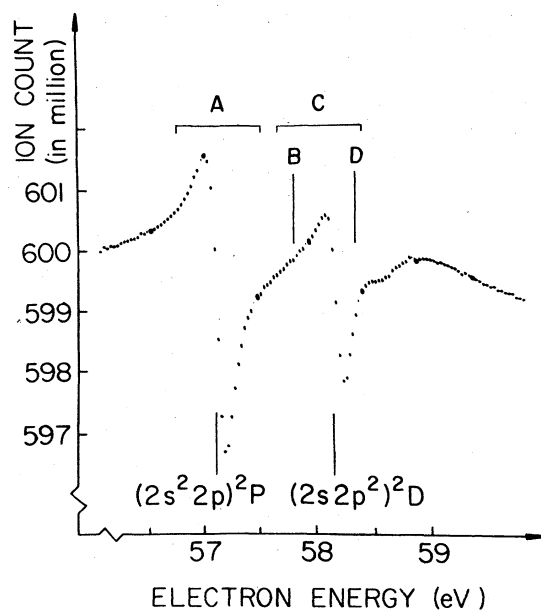


ELECTRON ENERGY (eV)

FIG. 33. Formation of He$^+$ by electron impact on He. The background ion formation is subtracted so that only the structure remains, representing ~0.8% of the total He$^+$ signal. The count rate is indicated. The structure results from the decay of the $(2s^22p)$ and $(2s2p^2)$ resonances by two-electron emission. [From Quéménér, Paquet, and Marmet (1971).]
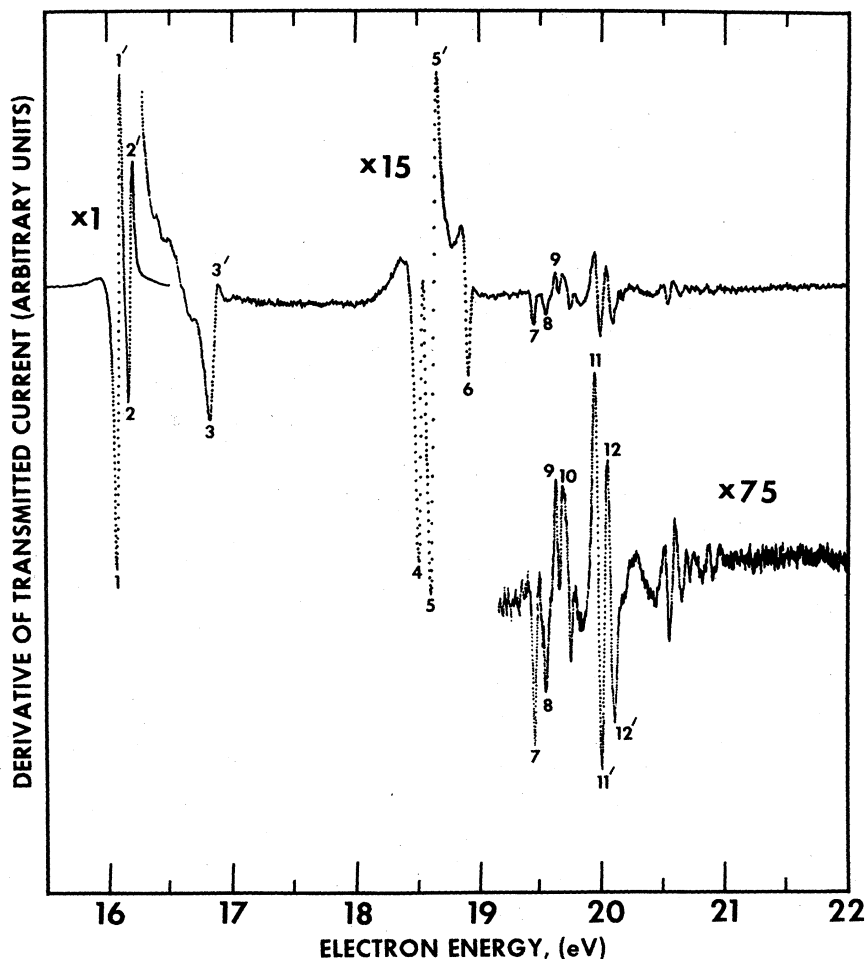
FIG. 34. Derivative of transmitted current vs electron energy in neon. [From Sanche and Schulz (1972).]

Nevertheless, Kurepa and Heddle (1972) propose that the large feature at 22.95±0.02 eV which appears in many of the excitation functions, be assigned to the $1s4s^2$ state of $He^-$. Similarly, the feature at 23.94±0.02 eV is assigned to the $5s^2$ configuration. It is, of course, understood that the above orbitals represent the dominant wavefunctions and that admixtures of other states are expected to contribute.

Figure 29(a) shows the results of Kurepa and Heddle

TABLE II. Values of the splitting between the $^2P_{3/2}$ and $^2P_{1/2}$ levels in the positive ion and in the compound state for Ne, Ar, Kr, and Xe.

| Gas | Compound state | | Positive ion |
| | Sanche and Schulz (1972) | Kuyatt, Simpson, Mielczarek (1965) | |
| --- | --- | --- | --- |
| Ne | 0.095 | 0.095 | 0.097 |
| Ar | 0.172 | 0.172 | 0.177 |
| Kr | 0.66 | 0.64 | 0.666 |
| Xe | ~1.2 | 1.25 | 1.306 |

(1972), as analyzed by Heddle *et al.* (1973) who have added all data from all their runs to aid in the distinction of real features from small fluctuations. The peak near 23.94±0.02 eV is very clearly exhibited in Fig. 29(a).

Figure 29(b) shows the optical excitation functions to two $D$ states, and Fig. 29(c) the excitation functions to three $P$ states, obtained by observing the wavelength indicated in the appropriate figure caption.

C. Resonances above the Ionization Potential: $(2s^22p)^2P$ and $(2s2p^2)^2D$

The lowest doubly excited states of helium are the $(2s^2)^1S$ state at 57.82 eV, and the $(2s2p)^3P$ state at 58.34 eV (Rudd, 1964, 1965). Kuyatt, Simpson, and Mielczarek (1965) discovered, using a transmission experiment, that resonances of the Feshbach type are associated with these states. Golden and Zecca (1970), as well as Sanche and Schulz (1972), confirmed the position of these resonances using the transmission method (Fig. 30). Appendix IV lists the values for these resonances, as found by different experiments. Fano and Cooper (1965) classified these resonances as $(2s^22p)^2P$ for the lowest (~57.16 eV) and $(2s2p^2)^2D$ for the second (~58.25 eV). Various theoretical
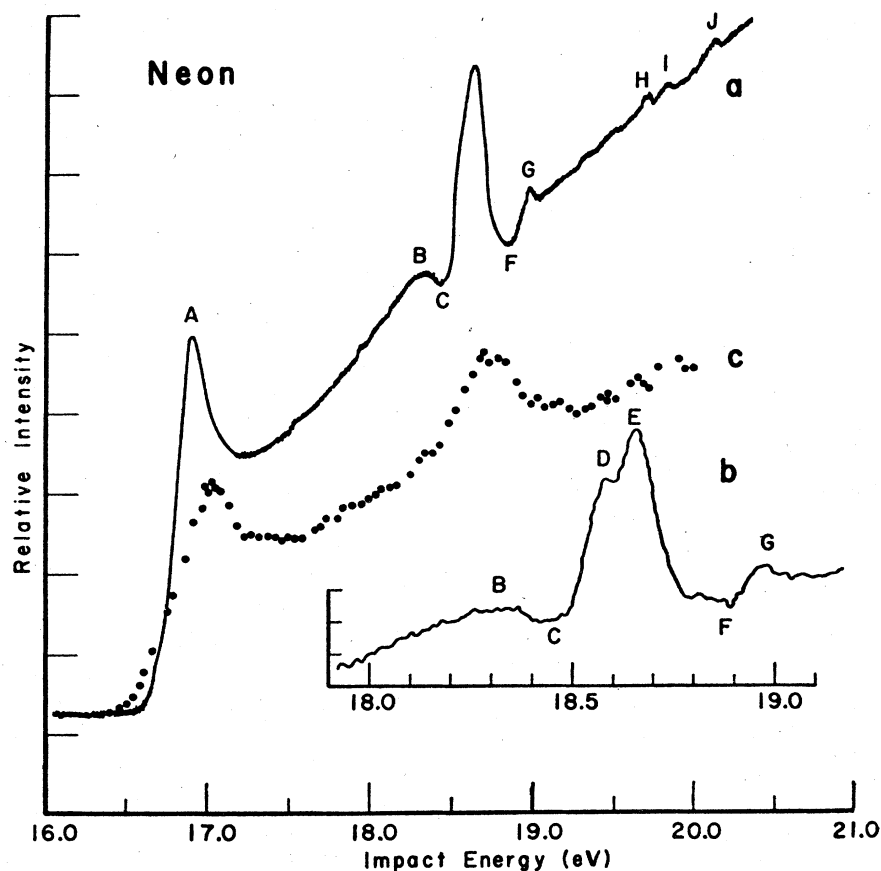
FIG. 35. Total metastable cross section for neon vs electron energy. Curve (a) is from Pichanick and Simpson (1968) with 50-meV resolution; curve (b) is the detail in the 18–19-eV range by the same authors, with 35-meV resolution; curve (c) is from Olmsted *et al.* (1965). [From Pichanick and Simpson (1968).]

approaches confirm the above assignment. Eliezer and Pan (1970) use the stabilization method to calculate the position of the $2s^2 2p$ and $2s2p^2$ states and Nicolaides (1972) uses a variational principle applied to the projection method with correlation included. Both theoretical methods give good agreement with the energies observed experimentally (see Appendix IV) and thus the assignment of the leading term ($2s^2 2p$ and $2s2p^2$) for the two resonances seems well established. In fact, Nicolaides (private communication) finds that the $2s^2 2p$ configuration contributes 73% to the square of the wave function of the $^2P$ resonance, with the remainder in terms like $2p^3$ and $2s2pnd$. For the $^2D$ resonance, the leading term, $2s2p^2$, contributes 83%, with the remainder in terms such as $2s^2nd$ and $2p^2nd$.

Figure 31 shows an energy level diagram in the region 57–60 eV. The $^2P$ and $^2D$ resonances can decay by the emission of a single electron into various excited states of helium. Decay into the $2^3S$, $2^1S$, and $2^1P$ states has been studied by Simpson, Menendez, and Mielczarek (1966) whose data are shown in Fig. 32.

The same resonances can also decay by the emission of two electrons, yielding $He^+ + 2e$. This type of decay has been found by Burrow and Schulz (1969) by studying the interference of zero-energy electrons produced in the two-electron decay. The trapped-electron method was used for these studies. This two-electron decay

also causes structure when one observes the energy dependence of the formation of $He^+$, as was done by Grissom, Compton, and Garrett (1969). Quéméner, Paquet, and Marmet (1971) have improved the sensitivity for the detection of structure in positive ion curves by several orders of magnitude. Their results are shown in Fig. 33. An analysis of the peak shapes yields, for the $^2P$ state, $\Gamma = 0.045 \pm 0.007$ eV ($q = -0.75 \pm 0.12$) and, for the $^2D$ state, $\Gamma = 0.025 \pm 0.010$ eV ($q = -0.95 \pm 0.25$). Here, $\Gamma$ is the width of the state and $q$ is the "line profile index" (see Sec. I).

An unusual feature has been recently observed in the $2^3S$ excitation cross section near 50 eV by Crooks *et al.* (1972). When the energy dependence of the differential cross section for the electrons having excited the $2^3S$ state is examined around 90 degrees, a precipitous dip in the cross section is observed near 50 eV. Such behavior is reminiscent of interference phenomena, and calculations show (Macek and Wooten, unpublished) that the $s$ and $d$ waves exhibit interference. When the differential cross sections for excitation to the $2^3S$ state are integrated, the resulting total cross section exhibits a peak near 50 eV, which is 15 eV wide. Crooks *et al.* interpret this peak in terms of a $p$-wave resonance. It therefore appears that near 50 eV in helium, there is interference of partial waves and, in addition, a broad resonance.

The resonance itself could be understood by con-

sidering a state of He⁻ in which the three electrons comprising He⁻ are equidistant from the nucleus. Such a quasistationary state was calculated by Herzenberg and Ton-That (1973) to exist around 45.9 eV. It is of a similar nature as the state of H⁻ ⁻ discussed in Sec. IIC, with the wave function having no radial nodes. The $2s^2 2p$ state at 57.16 eV, which has the same $^2P$ symmetry, has a radial node in each of the $2s$ factors.
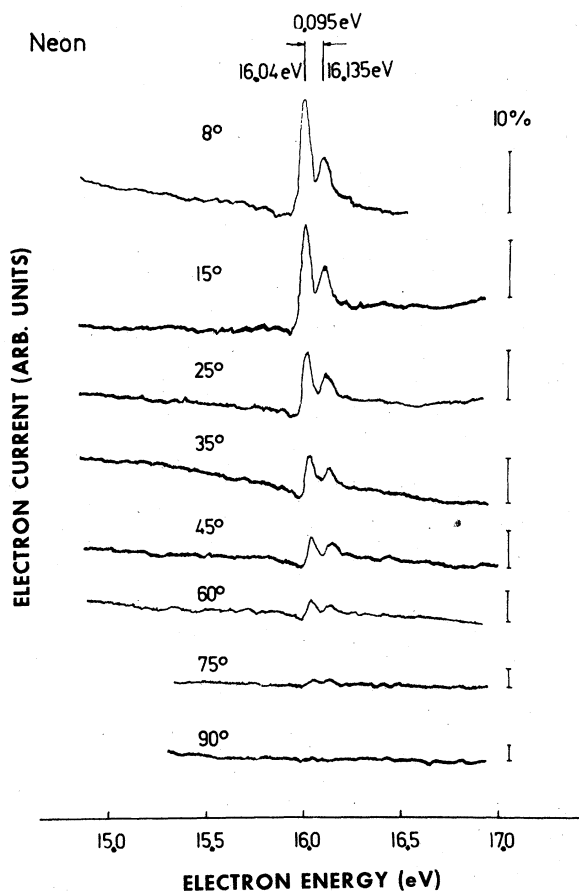


FIG. 36. Elastic cross section vs electron energy at designated angles of observation in neon. The vertical bars designate a 10% change in cross sections. The angular dependence of the resonances is characteristic of the $p$ wave. [From Andrick and Ehrhardt (1966).]

## IV. NEON, ARGON, KRYPTON, AND XENON

The rare gases Ne, Ar, Kr, and Xe exhibit marked similarities in terms of their resonances so that it is appropriate to consider them under a single heading.

### A. Resonances Below the Ionization Potential

The first resonances in all the rare gases discussed in this section consist of two $s$ electrons attached to the positive ion core (Simpson and Fano, 1963). Since the positive ion core is a doublet ($J = \frac{1}{2}$ and $J = \frac{3}{2}$), the resonances are also split. In fact, the splitting of the resonances is in very good agreement with the splitting
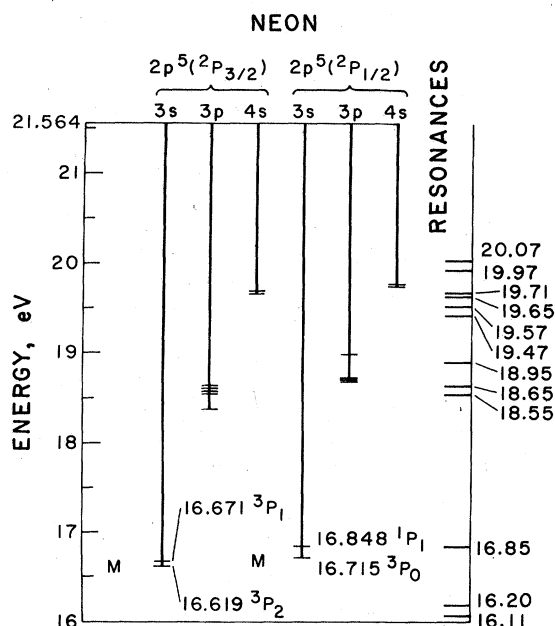


FIG. 37. Energy level diagram for neon, showing states of neon and the associated resonances. The values for the resonances are taken from Sanche and Schulz (1972) and a comparison with other values is shown in Appendix V. Metastable states are denoted by the letter M.

of the ion core, as shown in Table II, where comparison is made between the two available experiments on resonances and the known splitting of the ion core. The agreement between the splitting of the resonances and the positive ion core assures that the designations advanced by Simpson and Fano (1963) are correct. Thus, the lowest resonances in Ne, Ar, Kr, and Xe have
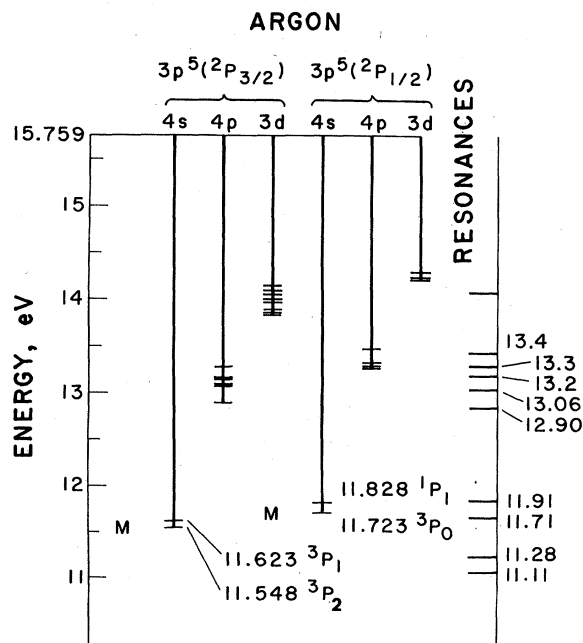


FIG. 38. Energy level diagram for argon. Numerical values are listed in Appendix VI.
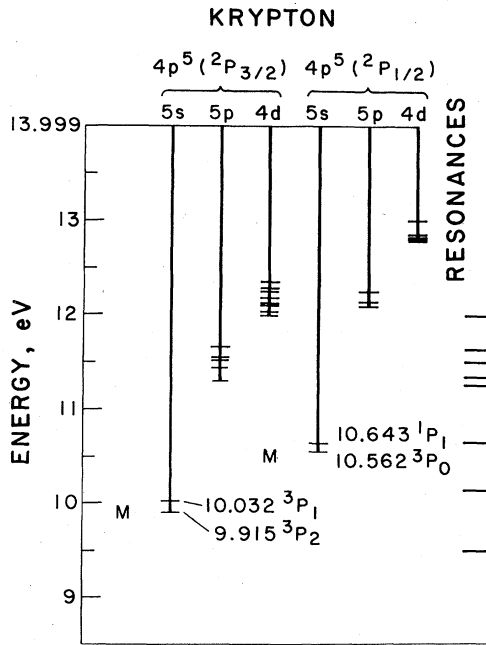
## KRYPTON



FIG. 39. Energy level diagram for krypton. Numerical values are listed in Appendix VII.

the form $(2p^5 3s^2)$, $(3p^5 4s^2)$, $(4p^5 5s^2)$, and $(5p^5 6s^2)$, respectively, each resonance being split by the amount indicated in Table II into a $^2P_{3/2}$ and a $^2P_{1/2}$ component.

Just as in the case of helium, our knowledge of resonances in Ne, Ar, Kr, and Xe comes from transmission experiments (Kuyatt et al., 1965; Sanche and Schulz, 1972), from experiments on total metastable production (Olmsted et al., 1965; Pichanick and Simpson, 1968) and from differential elastic scattering ex-
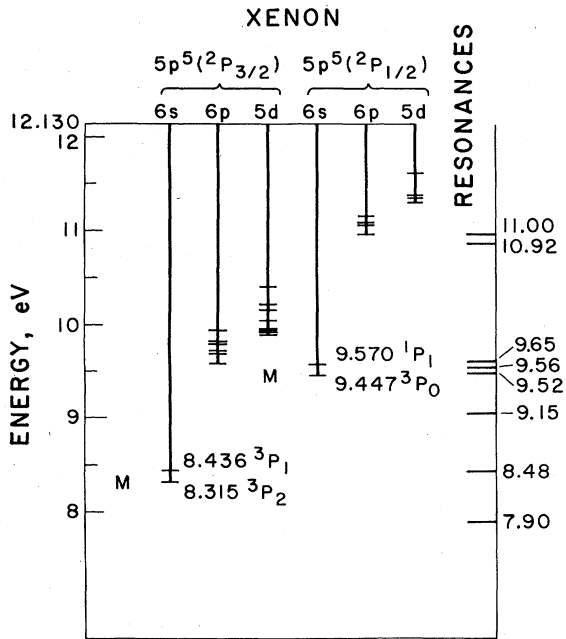
## XENON



FIG. 40. Energy level diagram for xenon. Numerical values are listed in Appendix VIII.
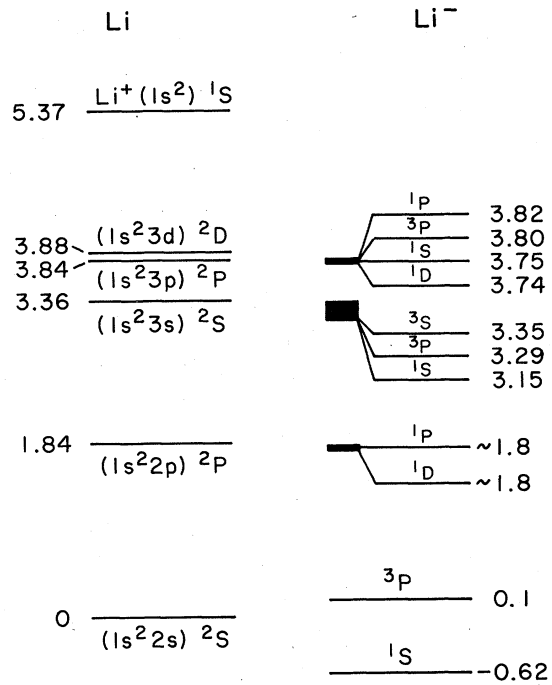


FIG. 41. Approximate energy level diagram for lithium and the compound states calculated theoretically. Values for the compound states are taken mainly from the work of Moores and Norcross (1972) and Fung and Matese (1972). The energy values, in eV, are only approximate. The electron affinity is taken from Weiss (1968).
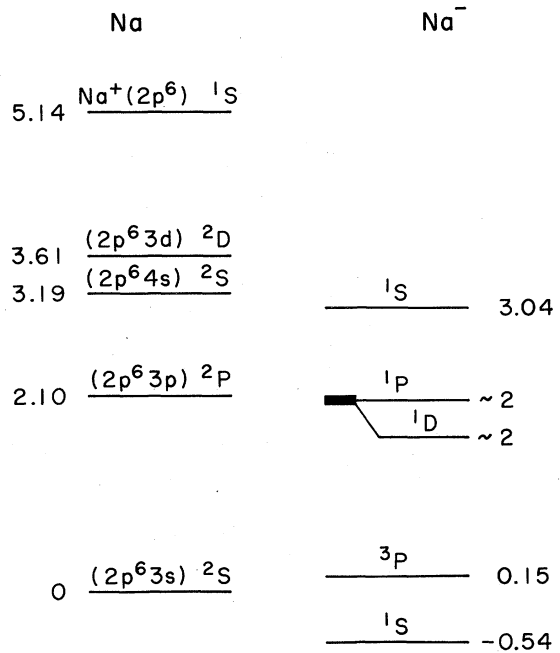


FIG. 42. Approximate energy level diagram for sodium and the compound states calculated theoretically. Values for the compound states are taken mainly from the work of Moores and Norcross (1972) and Fung and Matese (1972). The energy values, in eV, are only approximate. The electron affinity is taken from Weiss (1968), whose calculated value of 0.539 eV is in excellent agreement with recent photodetachment experiments of Hotop, Patterson, and Lineberger (0.542±0.01 eV).

FIG. 43. Total cross section for scattering of electrons by sodium. Full curve—theory of Moores and Norcross (1972); X—experiment of Brode (1929) divided by two; O—experiment of Perel, Englander, and Bederson (1962) normalized to theory at 5 eV. [From Moores and Norcross (1972).]
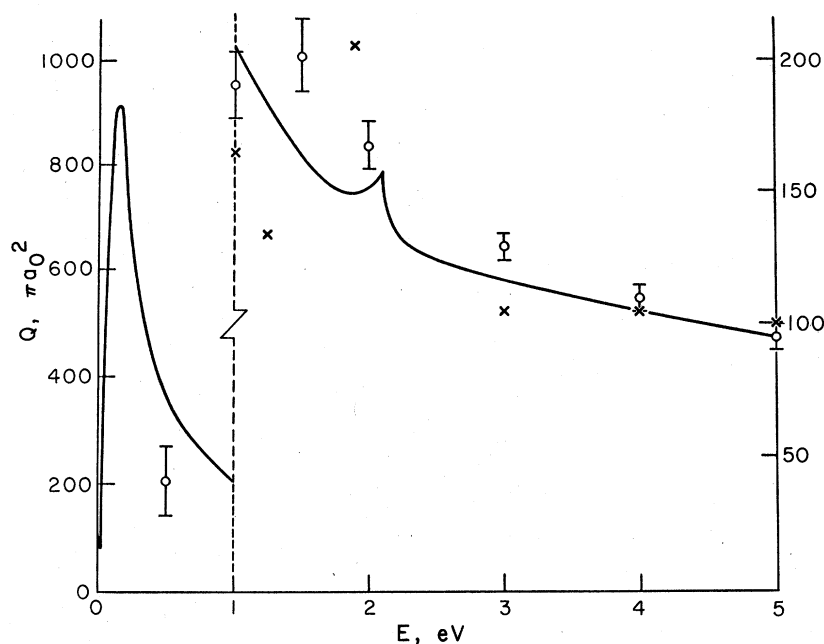
periments (Andrick and Ehrhardt, 1966). The information in these rare gases is more limited than in the case of He, since information on the excitation of electronically excited states of these gases is only now becoming available (Swanson *et al.*, 1971, 1973). Optical experiments with a good energy resolution in the electron beam are also very sparse [Sharpton *et al.* (1970) observe a sharp structure in photon emission at 18.6 eV in neon.]

Figures 34–36 show the experimental evidence for resonances in neon, and Fig. 37 shows an energy level diagram of Ne with the resonances included. Appendix V gives a comparison between the available experiments in tabulated form. A clearcut assignment of the higher-lying compound states is not yet available. The characteristics of Ar, Kr, and Xe are similar to those of neon. Energy level diagrams are shown in Figs. 38–40 and the energy values are listed in Appendixes VI–VIII.

### B. Resonances above the Ionization Potential

Above the ionization potential of Ne, Ar, Kr, and Xe, a number of features have been detected, some of which are undoubtedly resonances associated with singly excited states of the neutral atom. The energy range of these features spans the regions 42–50 eV in Ne, 24–32 eV in Ar, 22–27 eV in Kr, and 18–20 eV in Xe. These features are discussed in connection with the transmission experiment by Sanche and Schulz (1972), in connection with the trapped-electron method by Grissom, Garrett, and Compton (1969), and in connection with positive ion detection by Bolduc, Quéméner, and Marmet (1972). The reader is referred to these papers for an up-to-date discussion and for a list of previous references. One of the difficulties inherent

in these studies lies in distinguishing between resonances and the onset of highly excited autoionizing states of the neutral atom. Thus one has to rely heavily on measurements of the structure in the photoionization continuum, which provides the location of optically allowed transitions to highly excited states (see, e.g., Ederer, 1971). Some of the energies at which resonances are believed to occur in Ne and Ar are listed in Appendix IX.

### V. LITHIUM AND SODIUM

Electron scattering in alkali atoms has been of considerable interest in the past years (Bederson and Kieffer, 1971), but high-resolution experiments with monochromatic electron beams have only recently become available. Thus much of our knowledge regarding resonances in these atoms comes from theory. There is general agreement that at low energies ($\sim$0.15 eV) the spin exchange cross section in both Li and Na has a sharp rise (Karule, 1965; Burke and Taylor, 1969; Norcross, 1971; Moores and Norcross, 1972). This sharp rise is attributed to the existence of a $^3P$ compound state at about 0.15 eV. The width of this resonance is believed to be relatively large ($>$0.1 eV). The $^3P$ resonance also affects the phase shift of the elastic cross section (Moores and Norcross, 1972). The elastic cross section calculated from these phase shifts agrees with the cross section measured by Rubin *et al.* (unpublished).

In the vicinity of the $(1s^2 2p)\,^2P$ state of lithium, two resonances, $^1D$ and $^1P$, are postulated (Burke and Taylor, 1969). For reasons which are not entirely clear, Fung and Matese (1972) do not find these states using their multiconfiguration Hartree–Fock method; possibly the width of these states is too large. However Fung and
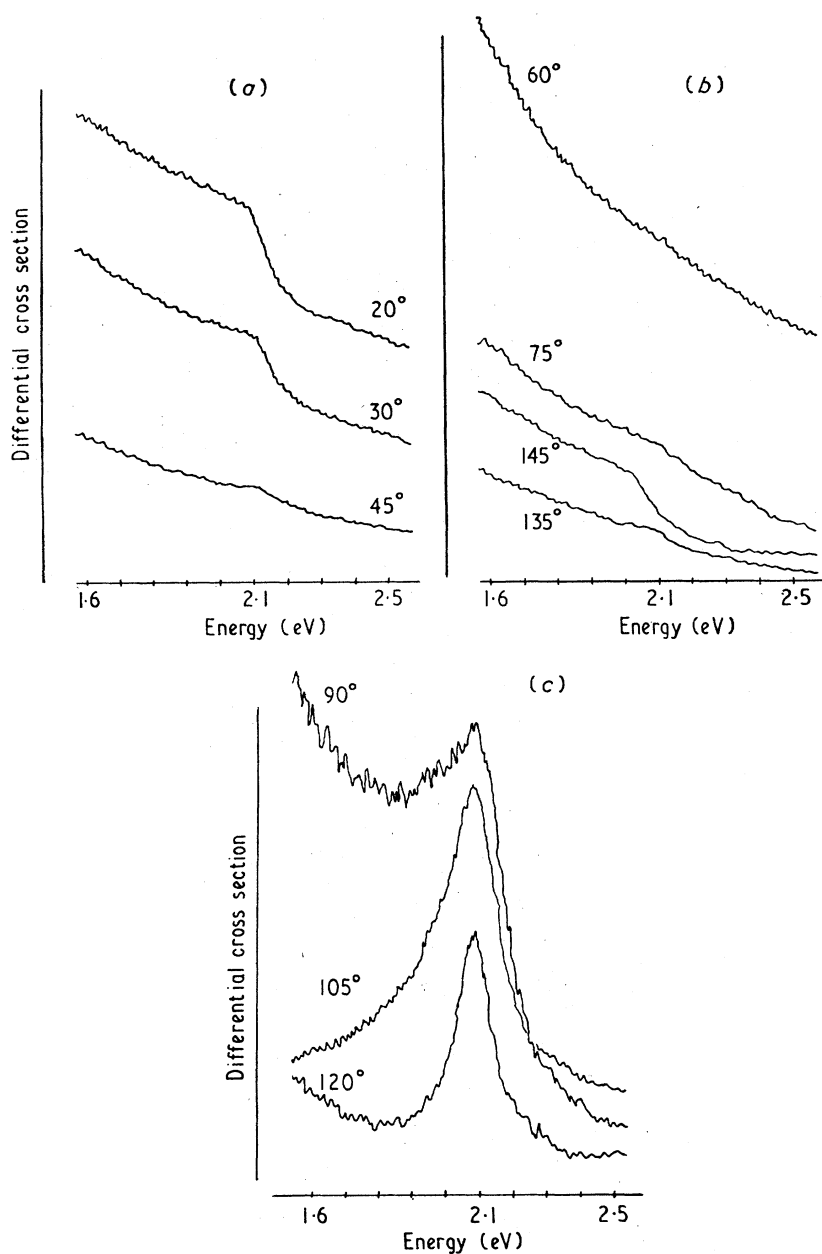
FIG. 44. Differential experimental cross section for elastic scattering of electrons on sodium. The angle of observation is indicated. Scales (b) and (c) are expanded with respect to scale (a) by factors of 3.7 and 25, respectively. [From Andrick, Eyb, and Hofmann (1972).]

Matese find three compound states lying below the $(1s^23s)^2S$ state and four states below the $(1s^23p)^2P$ state of Li. A schematic diagram, constructed from the results discussed above is shown in Fig. 41.

In sodium, an analogous situation prevails (Moores and Norcross, 1972) and the appropriate energy level diagram is shown in Fig. 42. Fung and Matese find only a single compound state in the 3-eV region of Na.

The existence of the $^1P$ and $^1D$ resonances just below the threshold of the first electronic state should dominate the excitation function to that state, and it appears that this is the case in Na (Enemark and Gallagher, 1972; Moores and Norcross, 1972).

The energy dependence of the total elastic and the differential elastic cross section in sodium exhibit a dramatic cusp at the energy of the $^2P$ state at 2.1 eV. This cusp is shown in Fig. 43 for the total cross section, as derived from the close-coupling theory of Moores and Norcross. The experimental results of Andrick, Eyb, and Hofmann (1972) for the differential elastic cross section are shown in Fig. 44. The close-coupling theory of Moores and Norcross is in very good agreement with the experiment. The structure shown in Figs. 43 and 44 is strongly influenced by the presence of the $^1P$ and $^1D$ states near 2 eV (Norcross and Moores, 1972).

It is noteworthy that the calculated cross sections for photodetachment of electrons from $Li^-$ and $Na^-$ in

FIG. 45. Transmission experiment in Hg. The three low-lying resonances are clearly visible as dips in the transmitted current. [From Fano and Cooper (1965).]
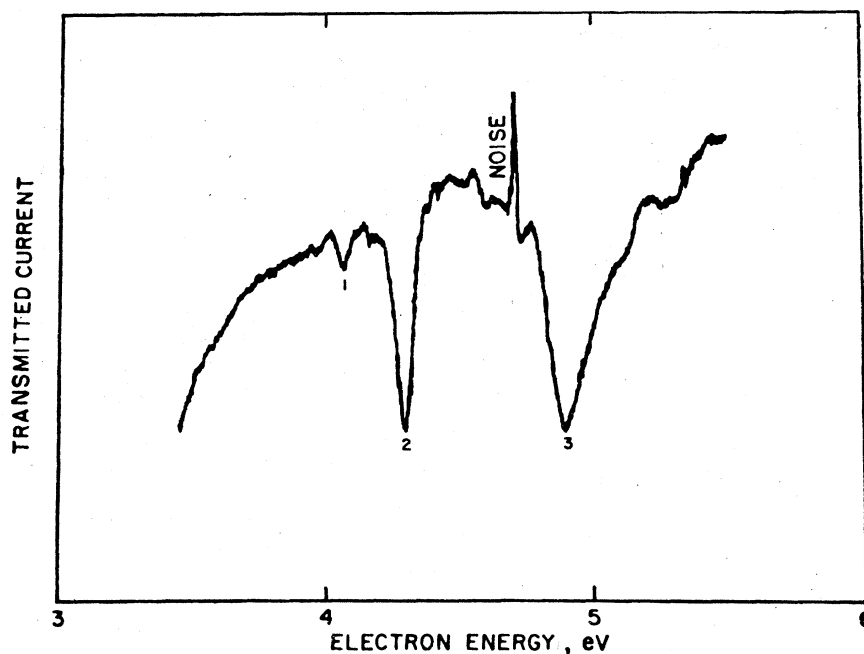
their ground states show a sharp peak near 2 eV (Norcross and Moores, 1972). This effect is attributed to the presence of the $^1P$ resonance near the threshold of the first excited state of the neutral atom.

## VI. MERCURY

Kuyatt, Simpson, and Mielczarek (1965) observe many resonances in their study of transmission of electrons through mercury. All resonances appear as dips in the transmitted current. An example of their data is shown in Fig. 45 and the positions of these resonances are shown on the energy level diagram of Fig. 46 in conjunction with the known electronically excited states of Hg. The lowest three resonances (marked 1, 2, 3) have been given the assignment $(6s6p^2)^4P_{1/2}$, $^4P_{3/2}$, $^4P_{5/2}$ (Fano and Cooper, 1965). The ground state of Hg is $(5d^{10}6s^2)^1S_0$.

Kuyatt et al. point out that the resonances at higher energies (near 8 eV) lie too high in energy to be attributed to higher levels $(^2D, {}^2S, {}^2P)$ of the $6s6p^2$ configuration. Rather, Kuyatt et al. suggest that the parents of some of the resonances in the 8-eV region are
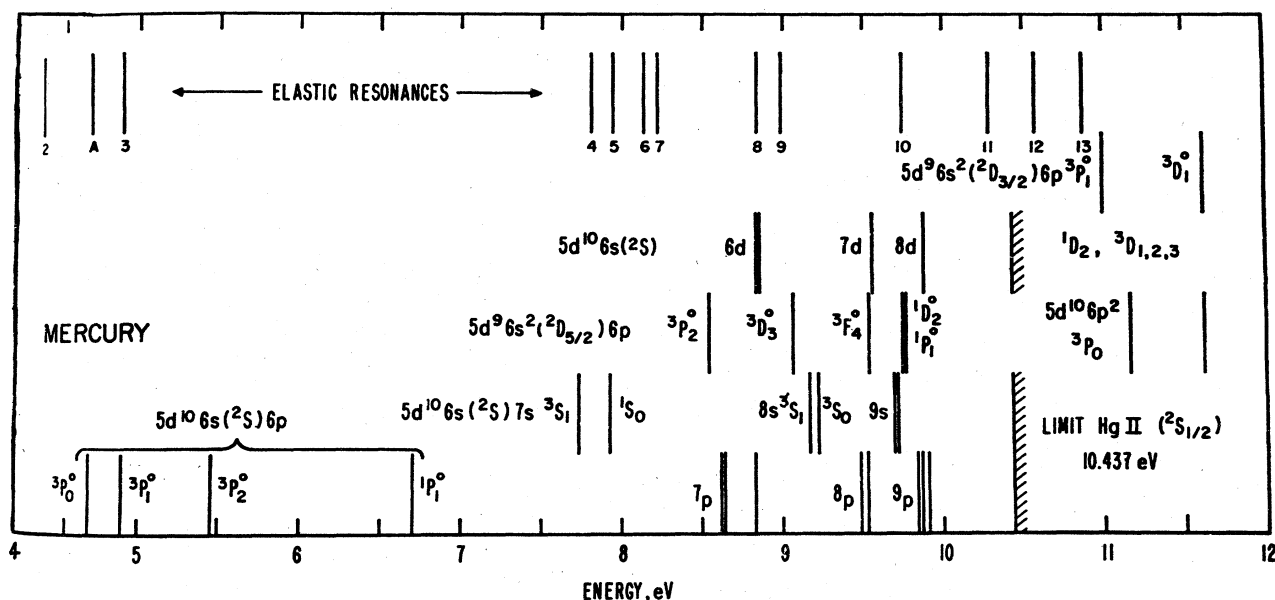


FIG. 46. Energy level diagram for Hg and the associated resonances. The resonances are numbered and their energies are listed in Appendix IX. [From Kuyatt, Simpson, and Mielczarek (1965).]
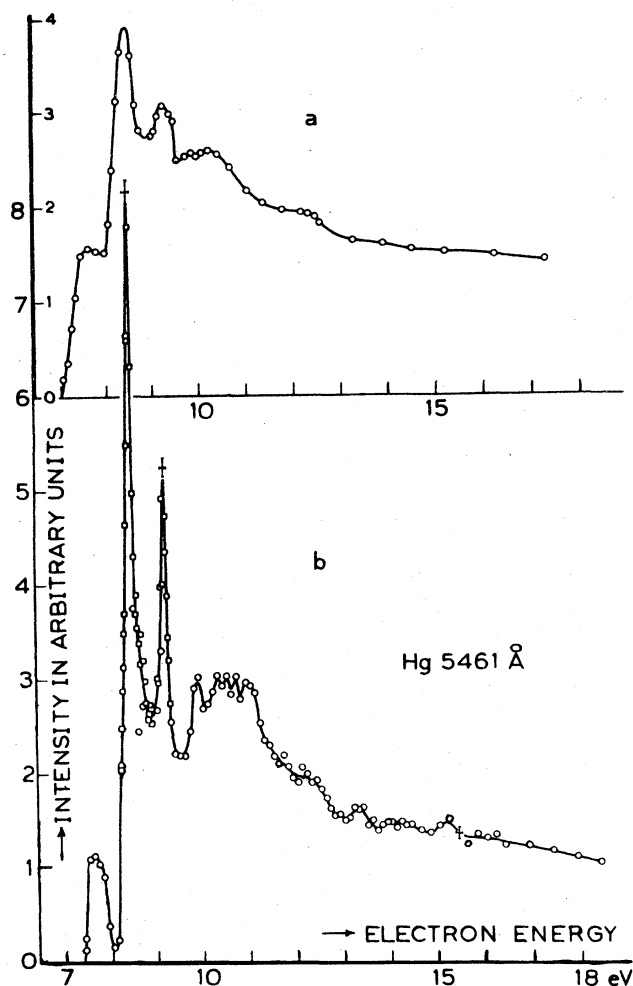
FIG. 47. Excitation function of the 5461-Å line of Hg. (a) Low-resolution results of Jongerius; (b) result obtained by Smit and Fijnaut (1965) using the retarding-potential difference method with a resolution of 0.1 eV. [From Smit and Fijnaut (1965).]

states of the configuration $5d^96s^26p$. The resonances would then have configurations such as $5d^96s^26p^2$.

The structures observed in transmission experiments can be compared with structures observed in optical excitation functions; care must be exercised in excluding structures resulting from sharp thresholds of higher energy levels which may contribute structure in low levels due to cascading.

Figure 47 shows the structure obtained by Smit and Fijnaut (1965) using a relatively narrow electron energy distribution (~0.1 eV) and observing the 5461-Å line in Hg. These results are in very good agreement with the work of Zapesochnyi and Shpenik (1966) who also used monoenergetic electrons for their observations and in addition to Hg ($\lambda = 2537$ Å, 5461 Å, 3650 Å, 4916 Å) examined a wide variety of optical excitation functions in He, Zn, Cd, Na, and K. Zapeso-

chnyi and Shpenik list the positions of the structure they observe. Appendix X compares their observed structures with the structures listed by Kuyatt et al. (1965). On the whole, there seems to be good agreement. It should be noted that Zapesochnyi and Shpenik interpret the observed structures in terms of cascading. However, it appears that the interpretation in terms of resonances could be equally valid.

## VII. OXYGEN (O)

The determination of the location of compound states in atomic species which occur naturally as molecules is very difficult, as pointed out in connection with the discussion of atomic hydrogen. Normally, one attempts to form a beam of the atomic species and crosses this beam with monochromatic electrons. A novel method for measuring compound states has been recently presented by Edwards, Risley, and Geballe (1971) and applied to atomic oxygen. In this method, a beam of stable O⁻ ions with about 2 keV of kinetic energy is incident on a rare gas target (He) and the electrons resulting from this interaction are energy-analyzed and recorded. Structure in the energy spectrum of the electrons is observed and is associated with the existence of resonances. Figure 48 shows an example. The peaks in Fig. 48 seem to arise from the reaction

$$O^- + He \rightarrow O^{-*} + He \rightarrow O + He + e,$$
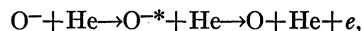
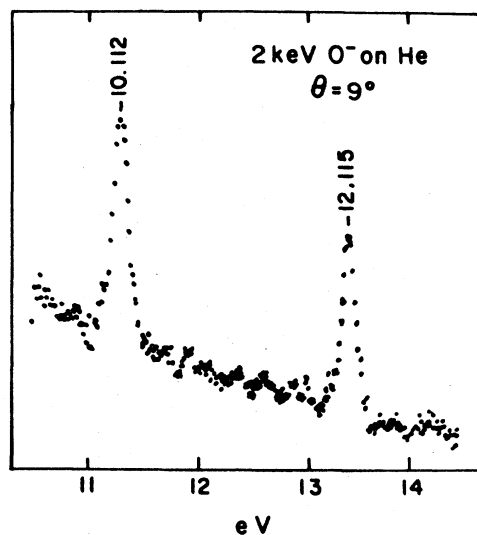where $O^{-*}$ denotes the compound state.



FIG. 48. Electron energy spectrum obtained after colliding a 2-keV beam of O⁻ with He. The electron energies given above the peaks are corrected for the velocity of O⁻ and are the proper energies for compound states. The peaks are interpreted as resulting from the formation of compound states up atomic oxygen. [From Edwards, Risley, and Geballe (1971).]

Since the electrons are ejected from a moving O⁻ particle, the measured electron energy must be corrected, and the "unshifted" energy must be determined. The energies indicated above the peaks of Fig. 48 refer to these corrected, "unshifted" values. Edwards *et al.* calibrate their energy scale by observing the reactions O⁻+H₂ and O⁻+Ar. In the former reaction, electrons resulting from compound states H⁻($^1D$) at 10.13 eV and from H⁻($^1S$) and H⁻($^3P$) were observed, although the latter two states could not be clearly resolved. In the reaction O⁻+Ar, the two low-lying resonances of Ar could be observed, and in fact the observed splitting (173 meV) is in agreement with other experiments (see Table II). These calibration experiments establish the reliability of the observations in oxygen. The energy level diagram of Fig. 49 shows schematically the configuration suggested by Edwards *et al.* to interpret their observations.

In order to test the results of the above experiment, Ormonde, Smith, Torres, and Davies (1973) performed a multi-configuration close-coupling calculation. They calculate elastic and inelastic cross sections and search for resonances. The $^3P$ and $^3D$ terms, which are possible parents for resonances are retained in the theory. A single resonance is found at 10.38 eV (0.25 eV above the experimental value quoted above), with a width of 20 meV. The discrepancy between theory and experiment in the energy of the resonance is attributed by Ormonde *et al.* (1973) to limitations of the theory. The assignment of the resonance given by Edwards *et al.* (1971) does not appear to be altered by the results of the theory.

A search for the higher-lying resonance (12.115 eV) found experimentally by Edwards *et al.* was also undertaken by Ormonde *et al.* (1973) using the close-coupling theory. No sharp resonances were found, but a shape resonance in the $^2P°$ partial wave was found near 11.5 eV, with a width about 1 eV. This shape resonance is probably in addition to the sharp structure at 12.115 eV found by Edwards *et al.*

Very recently, Matese, Rountree, and Henry (1973) undertook a configuration-interaction study of doublet resonances in atomic oxygen. They calculate the following levels of O⁻:

$$2p^3(^4S°)3s3p(^2P) \text{ at } 9.50 \text{ eV},$$

$$2p^3(^2D°)3s^2(^2D°) \text{ at } 12.05 \text{ eV},$$

$$2p^3(^2P°)3s^2(^2P°) \text{ at } 13.65 \text{ eV},$$

$$2p^3(^4S°)3p^2(^2P°) \text{ at } 10.87 \text{ eV}.$$

A reasonable estimate of possible errors in the above-quoted energies is ±0.1 eV. Matese *et al.* suggest that the 12.115-eV peak observed experimentally by Edwards, Risley, and Geballe corresponds to the $2p^3(^2D°)3s^2(^2D°)$ state, thus confirming the original
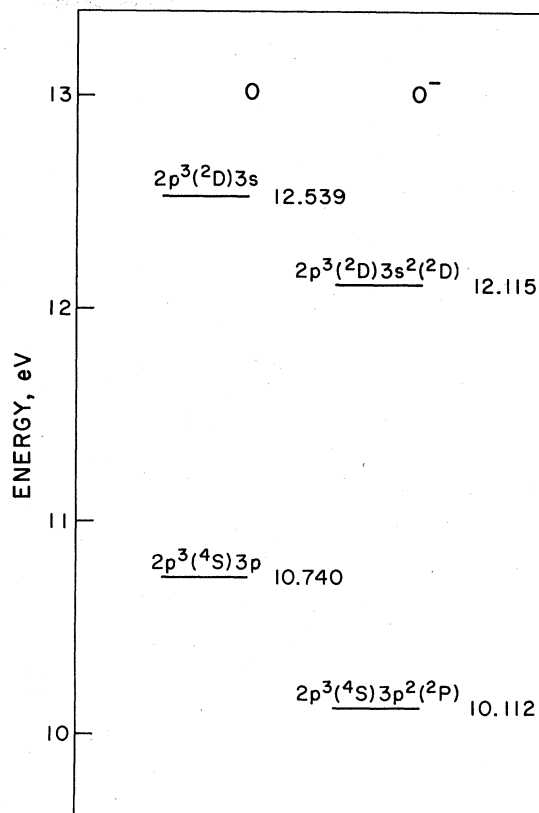


FIG. 49. Energy level diagram for O and O⁻, invoked by Edwards *et al.* (1971) to interpret the data of Fig. 48. The two states of O are considered to be parents of the compound states (O⁻) indicated. Energies are given in eV. The interpretation must be considered preliminary.

assignment for the upper state of Edwards *et al.*, as plotted on Fig. 49.

## ACKNOWLEDGMENTS

## APPENDIX I

Resonances in H (below $n=2$).

| State | Energy (eV) | Width (eV) | Method | Author |
|---|---|---|---|---|
| $^1S$ | 9.61 | 0.109 | cc | Burke and Schey (1962), Smith *et al.* (1962) |
| | 9.559 | | var | O'Malley and Geltman (1965) |
| | 9.557 | | var | Bhatia *et al.* (1967) |
| | 9.56 | | | Gailitis (1965) |
| | 9.55 | | | Holøien and Midtdal (1966) |
| | 9.56 | 0.048 | | Burke and Taylor (1966) |
| | 9.575 | 0.0543 | cc | Burke (1968) |
| | 9.560 | 0.0475 | ccc | Burke (1968) |
| | 9.587 | 0.0501 | ps. st. | Burke, Gallaher, and Geltman (1969) |
| | 9.56±0.01 | 0.043±0.006 | Exp | McGowan (1967) |
| | 9.558±0.01 | | Exp | Sanche and Burrow (1972) |
| $^1S$ | 10.178 | | var | O'Malley and Geltman (1965) |
| | 10.177 | | var | Bhatia *et al.* (1967) |
| | 10.178 | 0.00241 | cc | Burke (1968) |
| | 10.178 | 0.00219 | ccc | Burke (1968) |
| $^3S$ | 10.149 | | var | O'Malley and Geltman (1965) |
| | 10.146 | | var | Bhatia *et al.* (1967) |
| | 10.151 | $1.89 \times 10^{-5}$ | cc | Burke (1968) |
| | 10.150 | $2.06 \times 10^{-4}$ | ccc | Burke (1968) |
| $^1P$ | 10.178 | | var | O'Malley and Geltman (1965) |
| | 10.179 | $2.26 \times 10^{-5}$ | cc | Burke (1968) |
| | 10.177 | $4.50 \times 10^{-5}$ | ccc | Burke (1968) |
| $^3P$ | 9.727 | | var | O'Malley and Geltman (1965) |
| | 9.731 | | var | Bhatia *et al.* (1967) |
| | 9.768 | 0.00797 | cc | Burke (1968) |
| | 9.740 | 0.00594 | ccc | Burke (1968) |
| | 9.759 | 0.00571 | ps. st. | Burke, Gallaher, and Geltman (1969) |
| | 9.71±0.03 | >0.009 | Exp | McGowan (1967) |
| | 9.73±0.12 | | Exp | Kleinpoppen and Raible (1965) |
| | 9.70±0.15 | | Exp | Schulz (1964) |
| | 9.738±0.01 | 0.0056±0.0005 | Exp | Sanche and Burrow (1972) |
| $^1D$ | 10.160 | 0.0078 | cc | Burke (1968) |
| | 10.125 | 0.0088 | ccc | Burke (1968) |
| | 10.128±0.01 | 0.0073±0.002 | Exp | Sanche and Burrow (1972) |
| | 10.13±0.015 | | Exp | Ormonde *et al.* (1969) |
| $^3P$ | 10.194 | 0.0008 | cc | Ormonde *et al.* (1969) |
| | 10.190 | 0.0002 | 6-state | Ormonde *et al.* (1969) |
| | 10.198 | | var | O'Malley and Geltman (1965) |
| $^3S$ | 10.202 | | var | O'Malley and Geltman (1965) |
| $^1P$ | 10.203 | | var | O'Malley and Geltman (1965) |

Abbreviations: cc: close-coupling calculations. ccc: close-coupling plus correlation. ps.st: pseudo-state calculations. var: variational calculations. Exp: experiment.

## APPENDIX II

Values for the $1s(2s)^2\,^2S$ resonance in helium.

| Energy | Width | Method | Author |
|---|---|---|---|
| | | Experiment | |
| 19.30±0.05 | ... | 72° elastic | Schulz (1963) |
| 19.31±0.03 | ... | Transmission | Kuyatt et al. (1965) |
| 19.285±0.025 | ... | Total (elastic) | Golden and Bandel (1965) |
| 19.3±0.1 | ... | 90° elastic | McGowan (1965) |
| 19.30±0.01 | 0.008 | Transmission | Golden and Zecca (1970, 1971) |
| 19.34±0.02 | ... | Transmission | Sanche and Schulz (1972) |
| 19.35±0.02 | ... | 90° elastic | Mazeau et al. (1972) |
| | 0.008 | Differential | Gibson and Dolder (1969) |
| | 0.015–0.020 | Differential | Andrick and Ehrhardt (1966) |
| 19.355±0.008 | ... | Differential | Cvejanovic et al. (1973) |
| | | Theory | |
| 19.5(+0.1, −0.2) | 0.008 | Variational | Kwok and Mandel (1965) |
| | 0.03 | | |
| 19.33 | 0.039 | Close-coupling | Burke et al. (1966) |
| 19.67 | ... | Variational | Young (1968) |
| 19.3 | ... | Stabilization | Eliezer (1970) |
| 19.34 | ... | Bound-state | Weiss and Krauss (1970) |
| 19.69 | ... | | Perkins (1971) |
| 19.363 | 0.014 | Quasi-projection | Temkin et al. (1972) |
| 19.4 | 0.015 | Variational | Sinfailam and Nesbet (1972) |

## APPENDIX III

Position of resonances below ionization in helium (eV).

| Feature number (Fig. 13) | Transmission experiments | | Metastable production | Differential | Designation |
|---|---|---|---|---|---|
| | Sanche and Schulz (1972) | Kuyatt et al. (1965) | Pichanick and Simpson (1968) | Ehrhardt and co-workers | |
| 1–1' | 19.30–19.37 | 19.31–19.37 | | | $2^2S$ |
| | | 19.43–19.47 | | | |
| 2–2' | 19.80–19.90 | 19.818 | | | Wigner cusp+$2^3S$ |
| | | | 20.34 | 20.45 | $2^2P$ |
| 3–3' | 20.58–20.62 | 20.59 | | | Wigner cusp+$2^1S$ |
| | | | 20.99 | 21.00 | $2^2D$ |
| 4 | 21.19 | | | | |
| | | 21.50–21.55 | | | |
| 5–5'–5" | 22.34–22.42–22.50 | 22.34–22.39 | 22.44 | 22.42 | $3^2S$ |
| 6–6'–6" | 22.60–22.65–22.73 | 22.54–22.60 | 22.55/22.67 | 22.55/22.60 | $3^2P$ |
| 7–7'–7" | 22.88–22.92–22.97 | 22.81–22.85 | 22.75/22.86 | 22.75/22.85 | |
| 8 | 23.05 | | 23.05 | | |
| 9–9' | 23.35–23.43 | 23.30–23.44 | 23.39 | | $n=4$ |
| 10–10' | 23.48–23.55 | 23.49 | | | |
| 11–11'–11" | 23.82–23.88–23.93 | 23.75–23.82 | | | $n=5$ |
| 12 | 24.03 | | | | |

## APPENDIX IIIa

Larger structures in the optical excitation functions of He.

Preliminary data.

| Energy eV | Wavelength of observation (Å) | Ref. | Possible designation | Energy eV | Wavelength of observation (Å) | Ref. | Possible designation |
|---|---|---|---|---|---|---|---|
| 22.96 | 7065 | (a) | $4^2S$ | | 4713 | (c) | |
| 23.12 | 7065 | (a) | | 24.0 | 4472 | (a) | |
| 23.25 | 7065 | (a) | | | 4922 | (a) | |
| 23.31 | 7065 | (a) | | | 3188 | (b) | |
| 23.47–23.62 | 3889 | (b) | $^2P(?)$ | 24.08 | 5047 | (a) | |
| 23.41 | 5876 | (a) | | | 4713 | (a) | |
| 23.50 | 5876 | | | | | | |
| 23.86 | 5876 | (a) | | | | | |
| | 4472 | (a) | | | | | |
| | 4922 | (a) | | | | | |
| 23.94 | 5876 | (a) | | | | | |
| | 4472 | (a) | $5^2S$ | | | | |
| | 5047 | (c) | | | | | |

| Transition | $3^3S$–$2^3P$ | $3^3D$–$2^3P$ | $4^3D$–$2^3P$ | $4^1D$–$2^1P$ |
|---|---|---|---|---|
| Wavelength (Å) | 7065 | 5876 | 4472 | 4922 |
| Transition | $4^1S$–$2^1P$ | $4^3S$–$2^3P$ | $3^3P$–$2^3S$ | $4^3P$–$2^3S$ |
| Wavelength (Å) | 5047 | 4713 | 3889 | 3188 |

a Kurepa and Heddle (1972).
b Kisker (1972b).
c Heddle, Keesing, and Kurepa (1973).

The data have been arbitrarily selected by the author to indicate the main peaks observed in optical spectra. Many more, smaller structures have been reported. This table must therefore be considered preliminary, subject to change. This does not apply to the structures for which the wavelength is *underlined*. These are large and well-defined. The structure for which the wavelength is doubly underlined is "enormous".

## APPENDIX IV

Position of resonances above the ionization potential in He.

| Authors | $(2s^22p)^2P$ | $(2s2p^2)^2D$ | Authors | $(2s^22p)^2P$ | $(2s2p^2)^2D$ |
|---|---|---|---|---|---|
| Experiments | | | Quéméner et al. (1971) | 57.15±0.04 | 58.23±0.04 |
| Kuyatt et al. (1965) | 57.1±0.1 | 58.2±0.1 | Grissom et al. (1969) | 57.21 | 58.31 |
| Golden and Zecca (1970) | 56.7/56.93 | 57.87/58.08 | Theories | | |
| Burrow and Schulz (1969) | 56.93±0.1 | 58.04±0.1 | Eliezer and Pan (1970) (stabilization) | 57.3 | 58.3 |
| Sanche and Schulz (1972) | 57.16±0.05 | 58.25±0.05 | Nicolaides (1972) (projection and correlation) | 57.3 | 58.4 |

## APPENDIX V

Position of resonances in neon (eV).

| Feature designations[a] | Transmission experiments | | Metastable production | |
|---|---|---|---|---|
| | Sanche and Schulz (1972) | Kuyatt *et al.* (1965) | Pichanick and Simpson (1968) | Designation |
| 1–1' | 16.10–16.12[c] | 16.04 | | $(2p)^5(3s)^2\,{}^2P_{3/2}$ |
| 2–2' | 16.19–16.22[c] | 16.135 | | $(2p)^5(3s)^2\,{}^2P_{1/2}$ |
| 3–3'(*A*) | 16.85–16.91 | | 16.92 | |
| ... | ... | 18.18 | | |
| ... | ... | 18.29 | | |
| 4(*B, C*) | 18.55 | 18.46 | 18.35–18.43 | Optical excitation[b] 5852 Å |
| 5–5'(*D, E*) | 18.65–18.70 | 18.56 | 18.58–18.66 | Kisker (1972b) |
| 6(*F, G*) | 18.95 | | 18.86–18.97 | |
| 7 | 19.47 | | | 19.50–19.54 |
| 8 | 19.57 | | | 19.60– |
| 9 | 19.65 | | | |
| 10(*H*) | 19.71 | | 19.69 | –19.70 |
| | | | | 19.77–19.82 |
| 11–11'(*I*) | 19.97–20.03 | | 19.83 | 19.91–19.99 |
| 12–12'(*J*) | 20.07–20.13 | | 20.1 | 20.03–20.07 |
| | | | | –20.19 |
| | | | | 20.60–20.64 |
| | | | | 20.70–20.74 |

[a] The "feature designations" refer to Fig. 25 (numbers) and Fig. 26 (letters), respectively.

[b] The first energy refers to a maximum, the second to a minimum.

[c] The widths of the ${}^2P_{3/2}$, ${}^2P_{1/2}$ resonances have been deduced from experiment by Haselton (1973). He finds $\Gamma = 8.95 \pm 0.34$ meV.

## APPENDIX VI

Position of resonances in argon (eV).

| Transmission experiments | | Metastable production | |
|---|---|---|---|
| Sanche and Schulz (1972) | Kuyatt *et al.* (1965) | Pichanick and Simpson (1968) | Designation |
| 11.10–11.13 | 11.064–11.094 | | $3p^5 4s^2\,{}^2P_{3/2}$ |
| 11.27–11.30 | 11.235–11.267 | | ${}^2P_{1/2}$ |
| 11.71 | | 11.72 | $3p^5 4s4p(?)$ |
| 11.91 | | 11.88–11.98 | $3p^5 4s4p(?)$ |
| 12.89–12.92 | | 12.80–12.93 | |
| 12.95–13.06–13.11 | | 13.08 | |
| 13.22–13.28 | | 13.17–13.24 | |
| 13.33 | | 13.37 | |
| 13.45–13.50 | | 13.55 | |
| 14.03–14.07–14.10 | | | |

## APPENDIX VII

### Position of resonances in krypton (eV).

| Transmission exp. | Differential elastic and inelastic | Metastable production | |
|---|---|---|---|
| Sanche and Schulz (1972) | Swanson et al. (1973) | Pichanick and Simpson (1968) | Designation |
| 9.50–9.53 | 9.52 | | $4p^5 5s^2 \, ^2P_{3/2}$ |
| 10.16–10.19 | 10.14 | 10.05 | $^2P_{1/2}$ |
| 10.66–10.69 | 10.67 | 10.63 | |
| 11.29 | 11.29 | 11.10–11.20 | |
| 11.40 | 11.42 | | |
| 11.54 | | 11.42 | |
| 11.67 | 11.67 | 11.70 | |
| 11.97–12.04–12.10 | 11.97 | 11.94–12.04 | |
| | 12.04 | 12.28 | |
| | 12.10 | 13.08 | |

### Optical excitation experiments in krypton[a] (Kisker, 1972b).

| 4502 Å | 4464 Å | 4274 Å | 4376 Å |
|---|---|---|---|
| 12.90–12.95 | | | |
| | 12.93–13.00 | | 12.97–13.04 |
| | 13.19–13.25 | 13.13–13.18 | 13.11–13.18 |
| | | 13.23– | 13.24–13.30 |
| | | | 13.36– |

[a] Given are values for max–min.

Swanson, Cooper, and Kuyatt (1973) compare the resonances in krypton with optical absorption data of Rb I. Such a comparison leads them to interpret the resonances in the energy range 10.5 eV–12 eV (i.e., all but the two lowest states) as $4p^5 5s4d$ states. The $4p^5$ ion core can have $J=\frac{1}{2}$ or $\frac{3}{2}$.

## APPENDIX VIII

### Position of resonances in xenon (eV).

| Transmission experiments | | Metastable production | |
|---|---|---|---|
| Sanche and Schulz (1972) | Kuyatt et al. (1965) | Pichanick and Simpson (1968) | Designation |
| 7.80–7.90–7.92 | 7.74–7.77 | | $5p^5 6s^2 \, ^2P_{3/2}$ |
| 8.48 | | | |
| 9.11–9.26 | 9.02 | 9.0 | $^2P_{1/2}$ |
| 9.52 | | | |
| 9.56 | | 9.5 | |
| 9.65 | | | |
| 10.92 | 10.81–10.86 | 10.3 | |
| 11.00 | | | |

Appendix VIII—*Continued*

Optical excitation experiments[a] (Kisker, 1972c)

| 4624 Å | 4671 Å | 4079 Å | 4583 Å | 4734 Å |
|---|---|---|---|---|
| 11.02–11.05 | | | | |
| 11.12–11.15 | 11.11– | | 11.16–11.20 | |
| 11.22–11.31 | –11.27 | | | |
| 11.40–11.46 | 11.39–11.45 | | | |
| | 11.53–11.58 | 11.51–11.55 | | |
| | | 11.61–11.65 | | |
| | | 11.83–11.90 | 11.75–11.87 | 11.81–11.95 |
| | | | 12.03–12.09 | 12.03–12.10 |
| | 12.13–12.23 | 12.19–12.28 | 12.20–12.27 | –12.20 |

[a] In this table, the first energy corresponds to an observed maximum, the second energy value on the same line corresponds to an observed minimum.

## APPENDIX IX

Suggested resonances in Ne and Ar.

| Energy eV | Method | Observer | Designation |
|---|---|---|---|
| | | Neon | |
| 41.98 | Transmission | Sanche and Schulz (1972) | |
| 42.1 | Trapped electrons | Grissom *et al.* (1969) | |
| 43.05 | Transmission | Sanche and Schulz (1972) | |
| 44.35 | Transmission | Sanche and Schulz (1972) | |
| 44.25 | Trapped electrons | Grissom *et al.* (1969) | |
| 47.6 | Transmission | Sanche and Schulz (1972) | |
| 47.57 | Trapped electrons | Grissom *et al.* (1969) | |
| | | Argon | |
| 24.44 | Ar+ | Bolduc *et al.* (1972) | $3s3p^6 4s^2\ {}^2S$ |
| 24.53 | Transmission | Sanche and Schulz (1972) | |
| 26.87 | Transmission | Sanche and Schulz (1972) | |
| 27.91 | Transmission | Sanche and Schulz (1972) | |
| 28.9 | Transmission | Sanche and Schulz (1972) | |

## APPENDIX X

Position of resonances in mercury (eV).

| Feature No. (Fig. 38) | Kuyatt et al. (1965) Transmission | Zapesochnyi and Shpenik (1966) $6^3P_1$ $\lambda = 2537$ Å $E_x = 4.89$ eV | $7^3S_1$ 5461 Å 7.73 eV | $6^3D$ 3650 Å 8.9 eV | $8^1S_0$ 4916 Å 9.2 eV | Fano and Cooper (1965) Designation |
|---|---|---|---|---|---|---|
| 1 | 4.07 | ... | ... | ... | ... | $(6s6p^2)^4P_{1/2}$ |
| 2 | 4.30 | ... | ... | ... | ... | $(6s6p^2)^4P_{3/2}$ |
| 3 | 4.89 | ... | ... | ... | ... | $(6s6p^2)^4P_{5/2}$ |
|  | ... | 5.0 |  |  |  |  |
|  | ... | 5.3 |  |  |  |  |
|  | ... | 5.6 |  |  |  |  |
| 4 | 7.81 |  |  |  |  |  |
| 5 | 7.94 |  |  |  |  |  |
| 6 | 8.14 |  |  |  |  |  |
| 7 | 8.22 | 8.5 | 8.2 | ... |  |  |
| 8 | 8.83 | ... | 8.8 | ... |  |  |
| 9 | 8.99 | 9.0 | 9.0 | 9.1 |  |  |
| 10 | 9.75 | 9.7 | 9.6 | 9.8 | 9.5 |  |
| 11 | 10.29 | 10.0 | 10.2 | 10.2 | 10.2 |  |
| 12 | 10.58 | 10.4 | ... | ... | ... |  |
| 13 | 10.88 | ... | ... | ... | ... |  |
|  | ... | 11.2 | 11.1 | 11.1 | 11.4 |  |
|  | ... | ... | 11.9 | 11.7 | 11.9 |  |
|  | ... | ... | ... | ~12.2 | 12.4 |  |
|  | ... | 12.5 | ~12.5 | 12.6 |  |  |

Adams, A., and F. H. Read, 1972, J. Phys. E 5, 156.
Andrick, D., and H. Ehrhardt, 1966, Z. Phys. 192, 99.
Andrick, D., H. Ehrhardt, and M. Eyb, 1968, Z. Phys. 214, 388.
Andrick, D., M. Eyb, and M. Hofmann, 1972, J. Phys. B 5, L15.
Baranger, E., and E. Gerjuoy, 1957, Phys. Rev. 106, 1182.
Barker, R. B. and H. W. Berry, 1966, Phys. Rev. 151, 14.
Bauer, E., and N. H. Browne, 1964, in Atomic Collision Processes, edited by M. R. C. McDowell (North-Holland, Amsterdam), p. 16 (1964).
Baumann, H., E. Heinicke, H. J. Kaiser, and K. Bethge, 1971, Nucl. Instrum. Methods 95, 389.
Baz, A. I., 1957, Zh. Eksp. Teor. Fiz. 33, 923. [Sov. Phys.-JETP 6, 709.]
Bederson, B., 1968, Methods Exp. Phys. 7A, 67.
Bederson, B., and L. J. Kieffer, 1971, Rev. Mod. Phys. 43, 601
Bhatia, A. K., A. Temkin, and J. F. Perkins, 1967, Phys. Rev. 153, 177.
Blatt, J. M., and V. F. Weisskopf, 1952, Theoretical Nuclear Physics (Wiley, New York, 1952).

Bolduc, E., J.J. Quéméner, and P. Marmet, 1971, Can. J. Phys. 49, 3095.
Bolduc, E., J. J. Quéméner, and P. Marmet, 1972, J. Chem. Phys. 57, 1957.
Brode, R. B., 1929, Phys. Rev. 34, 673.
Burke, P. G., 1965, Advances in Physics, (Phil. Mag. Suppl.) 14, 521.
Burke, P. G., 1968, Adv. At. Mol. Phys. 4, 173.
Burke, P. G., J. W. Cooper, and S. Ormonde, 1966, Phys. Rev. Lett. 17, 345.
Burke, P. G., 1969, Phys. Rev. 183, 245.
Burke, P. G., D. F. Gallaher, and S. Geltman, 1969, J. Phys. B 2, 1142.
Burke, P. G., S. Ormonde, and W. Whitaker, 1967, Proc. Phys. Soc. Lond. 92, 319.
Burke, P. G., and H. M. Schey, 1962, Phys. Rev. 126, 147.
Burke, P. G., and A. J. Taylor, 1966, Proc. Phys. Soc. Lond. 88, 549.
Burke, P. G., 1969, J. Phys. B 2, 869.
Burrow, P. D., 1970, Phys. Rev. A 2, 1774.
Burrow, P. D., and G. J. Schulz, 1969, Phys. Rev. Lett. 22, 1271.
Chamberlain, G. E., 1967, Phys. Rev. 155, 46.
Chamberlain, G. E., and H. G. M. Heideman, 1965, Phys. Rev. Lett. 15, 337.
Chamberlain, G. E., S. J. Smith, and D. W. O. Heddle, 1964, Phys. Rev. Lett. 12, 647.
Comer, J., and F. H. Read, 1972, J. Phys. E 5, 211.
Cooper, J. W., and J. B. Martin, 1962, Phys. Rev. 126, 1482.
Crooks, G. B., R. D. DuBois, D. E. Golden, and M. E. Rudd, 1972, Phys. Rev. Lett. 29, 327.

Kuyatt, C. E., and J. A. Simpson, 1967, Rev. Sci. Instrum. **38**, 103.

Kuyatt, C. E., 1968, Methods Exp. Phys. **7A**, 1.

Kwok, K. L., and F. Mandl, 1965, Proc. Phys. Soc. Lond. **86**, 501.

LaBahn, R. W., and J. Callaway, 1964, Phys. Rev. **135**, A1539.

Long, R. L., D. M. Cox, and S. J. Smith, 1968, J. Res. Natl. Bur. Stand. (U.S.) A **72A**, 521.

Macek, J., 1967, Proc. Phys. Soc. Lond. **92**, 365.

Macek, J., and P. G. Burke, 1967, Proc. Phys. Soc. Lond. **92**, 351.

Marriott, R., and M. Rotenberg, 1968, Phys. Rev. Lett. **21**, 722.

Massey, A. S. W., and E. H. S. Burhop, 1969, *Electronic and Ionic Impact Phenomena* (Oxford University Press, London), Vols. I and II.

Matese, J. J., S. P. Rountree, and R. J. W. Henry, 1973, Phys. Rev. A **7**, 846.

Mazeau, J., F. Gresteau, G. Joyez, J..Reinhardt, and R. I. Hall, 1972, J. Phys. B **5**, 1890.

McDaniel, E..W., 1964, *Collision Phenomena in Ionized Gases* (Wiley, New York).

McGowan, J. W., 1966, Phys. Rev. Lett. **17**, 1207.

McGowan, J. W., 1967, Phys. Rev. **156**, 165.

McGowan, J. W., 1970, Science **167**, 1083.

McGowan, J. W., E. M. Clarke, and E. K. Curley, 1965, Phys. Rev. Lett. **15**, 917.

McGowan, J. W., J. F. Williams, and E. K. Curley, 1969, Phys. Rev. **180**, 132.

Moores, D. L., and D. W. Norcross, 1972, J. Phys. B **5**, 1482.

Myerscough, V. P., 1965, Phys. Lett. **19**, 120.

Neynaber, R. H., E. W. Rothe, L. L. Marino, and S. M. Trujillo, 1961, Phys. Rev. **123**, 148.

Nicolaides, C. A., 1972, Phys. Rev. A **6**, 2078.

Norcross, D. W., 1971, J. Phys. B **4**, 1458.

Norcross, D. W., and D. L. Moores, 1972, *Atomic Physics III, Proceedings IIIrd International Conference on Atomic Physics*, Boulder (Plenum, New York).

Olmsted, J. III, A. S. Newton, and K. Street, Jr., 1965, J. Chem. Phys. **42**, 2321.

O'Malley, T. F., and S. Geltman, 1965, Phys. Rev. **137**, A1344.

Ormonde, S., J. McEwen, and J. W. McGowan, 1969, Phys. Rev. Lett. **22**, 1165.

Ormonde, S., K. Smith, B. W. Torres, and A. R. Davies, 1973 (to be published).

Ott, W. R., W. Kauppila, and W. L. Fite, 1970, Phys. Rev. A **1**, 1089.

Pavlovic, Z., M. J. W. Boness, A. Herzenberg, and G. J. Schulz, 1972, Phys. Rev. A **6**, 676.

Peart, B., D. S. Walton, and K. Dolder, 1970, J. Phys. B **3**, 1346.

Perel, J., P. Englander, and B. Bederson, 1962, Phys. Rev. **128**, 1148.

Perkins, J. F., 1971, Phys. Rev. A **4**, 489.

Phelps, A. V., 1955, Phys. Rev. **99**, 1307.

Pichanick, F. M. J., and J. A. Simpson, 1968, Phys. Rev. **168**, 64.

Quéméner, J. J., C. Paquet, and P. Marmet, 1971, Phys. Rev. A **4**, 494.

Read, F. H., 1970, J. Phys. E **3**, 127.

Read, F. H., 1971, J. Phys. E **4**, 562.

Rudd, M. E., 1964, Phys. Rev. Lett. **13**, 503.

Rudd, M. E., 1965, Phys. Rev. Lett. **15**, 580.

Sanche, L., and G. J. Schulz, 1972, Phys. Rev. A **5**, 1672.

Sanche, L., and P. D. Burrow, 1972, Phys. Rev. Lett. **29**, 1639.

Sawada, T., J. E. Purcell, and A. E. S. Green, 1971, Phys. Rev. A **4**, 193.

Schowengerdt, F. D., S. R. Smart, and M. E. Rudd, 1973,

Cvejanovic, S., J. Comer, and F. H. Read, 1973, in *Eighth International Conference on the Physics of Electronic and Atomic Atomic Collisions: Abstracts of Papers* (Belgrade, Yugoslavia).

Drake, G. W. F., 1970, Phys. Rev. Lett. **24**, 126.

Ederer, D. L., 1971, Phys. Rev. A **4**, 2263.

Edwards, A. K., J. S. Risley, and R. Geballe, 1971, Phys. Rev. A **3**, 583.

Ehrhardt, H., 1969, in *Physics of the One- and Two-Electron Atoms*, edited by F. Bopp and H. Kleinpoppen (North-Holland, Amsterdam, 1969).

Ehrhardt, H., L. Langhans, and F. Linder, 1968, Z. Phys. **214**, 179.

Ehrhardt, H., and K. Willmann, 1967, Z. Phys. **203**, 1.

Eliezer, I., and Y. K. Pan, 1970, Theor. Chim. Acta **16**, 63.

Enemark, E. A., and A. Gallagher, 1972, Phys. Rev. A **6**, 192.

Fano, U., 1961, Phys. Rev. **124**, 1866.

Fano, U. and J. W. Cooper, 1965a, Phys. Rev. **137**, A1364.

Fano, U., and J. W. Cooper, 1965b, Phys. Rev. **138**, A400.

Fleming, R. J., and G. S. Higginson, 1963, Proc. Phys. Soc. Lond. **81**, 974.

Fung, A. C., and J. J. Matese, 1972, Phys. Rev. A **5**, 22.

Gailitis, M., 1965, in *IVth International Conference in the Physics of Electronic and Atomic Collisions: Abstracts of Papers*, edited by L. Kerwin and W. Fite (Science Bookcrafters, Hastings-on-Hudson, N. Y.), p. 10.

Gailitis, M., and R. Damburg, 1963, Proc. Phys. Soc. Lond. **82**, 192.

Geltman, S., and P. G. Burke, 1970, J. Math. Phys. **3**, 1062.

Gibson, J.R., and K. T. Dolder, 1969, J. Phys. B **2**, 741.

Golden, D. E., and H. W. Bandel, 1965, Phys. Rev. **38**, A14.

Golden, D. E., and A. Zecca, 1970, Phys. Rev. A **1**, 241.

Golden, D. E., and A. Zecca, 1971, Rev. Sci. Instrum. **42**, 210.

Grissom, J. T., R. N. Compton, and W. R. Garrett, 1969, Phys. Lett. **30A**, 117.

Grissom, J. T., W. R. Garrett, and R. N. Compton, 1969, Phys. Rev. Lett. **23**, 1011.

Hall, R. I., J. Reinhardt, G. Joyez, and J. Mazeau, 1972, J. Phys. B **5**, 66.

Haselton, H. H., 1973, Bull. Am. Phys. Soc. **18**, 710.

Hasted, J. B., 1964, *Physics of Atomic Collisions* (Butterworths, London).

Hazi, A. U., and H. S. Taylor, 1970, Phys. Rev. A **1**, 1109.

Heddle, D. W. O., 1970, JILA Rept. 104 (University of Colorado, Boulder, Colo.).

Heddle, D. W. O., R. G. W. Keesing, and J. M. Kurepa, 1973, (to be published).

Herzenberg, A., 1971, Phys. Bull. Inst. Phys. Phys. Soc. Lond. **22**, 521.

Herzenberg, A., 1972 (private communication).

Herzenberg, A., and D. Ton-That, 1973 (to be published).

Herzenberg, A., K. L. Kwok, and F. Mandl, 1964, Proc. Phys. Soc. Lond. **84**, 345.

Holøien, E., 1960, J. Chem. Phys. **33**, 301.

Holøien, E., and J. Midtdal, 1966, J. Chem. Phys. **45**, 2209.

Karule, E. M., 1965, in *Atomic Collisions III*, edited by V. Ia. Veldre (Akad. Nauk Latv. SSSR, Inst. Fiz. English translation, JILA Information Center Report #3, University of Colorado 1966. Available through SLA translation center, John Crerar Library, Chicago, Ill. Translation # TT-66-12939.

Karule, E. M., 1970, J. Phys. B **3**, 860.

Kisker, E., 1972a. Phys. Lett. **38A**, 79

Kisker, E., 1972b, Z. Phys. **256**, 121.

Kisker, E., 1972c, Z. Phys. **257**, 51.

Kleinpoppen, H., and V. Raible, 1965, Phys. Lett. **18**, 24.

Klemperer, O., 1965, Rep. Prog. Phys. **28**, 77.

Kurepa, J. M., and D. W. O. Heddle, 1972, Proceedings of the VI Yugoslav Symposium on Physics of Ionized Gases.

Kuyatt, C. E., J. A. Simpson, and J. A. Mielczarek, 1965, Phys. Rev. **138**, A385.

Phys. Rev. A 7, 560.

Schulz, G. J., 1959, Phys. Rev. 116, 1141.

Schulz, G. J., 1963, Phys. Rev. Lett. 10, 104.

Schulz, G. J., 1964a, Phys. Rev. Lett. 13, 583.

Schulz, G. J., 1964b, Phys. Rev. 136, A650.

Schulz, G. J., and R. E. Fox, 1957, Phys. Rev. 106, 1179.

Schulz, G. J., and J. W. Philbrick, 1964, Phys. Rev. Lett. 13, 477.

Sharpton, F. A., R. M. St. John, C. C. Lin, and F. E. Fajen, 1970, Phys. Rev. A 2, 1305.

Shore, B. W., 1967, Rev. Mod. Phys. 39, 439.

Simpson, J. A., 1964, Rev. Sci. Instrum. 35, 1698.

Simpson, J. A., 1967, Rev. Sci. Instrum. 38, 103.

Simpson, J. A., and U. Fano, 1963, Phys. Rev. Lett. 11, 158.

Simpson, J. A., M. G. Menendez, and S. R. Mielczarek, 1966, Phys. Rev. 150, 76.

Sinfailam, A. L., and R. K. Nesbet, 1972, Phys. Rev. A 6, 2118.

Smit, C., and H. M. Fijnaut, 1965, Phys. Lett. 19, 121.

Smith, K., 1966, Rep. Prog. Phys. 29, 373.

Smith, K., R. P. Eachran, and P. A. Fraser, 1962, Phys. Rev. 125, 553.

Stamatovic, A., and G. J. Schulz, 1970, Rev. Sci. Instrum. 41, 423.

Sunshine, G., B. B. Aubrey, and B. Bederson, 1967, Phys. Rev. 154, 1.

Swanson, N., J. W. Cooper, and C. E. Kuyatt, 1971, in *Electronic and Atomic Collisions*, Abstracts of Papers of the VIIth International Conference on the Physics of Electronic and Atomic Collisions (North-Holland, Amsterdam,), p. 323. See also, 1973, Phys. Rev. (to be published).

Taylor, A. J., and P. G. Burke, 1967, Proc. Phys. Soc. Lond. 92, 336.

Taylor, H. S., 1970, Adv. Chem. Phys. 18, 91.

Taylor, H. S., G. V. Nazaroff, and A. Golebiewski, 1966, J. Chem. Phys. 45, 2872.

Taylor, H. S., and L. D. Thomas, 1972, Phys. Rev. Lett. 28, 1091.

Temkin, A., 1957, Phys. Rev. 107, 1004.

Temkin, A., A. K. Bhatia, and J. N. Bardsley, 1972, Phys. Rev. A 5, 1663.

Walton, D. S., B. Peart, and K. Dolder, 1970, J. Phys. B 3, L148.

Weiss, A. W., 1968, Phys. Rev. 166, 70.

Weiss, A. W., and M. Krauss, 1970, J. Chem. Phys. 52, 4363.

Wigner, E. P., 1948, Phys. Rev. 73, 1002.

Young, A. D., 1968, J. Phys. B 1, 1073.

Zapesochnyi, I. P., and O. B. Shpenik, 1966, Sov. Phys.-JETP 23, 592.